

UNCLASSIFIED

| |
|--|
| |
| |
| |
| |
| AD NUMBER |
| AD865697 |
| NEW LIMITATION CHANGE |
| TO Approved for public release, distribution unlimited |
| FROM Distribution authorized to U.S. Gov't. agencies and their contractors; Administrative/Operational Use; FEB 1970. Other requests shall be referred to Air Force Flight Dynamics Lab., Attn: FDMM, Wright-Patterson AFB, OH 45433. |
| AUTHORITY |
| Air Force Flight Dynamics Lab. ltr dtd 13 Jul 1979 |

THIS PAGE IS UNCLASSIFIED

THIS REPORT HAS BEEN DELIMITED
AND CLEARED FOR PUBLIC RELEASE
UNDER LOD DIRECTIVE 5200.20 AND
NO RESTRICTIONS ARE IMPOSED UPON
ITS USE AND DISCLOSURE.

DISTRIBUTION STATEMENT A

APPROVED FOR PUBLIC RELEASE;
DISTRIBUTION UNLIMITED.

AFFDL-TR-69-117

AD 865697

JET FLAP INVESTIGATION AT TRANSONIC SPEEDS

W. E. Grahame

J. W. Headley

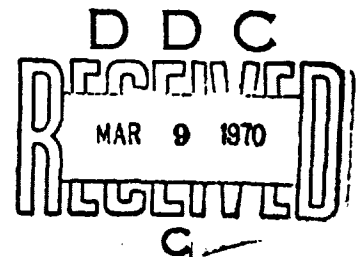
Northrop Corporation
Aircraft Division

TECHNICAL REPORT AFFDL-TR-69-117

February 1970

This document is subject to special export controls and each transmittal to foreign governments or foreign nationals may be made only with prior approval of the Flight Dynamics Laboratory (FDMM), Wright-Patterson Air Force Base, Ohio 45433.

Reproduced by the
CLEARINGHOUSE
for Federal Scientific & Technical
Information Springfield Va. 22151



AIR FORCE FLIGHT DYNAMICS LABORATORY
AIR FORCE SYSTEMS COMMAND
WRIGHT-PATTERSON AIR FORCE BASE, OHIO

| | |
|---------------------------------|---|
| ACCESSION FOR | |
| OFSTI | WHITE SECTION <input type="checkbox"/> |
| DDG | DIFF. SECTION <input checked="" type="checkbox"/> |
| UNANNOUNCED | <input type="checkbox"/> |
| JUSTIFICATION | |
| BY | |
| DISTRIBUTION/AVAILABILITY CODES | |
| DIST. | AVAIL. and/or SPECIAL |
| 2 | |

NOTICES

When Government drawings, specifications, or other data are used for any purpose other than in connection with a definitely related Government procurement operation, the United States Government thereby incurs no responsibility nor any obligation whatsoever; and the fact that the Government may have formulated, furnished, or in any way supplied the said drawings, specifications, or other data, is not to be regarded by implication or otherwise as in any manner licensing the holder or any other person or corporation, or conveying any rights or permission to manufacture, use, or sell any patented invention that may in any way be related thereto.

This document is subject to special export controls, and each transmittal to foreign governments or foreign nationals may be made only with prior approval of the Flight Dynamics Laboratory (FDMM), Wright-Patterson AFB, Ohio 45433.

The distribution of this report is limited because the report contains technology identifiable with items on the strategic embargo list excluded from export or re-export under U. S. Embargo Act of 1949 as implemented by AFR 40-10.

Copies of this report should not be returned unless return is required by security considerations, contractual obligations, or notice on a specific document.

AFFDL-TR-69-117

JET FLAP INVESTIGATION AT
TRANSONIC SPEEDS

W. E. Grahame

J. W. Headley

This document is subject to special export controls and each transmittal to foreign governments or foreign nationals may be made only with prior approval of the Flight Dynamics Laboratory (FDMM), Wright-Patterson Air Force Base, Ohio, 45433.

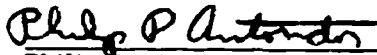
FOREWORD

This report describes a transonic wind tunnel investigation of a two-dimensional wing with a jet flap. It was prepared by the Aerodynamics and Propulsion Research and Technology Group of the Northrop Corporation Aircraft Division, Hawthorne, California under Air Force Contract F33615-69-C-1429. The work was under the direction of the Air Force Flight Dynamics Laboratory, with Mr. L. W. Rogers, FDMM, as Project Engineer.

The work reported here was performed during the period from 10 February 1969 to 10 November 1969. This report was submitted by the authors in November 1969.

The authors acknowledge the contributions made by the following members of the Northrop Corporation; Mr. F. Peltzman and Mr. A. Weddell of the Test Branch, and Messrs. C.W. Winter, K. Star and R. Edwards. Report number NOR-69-143 has been assigned for internal control.

This technical report has been reviewed and is approved.



Philip P. Antonatos
Chief, Flight Mechanics Division
Air Force Flight Dynamics Laboratory

ABSTRACT

A transonic wind tunnel test of a two-dimensional airfoil with a jet flap was conducted to obtain data relative to determining the feasibility of using a jet flap for transonic maneuvering. Tests were performed at Mach numbers of 0.70, 0.80, 0.85, 0.90, and 0.95 for an angle-of-attack range from zero up to the angle of attack corresponding to maximum lift coefficient at nominal jet flap angles of 0°, 30°, 45°, 60°, and 90°. Lift and drag characteristics were obtained by integrating pressures measured over the wing and by a wake rake. The results show significant lift improvement at low Mach number which diminished as Mach number increased. Test results were compared on the basis of lifting efficiency E_L and thrust recovery η_T at various jet angles and jet momentum values. The results indicated that the values of E_L and η_T obtained generally agreed with those which have been presented from other tests. The jet flap at the largest angle (θ_f nominally 90°) with a row of vane vortex generators positioned at 12% chord produced the greatest rearward movement of shock-induced separation. Effects of Reynolds number showed that lift characteristics were lower at $R_N = 5.5 \times 10^6/\text{ft}$ than at $R_N = 2.5 \times 10^6/\text{ft}$ while drag was higher throughout the Mach number range. A correlation of six methods, which predict the onset of buffet, illustrated the ability of the jet flap to improve the buffet boundary.

This abstract is subject to special export controls and each transmittal to foreign governments or foreign nationals may be made only with prior approval of the Flight Dynamics Laboratory (FDMM), Wright-Patterson AFB, Ohio 45433.

TABLE OF CONTENTS

| <u>Section</u> | <u>Title</u> | <u>Page</u> |
|----------------|--|-------------|
| I | INTRODUCTION | 1 |
| II | WIND TUNNEL TEST PROGRAM | 3 |
| | Aerodynamic Design of the Model | 3 |
| | Model Construction | 5 |
| | Instrumentation | 6 |
| | Data Reduction | 6 |
| | Vortex Generators | 6 |
| | Static Calibrations | 9 |
| | Wind Tunnel Test Conditions | 12 |
| III | DISCUSSION OF RESULTS | 13 |
| | Effect of Blowing Momentum on Longitudinal Characteristics, $\theta_f = 88^\circ$ | 13 |
| | Effect of Blowing Momentum on Pressure Distributions $\theta_f = 88^\circ$. | 15 |
| | Effect of Jet Flap Angle | 16 |
| | Effect of Mach Number | 18 |
| | Effect of Vortex Generators | 21 |
| | Effect of Reynolds Number | 21 |
| | Evaluation of Thrust Recovery and Residual Drag | 23 |
| | Thrust Recovery | 23 |
| | Residual Drag | 25 |
| | Buffet Onset Analysis | 26 |
| | Shock Locations and Separation | 27 |
| | Comparison of Test Airfoil with NACA 64A406 | 30 |
| | Spanwise Pressure Distribution | 30 |
| IV | CONCLUSIONS | 31 |
| V | REFERENCES | 32 |
| APPENDIX | LIST OF RELATED FIGURES | 33 |

LIST OF ILLUSTRATIONS

| <u>Figure</u> | <u>Title</u> | <u>Page</u> |
|---------------|---|-------------|
| 1 | Basic (NACA 64A406) and Modified Airfoils | 4 |
| 2 | Typical Jet Flap Exit Configurations | 4 |
| 3 | Schematic of Jet Flap Airfoil Installation | 7 |
| 4 | Wing Model with Sting Support and Wake Rake. | 8 |
| 5 | Jet Flap Model Mounted to Endplates in AEDC Tunnel | 8 |
| 6 | Vortex Generator Installation. | 9 |
| 7 | Oil Flow Pattern (θ_f nominally 90°) at Plenum Pressure = 31.0 psia. | 10 |
| 8 | Variation of Jet Circulation Lift Coefficient with Mach Number | 15 |
| 9 | Jet Sheet Trajectories | 17 |
| 10 | Incompressible Values of E_L | 18 |
| 11 | Comparison of Blowing at Low and High Mach Numbers | 19 |
| 12 | Effect of Mach Number on Lift Coefficient | 20 |
| 13 | Oil Flow Visualization at $M = 0.85$, $\alpha = 8^\circ$, $\theta_f = 88^\circ$ | 22 |
| 14 | Effect of Reynolds Number on Displacement Thickness | 24 |
| 15 | Variation of Shock Location with Reynolds Number | 24 |
| 16 | Definition of Thrust Recovery and Residual Drag | 26 |
| 17 | Buffet Onset Methods | 27 |
| 18 | Flow Pattern Comparison | 28 |
| 19 | Definition of Shock Location. | 29 |

LIST OF TABLES

| <u>Table</u> | <u>Title</u> | <u>Page</u> |
|--------------|---|-------------|
| I | Jet Flap Airfoil Coordinates (Modified NACA 64A406) | 5 |
| II | Experimental Flow Coefficients | 11 |
| III | Static Jet Reactions at Plenum Pressure = 60 psia | 12 |
| IV | Comparison of Longitudinal Characteristics at Maximum Angle of Attack, $\theta_f = 88^\circ$ | 14 |
| V | Effect of C_μ on Lift Efficiency and Circulation Lift | 20 |

LIST OF SYMBOLS

| | |
|--------------|---|
| A_j | — Area of the Jet Slot |
| c | — Airfoil Chord |
| C_a | — Section Axial Force Coefficient |
| C_d | — Section Drag Coefficient |
| C'_d | — Unseparated Drag Coefficient, (Jet Off), See Equation (8) |
| C_{d_o} | — Section Drag Coefficient at Zero Lift |
| C_{d_r} | — Section Residual Drag, See Figure 16 |
| C_l | — Section Lift Coefficient |
| C_{l_r} | — Supercirculation Lift Coefficient, See Equation (5) |
| C_m | — Section Moment Coefficient About Quarter Chord Point |
| C_n | — Jet Flap Flow Coefficient |
| C_p | — Local Pressure Coefficient, $\frac{p-p_o}{q_o}$ |
| $C_{p_{TE}}$ | — Local Pressure Coefficient at the Trailing Edge |
| C_μ | — Blowing Momentum Coefficient, See Equation (1) |
| E_L | — Lift Efficiency, See Equation (6) |
| K | — Constant In Equation (8) |
| M | — Mach Number |

| | |
|------------|--|
| m_j | — Mass Flow Through Jet Slot |
| p | — Local Static Pressure |
| p_o | — Free Stream Static Pressure |
| P_j | — Static Pressure at Jet Exit |
| P_T | — Jet Flap Plenum Total Pressure |
| q_o | — Free Stream Dynamic Pressure |
| R_a | — Static Jet Axial Reaction, See Equation (3) |
| R_j | — Static Jet Reaction, See Equation (2) |
| R_n | — Static Jet Normal Reaction, See Equation (4) |
| R_N | — Reynolds Number |
| S | — Wing Span |
| t_s | — Jet Slot Width |
| V_j | — Jet Exit Velocity |
| x | — Distance Along Chord from Leading Edge |
| x_s | — Distance of Shock from Leading Edge |
| y | — Distance Along Span |
| z | — Distance Above Chord |
| α | — Section Angle of Attack |
| δ^* | — Boundary Layer Displacement Thickness |
| η_T | — Thrust Recovery, Defined in Equation (7) |
| θ_f | — Jet Flap Deflection Angle |

SECTION I

INTRODUCTION

With increasing emphasis being placed on improved transonic maneuvering performance of fighter aircraft, it has become necessary to investigate the feasibility of applying high-lift devices which appear to hold promise but heretofore have not received much attention. From the limited amount of transonic tests which have been conducted in the past, it has been shown that the jet flap can have a beneficial effect on airfoil lift and drag characteristics. It remained, however, to understand more about other characteristics of the jet flap such as its ability to reduce or eliminate shock-induced separation at angle of attack throughout the transonic Mach regime. Also, it was of importance to determine pitching moment effects, Reynolds number effects, thrust recovery and lifting efficiency at various jet angles and blowing momentum.

Extensive theoretical and experimental work over the past 16 years by various organizations has shown that the jet flap is a powerful device for increasing the lift of a wing. The lift improvement derives from supercirculation around an airfoil resulting from an increase in effective camber due to the jet sheet. Most of the work has involved the determination of low speed jet flap characteristics, although a limited amount of work has been performed at transonic speeds. A survey of available data indicated that the parameters used to measure low-speed jet flap performance such as thrust recovery and lifting efficiency applied at transonic speeds as well. Two-dimensional results at transonic speeds in Reference 7, showed that 100% thrust recovery and lifting efficiencies as high as 16 were possible.

A review of jet flap investigations on two- and three-dimensional wings has shown a lack of surface pressure measurements particularly at transonic speeds. Such measurements are of importance in the analysis of shock-induced separation effects. One method which has been applied in flow separation analysis is oil flow visualization, whereby oil is emitted through orifices in the leading edge of a wing and allowed to flow over the upper surface. The resulting oil flow patterns aid in the determination of separated flow regions.

A correlation then of the upper surface pressures and oil flow visualization results would therefore yield important evidence of shock location and shock-induced separation. From this correlation, a greater understanding of the effectiveness of the jet flap in reducing separation would be provided. A reduction in flow separation over the wing has a direct bearing on improving buffet characteristics and consequently an evaluation of the jet flap based on standard buffet methods is of interest.

The investigation was therefore initiated with the following objectives:

1. To provide wind tunnel test data of a jet flap at various transonic Mach numbers.
2. To provide information from flow visualization and pressure tests concerning the capability of a jet flap to reduce or eliminate flow separation.

SECTION II

WIND TUNNEL TEST PROGRAM

The purpose of this program was to investigate the feasibility of using a jet flapped airfoil for transonic maneuvering by means of wind tunnel tests. To provide information on jet flap characteristics in the transonic regime for this study, an experimental wind tunnel program was conducted on a two-dimensional unswept wing which included a variable angle jet flap.

This model was tested in the 4T Tunnel at the Arnold Engineering Development Center (AEDC), Tullahoma, Tennessee, in June 1969. The following paragraphs discuss the model design, the test programs, and the data reduction techniques.

AERODYNAMIC DESIGN OF THE MODEL

The airfoil selected for the investigation was NACA 64A406 modified where necessary to permit installation of the jet flap. These modifications were aft of the 62% x/c station and consisted of a gradual thickening of the airfoil up to the 90% x/c location where the airfoil was then truncated. The modified airfoil maximum thickness was 6.6%. See Figure 1 for basic and modified airfoils.

These modifications enabled a satisfactory plenum chamber to be put inside the airfoil permitting a sufficient wall thickness to contain the required plenum pressures. Sufficient material at the trailing edge was also available to give direction to the jet sheet. In the design of the jet nozzle system an attempt was made to produce a configuration which could be representative of fullscale practice. With this in mind a semicircular trailing edge profile with a radial slot was devised providing the necessary direction for the jet.

The test airfoil, the coordinates of which are given in Table I, contained the jet nozzle configurations shown in Figure 2.

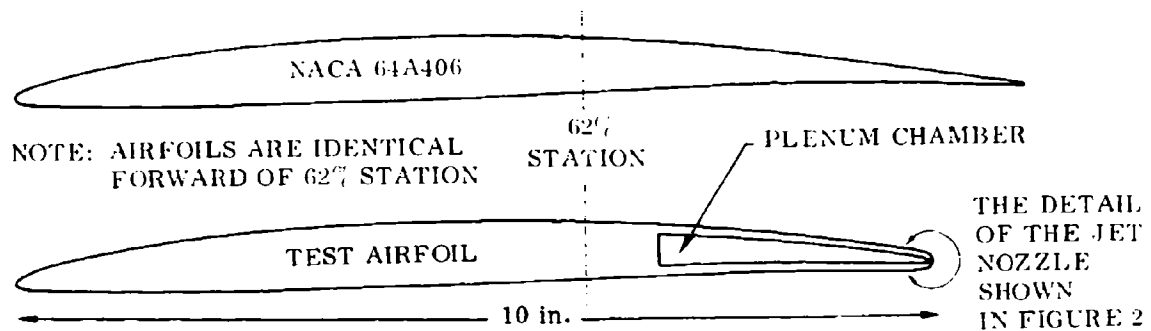


Figure 1. Basic (NACA 64A406) and Modified Airfoils

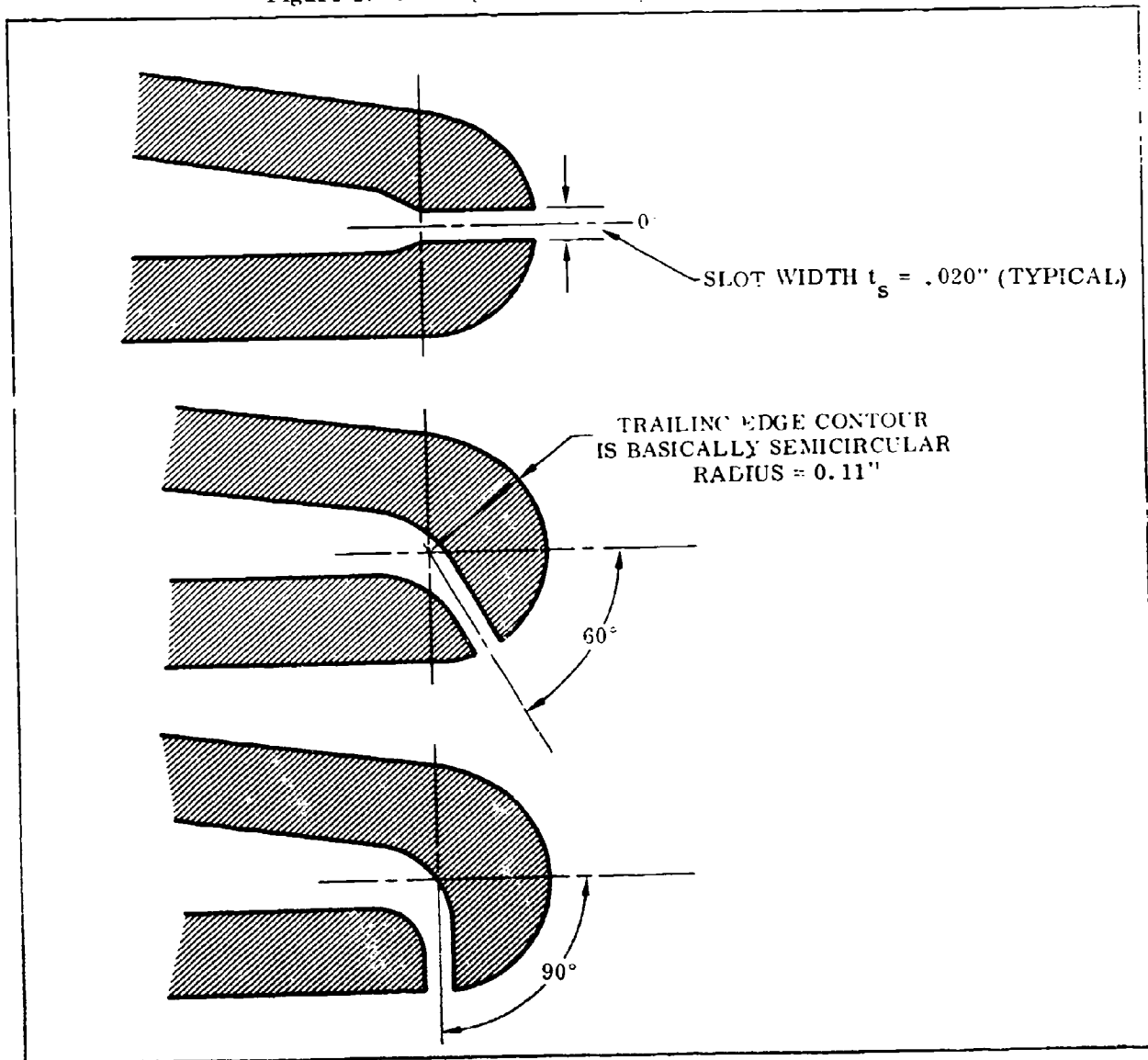


Figure 2. Typical Jet Flap Exit Configurations

TABLE I. JET FLAP AIRFOIL COORDINATES
(MODIFIED NACA 64A406)

| $\% x/c$ | Upper (in.) | Lower (in.) |
|----------|----------------|----------------|
| 0 | .005 | .005 |
| 1.25 | .107 | -.051 |
| 2.5 | .155 | -.063 |
| 3.75 | .192 | -.069 |
| 5.0 | .225 | -.073 |
| 7.5 | .281 | -.077 |
| 10.0 | .329 | -.079 |
| 12.5 | .370 | -.080 |
| 15.0 | .406 | -.080 |
| 20.0 | .468 | -.078 |
| 25.0 | .518 | -.075 |
| 30.0 | .557 | -.070 |
| 35.0 | .586 | -.064 |
| 40.0 | .607 | -.057 |
| 45.0 | .618 | -.048 |
| 50.0 | .619 | -.035 |
| 55.0 | .610 | -.020 |
| 60.0 | .594 | -.004 |
| 65.0 | .575 | .011 |
| 69.0 | .559 | .020 |
| 75.0 | .527 | .026 |
| 80.0 | .490 | .030 |
| 85.0 | .441 | .030 |
| 90.0 | .379 | .024 |
| 95.0 | .304 | .016 |
| 97.0 | .269 | .013 |
| 97.5 | .260 | .012 |
| 99.0 | .232 | .008 |
| 100.0 | .110 | .110 |

MODEL CONSTRUCTION

The model assembly consisted of a steel wing of 10-inch chord and 20-inch span supported by two steel side plates which were connected at the aft end by a cross strut, in a manner similar to the standard Northrop two-dimensional test apparatus described in Reference 2. This complete assembly was attached to the tunnel sting support system.

The wing was built in two parts. The forward portion of 17-4 stainless steel; the aft portion, which was hollow, was electroformed in nickel. This hollow structure was used as a plenum chamber for the jet flap air. A full length slot ran along the trailing edge of the wing. Six different aft portions were constructed, consisting of

the five different jet flap angles and a blank section to provide the basic airfoil data. Surface pressure taps were located at the 50%, 37% and 23.7% y/s stations, and pressure tubes were run from these locations to Scanivalves in the support strut.

The jet flap was supplied with high pressure air from piping run along the out-sides of both side plates. This was then fed into the plenum chamber through fixed orifices, and exhausted through the trailing edge slot.

Figure 3 shows a schematic of the model assembly. Figures 4 and 5 are photographs of the apparatus installed in the AEDC wind tunnel.

INSTRUMENTATION

Test instrumentation consisted of static pressure taps on both upper and lower surfaces of the wing, and a total pressure rake located on the wing center line one model chord behind the wing. The wing static taps were mainly on the center span station ($y/s = 0.5$) with somewhat fewer taps on the $y/s = 0.425$ and $y/s = 0.35$ stations. The rake was of a 16-inch span with the majority of its tubes in the central region.

The model angle of attack was measured locally on the model side plates. Plenum pressures for the jet flap were measured at three different locations in the plenum chamber; an average value was used for setting the required pressure level.

Scanivalves were located in the model support strut and were used to measure the wing and wake rake pressures. An oil supply tube was located at the 7.5% x/c station, and bleed holes at this position permitted a dyed oil to be pumped over the wing surface for flow visualization.

DATA REDUCTION

Data reduction consisted of converting the surface measurements to pressure coefficients and the wake rake pressures to total pressure loss coefficients. The reduced wing data was then integrated over the wing surface to obtain normal, axial lift and drag forces. Integration of the rake pressure coefficients gave the momentum drag coefficient C_d .

A complete description of the data measuring and reduction procedure is given in Reference 3.

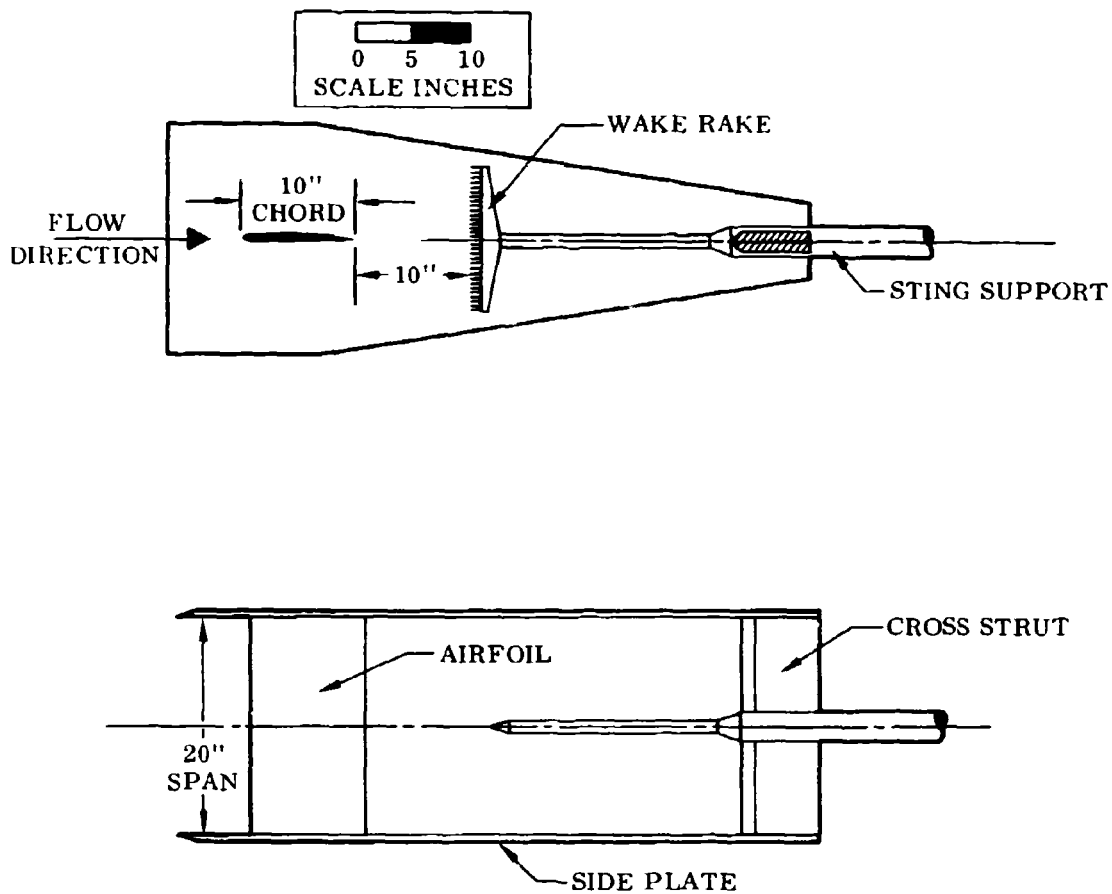


Figure 3. Schematic of Jet Flap Airfoil Installation

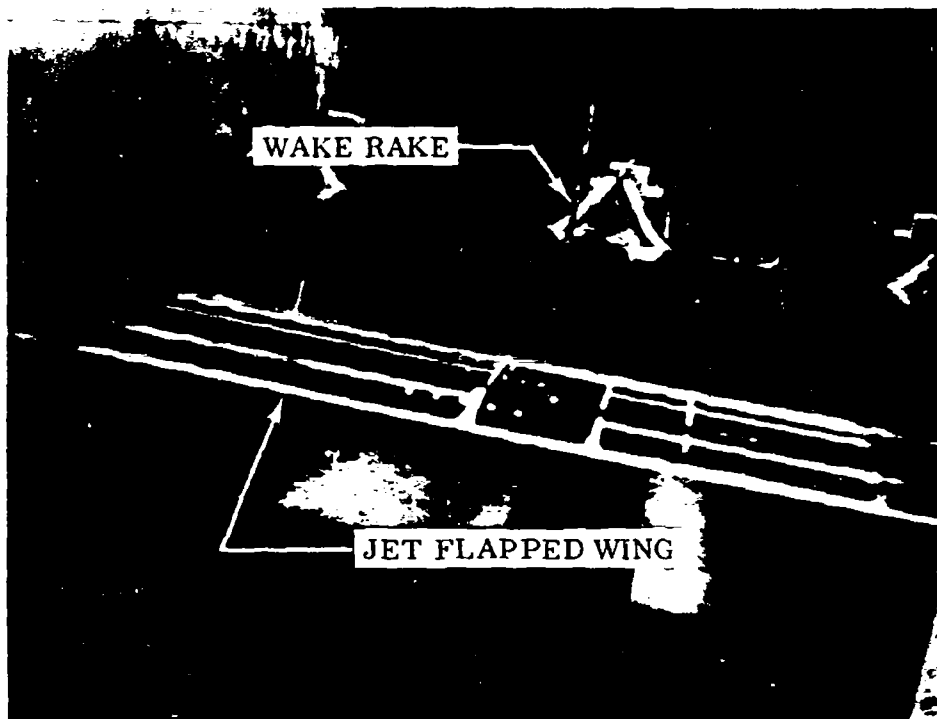


Figure 4. Wing Model with Sting Support and Wake Rake



Figure 5. Jet Flap Model Mounted to Endplates in AEDC Wind Tunnel

VORTEX GENERATORS

A brief study of the effect of adding vortex generators to the airfoil was carried out at the end of the program. The configuration and location of the generators is shown in Figure 6. A series of 6 co-rotating vortex generators equally spaced about the midspan was located at the 12% chord point.

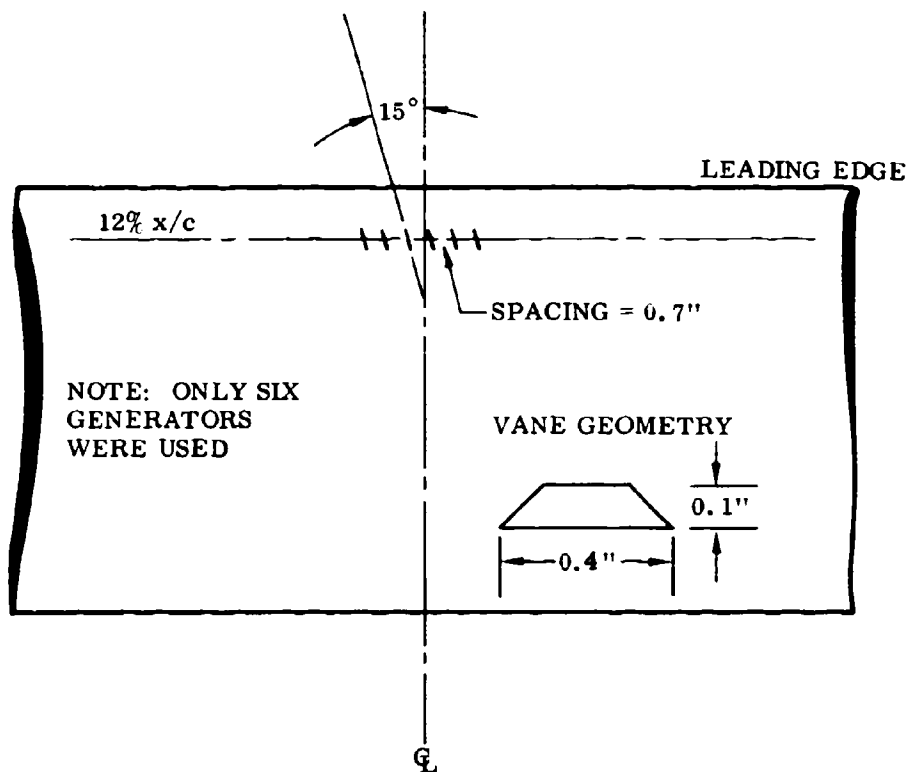
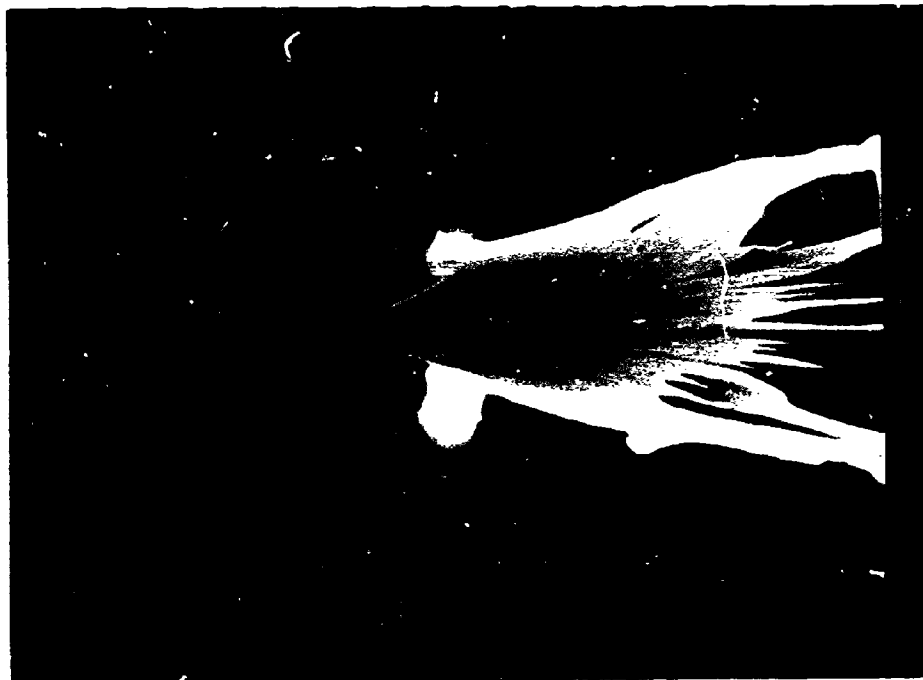


Figure 6. Vortex Generator Installation

STATIC CALIBRATIONS

Static calibrations were performed on the various trailing edge sections to determine the actual jet efflux angle, the efficiency of the jet nozzle, and the static jet reaction for the test range of mass flows.

Jet angles were obtained by first visualizing the jet sheet on a splitter plate coated with fluorescent oil, then measuring the jet angle from a photograph of the plate. A typical oil flow pattern is shown in Figure 7.



6904406

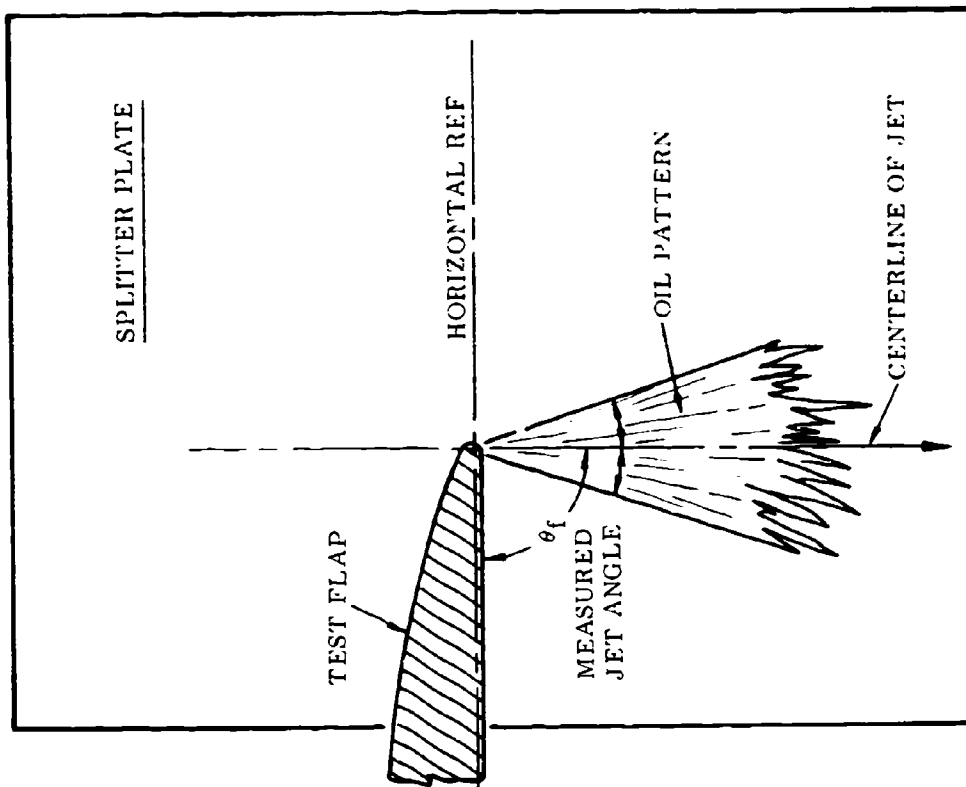


Figure 7. Oil Flow on Splitter Plate (θ_f nominally 90°) at Plenum Pressure = 31.0 psia

The measured jet angles were found to be nominally as designed, at low plenum pressure, with the exception of the $\theta_f = 45^\circ$ jet, which was determined to be 35° . An effect of plenum pressure on jet angle was also noted, the jets tending to "straighten out" as pressure was increased. Because of the similarity to the data for $\theta_f = 30^\circ$, it was decided to present data for just four flap angles. To identify the various flaps the measured flap angles were chosen at 60 psia plenum pressure, and the final angles selected were $\theta_f = 0^\circ, 35^\circ, 55^\circ$ and 88° which corresponded to the design values of $0^\circ, 45^\circ, 60^\circ$ and 90° .

Values of flow coefficient C_n determined from the static tests for the jet nozzles are the ratio of the actual weight flows to the theoretical weight flows, shown in Table II.

TABLE II. EXPERIMENTAL FLOW COEFFICIENTS

| Measured Jet Angle | Flow Coefficient, C_n |
|--------------------|-------------------------|
| 0° | .667 |
| 35° | .754 |
| 55° | .719 |
| 88° | .727 |

Applying the flow coefficient C_n to the basic equation for the momentum coefficient yields the following equation:

$$C_\mu = 1.8 \frac{P_T}{q_0} C_n \left[1 - \left(\frac{P_0}{P_T} \right)^{2/7} \right]^{1/2} \frac{t_s}{c} \quad (1)$$

The air issuing from the jet is assumed to expand isentropically from plenum pressure to sonic velocity at the slot exit and then expand to free stream static pressure.

Static jet reactions at the exit were calculated from the following equation:

$$R_j = m_j V_j + (p_j - p_o) A_j \quad (2)$$

It was assumed that the jet was always choked. Axial and normal reactions are then given by:

$$R_a = R_j \cos \theta_f \quad (3)$$

$$R_n = R_j \sin \theta_f \quad (4)$$

Table III summarizes the static calibration for the five nominal jet angles.

TABLE III. STATIC JET REACTIONS AT PLENUM PRESSURE = 60 psia

| Measured Jet Angle | R_j for $P_T = 60$ psia ($C_\mu = 0.02$ Approx) | R_a | R_n |
|--------------------|---|-------|-------|
| 0° | 13.55 | 13.55 | 0 |
| 35° | 15.25 | 12.48 | 8.74 |
| 55° | 13.05 | 7.48 | 10.68 |
| 88° | 14.25 | 0.495 | 14.25 |

A complete description of this static calibration is given in Reference 4.

WIND TUNNEL TEST CONDITIONS

The tests were carried out in the 4T Tunnel at AEDC, at Mach numbers of 0.7, 0.8, 0.85, 0.9, and 0.95, and for nominal Reynolds numbers of $2.5 \times 10^6/\text{ft}$ and $5.5 \times 10^6/\text{ft}$. The angle of attack range was from zero to that for maximum lift coefficient. Blowing momentum coefficients C_μ ranged from 0 to 0.06.

SECTION III

DISCUSSION OF RESULTS

The data that are presented in this Section have been organized to illustrate, first, the primary effects of the jet flap on airfoil characteristics which, in turn, include the effects of the varying amounts of blowing momentum and the effects of jet angle. Next, data comparisons are presented showing the effects of Mach number, vortex generators, and Reynolds number on airfoil characteristics with jet on and jet off. Finally, there is a comparison of basic and modified airfoils, thrust recovery and residual drag characteristics, buffet onset methods, and shock variations. An analysis of the trends established by the data in each case is also presented.

EFFECT OF BLOWING MOMENTUM ON LONGITUDINAL CHARACTERISTICS, $\theta_f = 88^\circ$

The longitudinal characteristics shown in Figures A-1 through A-5 of the Appendix illustrate the effects of various blowing momentum rates on lift, drag, and pitching moment at Mach numbers of 0.7, 0.8, 0.85, 0.90, and 0.95. The data are also compared to the jet off case for a jet angle of 88° .

Large increments of lift occurred tending to increase slightly with an increase in angle of attack. In Figure A1, for a $C_\mu = 0.029$, for example, a maximum lift increment of 0.44 is obtained at $\alpha = 11^\circ$, and the corresponding maximum lift coefficient developed at this condition is 1.51. Associated drag and pitching moment increments are $\Delta C_d = 0.01$ and $\Delta C_m = -0.17$.

A comparison of lift, drag, and moment increments at other Mach numbers is shown in Table IV.

It is evident in comparing the effects at various C_μ that there is some inconsistency in the variation of lift increment with C_μ at 0.70 Mach number. A cross plot of lift indicates that the data at $C_\mu = 0.015$ appear to be low when compared to the trends established at other jet angles. (Such trends are compared with low speed theory in a later discussion.) At $M = 0.80$, Figure A-2, the lift increments decrease with increasing C_μ and are more consistent with trends from low speed theory by Spence,

TABLE IV. COMPARISON OF LONGITUDINAL CHARACTERISTICS AT
MAXIMUM ANGLE OF ATTACK, $\theta_f = 88^\circ$

| M | $^a C_{l_{\max}}$ | $C_{l_{\max}}$ | $\Delta C_{l_{\max}}$ | C_μ | ΔC_d | ΔC_m |
|-----|-------------------|----------------|-----------------------|---------|--------------|--------------|
| .70 | 11° | 1.51 | 0.44 | .029 | 0.01 | -0.17 |
| .80 | 13° | 1.22 | 0.25 | .022 | 0.04 | -0.10 |
| .85 | 13° | 1.15 | 0.27 | .029 | * | -0.10 |
| .90 | 13° | 1.28 | 0.31 | .029 | * | -0.10 |
| .95 | 13^{**} | 1.28 | 0.21 | .029 | * | -0.10 |

Note: *Drag increment erroneous due to wake rake measurement limitation at high α .

**Maximum angle limited by model installation.

Reference 5, except at $C_\mu = 0.022$ and 0.029 . The effectiveness of the higher C_μ does show slight improvement at higher angles of attack. A definite break in the lift curve slope occurs at $\alpha = 6^\circ$ for jet off, due to a shock which forms in the vicinity of midchord. With jet on, a slight reduction in lift curve slope and C_l vs α break may be noted. At $M = 0.85$, in Figure A-3, the lift curve breaks at $\alpha \approx 4^\circ$ at all values of C_μ . Again, there is little difference in the data at $C_\mu = 0.022$ and 0.029 except at the higher angles of attack. At $M = 0.90$ the lift curve slopes reduce slightly for all blowing (jet on) rates.

The lift curve breaks at an angle of attack of 2° at this Mach number ($= 0.90$). For angles of attack above 8° , the drag is not accurate since the wake rake was not long enough to measure the total momentum change existing in the flow field above the rake. This condition also exists at $M = 0.95$ above an angle of attack of 6° .

The data for $M = 0.95$ are presented in Figure A-5, showing that the blowing momentum has a much smaller effect on lift increments, which is not the case at lower Mach numbers. Lift curve break occurs between 0° and 1° angle of attack. The curve in Figure 8 illustrates the decreasing lift increment with Mach number. As presented, lift increment is actually C_{l_f} , the supercirculation lift where:

$$C_{l_f} = C_l - C_{l_{C_\mu=0}} - C_\mu \sin(\theta_f + \alpha) \quad (5)$$

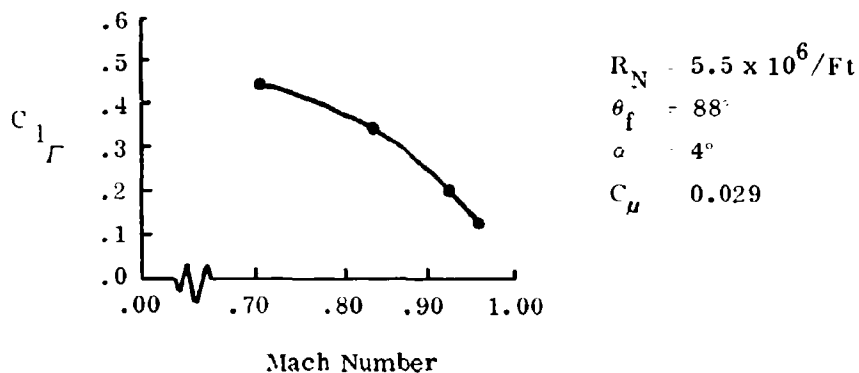


Figure 8. Variation of Jet Circulation Lift Coefficient with Mach Number.

It should be mentioned that the lift and moment data presented in the figures of the Appendix do not include the direct effects contributed by jet force such as the components $\Delta C_l = C_\mu \sin(\theta_f + \alpha)$ and $\Delta C_m = -3/4 c C_\mu \sin \theta_f$

EFFECT OF BLOWING MOMENTUM ON PRESSURE DISTRIBUTIONS, $\theta_f = 88^\circ$

The pressure distributions associated with the longitudinal characteristics which have been presented provide a good insight of the effects of blowing. In Figure A-6, pressure distributions are compared at $M = 0.70$ at an angle of attack of 8° . It is apparent that blowing influences pressures over the entire wing, particularly in the region between $x/c = 0.2$ and 0.4 on the upper surface and between $x/c = 0.7$ and 1.0 on both upper and lower surfaces. In the first case, a shock located at $x/c = 0.2$ is shifted to $x/c = 0.35$ for a $C_\mu = 0.029$ and in the second case large increments in negative and positive pressure are developed on upper and lower surfaces, respectively, near the trailing edge.

It should be noted that although a shock forms, separation does not occur as shown by subsonic pressure recovery aft of the shock. With blowing, lower pressures aft of the shock are still subsonic and flow remains attached. The pressure distribution near the trailing edge gives the appearance of separated flow, but this is not the case since the characteristic of the jet flap is to accelerate flow which results in lower pressure at the trailing edge. Additionally, oil flow visualization show attached flow over the entire upper surface at this Mach number. At $M = 0.80$, the effect of blowing on surface pressures is reduced somewhat as shown in Figure A-7. Separation has occurred from approximately 60% chord aft. With jet on, a rearward shift in shock

location of approximately $\Delta x/c = 0.06$ for $C_\mu = 0.029$ is shown. The flow on the upper surface aft of the shock is supersonic for the jet off case, and with a thicker boundary layer, flow separation develops. At higher Mach numbers, increased separation due to thicker boundary layers results as the pressure rise aft of the shock falls increasingly short of sonic pressure levels. These characteristics are shown in Figures A-8 and A-9. In both cases, blowing has a stronger influence on shifting shocks aft and reducing separated flow regions because of flow entrainment by the jet. For example, separation can be assumed to be shifted from $x/c = 0.6$ to 0.8 at $M = 0.85$ and from $x/c = 0.77$ to $x/c = 0.92$ at $M = 0.90$. A correlation of flow visualization photos with pressure distributions for jet on and jet off relative to separation location is described at the end of this section. At $M = 0.95$, in Figure A-10, the shock develops at approximately $x/c = 0.98$. Blowing eliminates separation over the remaining 2% as the flow accelerates around the trailing edge. It is of interest to note that at $M = 0.95$ the upper surface pressures are unaffected by blowing and that the increase in lower surface pressures provides about all of the lift increment developed at this condition.

EFFECT OF JET FLAP ANGLE

A plot comparing the effect of jet flap angle is presented in Figure A-11. The data shown are the longitudinal characteristics for jet angles of 0° , 35° , 55° , and 88° at $M = 0.90$ and $C_\mu = 0.015$. It is apparent that maximum lift improvement is obtained at $\theta_f = 88^\circ$ and that there is slight difference between the data at $\theta_f = 35^\circ$ and $\theta_f = 55^\circ$. Evidently a similarity in the effective jet angle exists for these cases. Drag is lowest for $\theta_f = 35^\circ$ over the C_l vs α range but between $C_l = 0.50$ and 0.90 drag differences are negligible for all θ_f . Pitching moment is increasingly negative with jet angle. The increment between $\theta_f = 0^\circ$ and $\theta_f = 88^\circ$ remaining constant at $\Delta C_m = -0.10$.

The pressure distributions over the wing for angles of 0° , 55° , and 88° are presented in Figure A-12. The data have been compared for an angle of attack of 8° . The comparison indicates that surface pressures for the angles of 0° and 55° are similar, a phenomenon which is peculiar to this Mach condition. Most noteworthy is the shift in shock on the upper surface from $x/c = 0.60$ to $x/c = 0.80$ for $\theta_f = 88^\circ$ and the large positive pressure increase on the lower surface.

To summarize the effects on lift coefficient of jet flap angle and blowing rate, Figure A-13 has been prepared. Here the lift C_{l_f} at $\alpha = 0^\circ$ has been plotted as a function of blowing momentum coefficient C_μ for the range of Mach numbers and jet

flap angles of 0° , 35° , 55° , and 88° . The dashed curve represents the lift obtained from Spence's incompressible theory (Reference 5) and is shown for comparison purposes.

A jet flap angle of 88° is seen to produce the maximum effect, which occurs at a C_μ value of around 0.025. Increasing C_μ beyond this value slightly decreases $C_{l\Gamma}$ at $\theta_f = 88^\circ$. A jet flap angle of 0° produces a slightly negative lift increment, which can be attributed to the slight uncambering effect due to the jet at zero degrees. Improvement in $C_{l\Gamma}$ above $\theta_f = 0^\circ$ at the intermediate jet angles may be observed. The data for $\theta_f = 55^\circ$ are higher than those for $\theta_f = 35^\circ$ although perhaps not quite as high as should be expected when compared to low speed theory.

The non-linear trend of $C_{l\Gamma}$ with C_μ is a characteristic of the jet flap as its effect progresses from boundary layer control to supercirculation. With increased blowing the "effective jet flap angle" increases, but in smaller increments.

As Figure 9 shows, this "effective flap angle" is representative of the initial curvature of the jet sheet for transonic flow conditions. The curvature of the jet sheet increases less rapidly with increasing C_μ . These curves were calculated from a modification of theory in Reference 6.

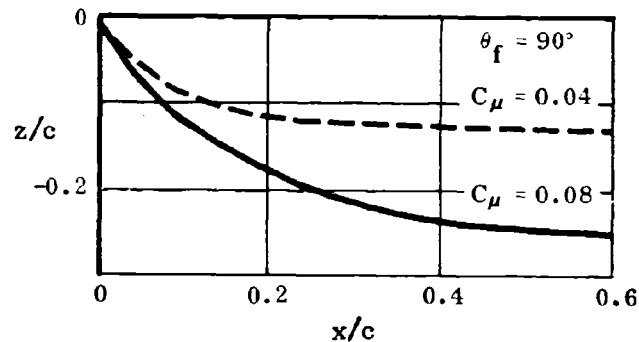


Figure 9. Jet Sheet Trajectories

A method which illustrates the magnitude of lift improvement resulting from jet flap effects can be developed by using the incompressible theory of Reference 5, and the definition of lift efficiency such that

$$E_L = \frac{[C_\mu^{1/2} + 0.325 C_\mu + 0.156 C_\mu^{3/2}] \theta_f}{C_\mu \sin \theta_f} = \frac{C_{l\Gamma}}{C_\mu \sin \theta_f} \quad (6)$$

which for small angles reduces to relatively constant values at low jet angles. This is shown in Figure 10 for various values of C_μ . It may be observed that above $\theta_f = 30^\circ$, values of E_L increase rapidly. Data from the present test at $M = 0.70$ at $C_\mu = 0.015$ show good agreement with the trends established by low speed theory. A further discussion of lift efficiency with Mach number is presented later in the text.

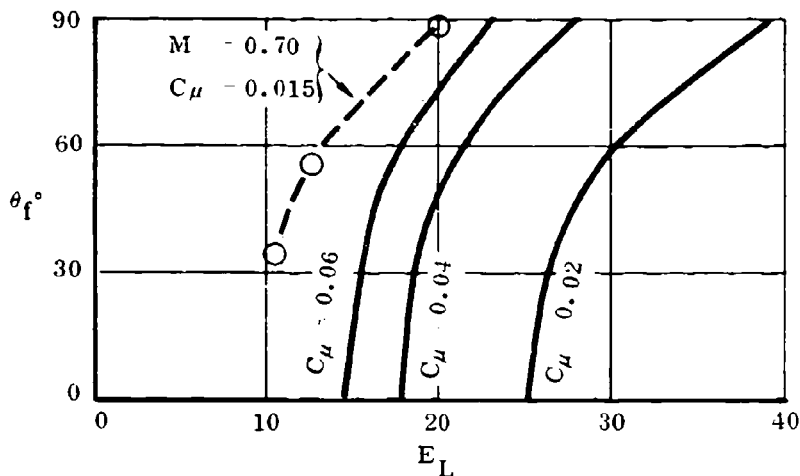


Figure 10. Incompressible Values of E_L

A summary of drag characteristics as a function of blowing momentum C_μ for jet angles of 0° , 55° , and 88° are shown in Figures A-14, A-15, and A-16. The data are presented for lift coefficients of 0.4, 0.6, and 0.80. In Figure A-14, the trends show decreasing drag as C_μ is increased such that at $\theta_f = 0^\circ$ and 55° drag is zero at approximately $C_\mu = 0.03$. For $\theta_f = 88^\circ$, drag increases from $C_\mu = 0$ to 0.007 and then tends to decrease and reach a level at $C_\mu = 0.029$ which approximates that for $C_\mu = 0$. At $M = 0.85$, in Figure A-15, similar trends are shown although the levels of drag are considerably higher than in Figure A-14, and there are larger incremental drag differences between the lift curves. However, at $\theta_f = 88^\circ$, there is much less spread in the drag data for the same lift coefficients. In Figure A-16, the drag data for $M = 0.95$ are shown; in this case the variation of drag with C_μ and drag level are similar for all three jet angles.

EFFECT OF MACH NUMBER

The variation of longitudinal characteristics with Mach number for $\theta_f = 88^\circ$ is presented in Figures A-17 through A-20. Figure A-17 shows the effect of compressibility which results in lift rising to peak values at $M = 0.85$ at angles of attack of 0° , 2° , and 4° . For higher angles of attack, peak lift values occur at $M = 0.80$. With blowing at $C_\mu = 0.022$, the level of lift over the entire Mach range is increased at all

angles of attack as shown in Figure A-18. However, the peak values of lift at angles of attack of 0° , 2° , and 4° are shown to occur at $M = 0.80$. Figure A-19 shows that the corresponding drag coefficients begin to rise at $M = 0.80$ at the lower angles of attack, while at the higher angles drag rise appears to occur between 0.70 and 0.80 Mach number. There is no apparent change in the Mach number for drag rise as a result of blowing as shown in Figure A-19, but at the lower angles of attack drag is held relatively constant. At the higher angles, $\alpha = 8^\circ$, drag increases over the no blowing case. But this might be expected since the jet thrust at these high angles has a forward component.

Figure A-20 shows that pitching moment increased negatively as Mach number increases for all angles of attack. This is caused by (1) higher pressures aft of the quarter chord, (2) a rearward shift of shock, and (3) the associated separation which develops aft of the shock on the wing upper surface. With blowing, there is a large increase in negative pitching moment. This is shown in Figure A-20, where at $M = 0.70$ compared with the no blowing case, the negative pitching moment increment is approximately -0.15 . Beyond a Mach number of 0.80 pitching moment increments diminish, since upper surface pressures forward of the shock remain relatively unaffected by jet flap blowing, and thus do not contribute to positive lift (negative moment) between the quarter chord point and the rear shock. As the shock moves further rearward at the higher Mach numbers, this effect is more apparent. Figure 11 shows this comparison.

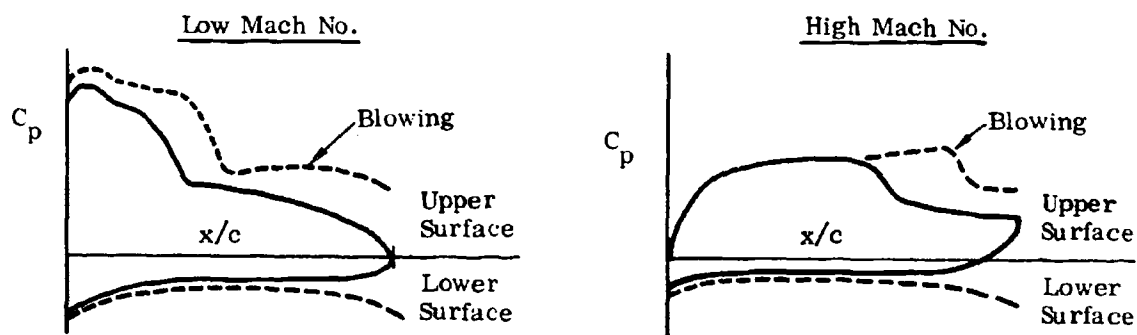


Figure 11. Comparison of Blowing at Low and High Mach Numbers

As a consequence, the pitching moment variation with Mach number in Figure A-20 for $M > 0.80$ remains relatively constant except at the higher angles of attack.

Lift efficiency E_L , as a function of Mach number, is shown in Figure A-21. In this figure, the lift efficiency E_L is plotted for jet flap angles of 35° , 55° , and 88° as obtained from data in Figure A-13. The trends show decreased efficiency at Mach numbers higher than 0.80. Lift efficiency improves significantly as the jet angle is increased to $\theta_f = 88^\circ$. It also may be noted that lift efficiency tends to be higher for the lower values of C_μ . It should be pointed out that although there is a reduction in lift efficiency with the higher value of C_μ jet induced circulation lift increases. Table V below shows this comparison.

TABLE V. EFFECT OF C_μ ON LIFT EFFICIENCY AND CIRCULATION LIFT

| $M = 0.8, \quad \alpha = 0^\circ, \quad R_N = 5.5 \times 10^6 / \text{FT}$ | | | |
|--|---------|-------|-----------|
| θ_f | C_μ | E_L | C_{l_f} |
| 55° | 0.015 | 11.5 | 0.14 |
| | 0.029 | 8.5 | 0.20 |
| 88° | 0.015 | 22.5 | 0.33 |
| | 0.029 | 14.5 | 0.42 |

A similar Mach number effect has been observed in other tests. Data from one of these is shown in Figure 12 compared to the test data. The airfoils were similar but not identical. However, good agreement is shown.

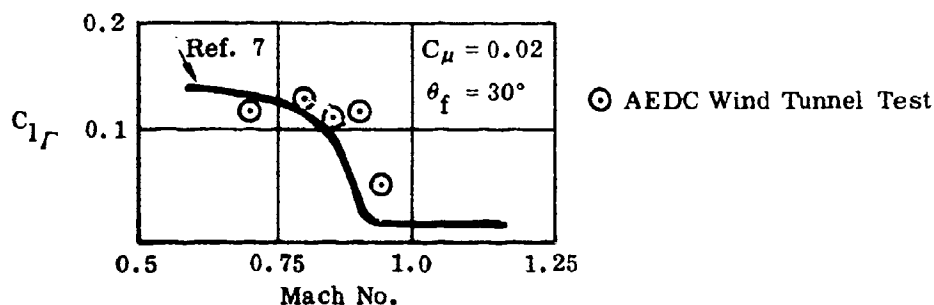


Figure 12. Effect of Mach Number on Lift Coefficient

EFFECT OF VORTEX GENERATORS

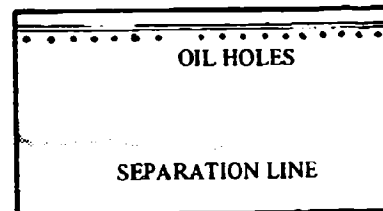
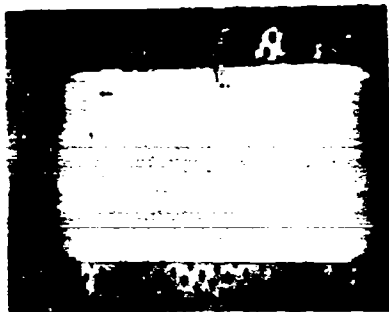
A brief series of runs were made during this test program to assess the effects of adding vortex generators to the jet flapped wing. Six generators were located on the 12% chord line and were evenly spaced around the 50% span station. Details of the installation are shown on Figure 6.

Longitudinal characteristics, with and without vortex generators, are shown on Figures A-22 to A-24 for three different Mach numbers. The effect of adding the generators is to delay separation, especially at the higher Mach numbers and angles of attack. A similar trend is shown when blowing is added. Figure A-25 illustrates more of the actual effects of the vortex generators, in terms of the chordwise pressure distributions. Addition of the vortex generators produces a rearward shock movement of $0.15 x/c$ for both jet flap on and off, and this is then equivalent to a ΔC_l of ~ 0.1 . The jet flap alone for a C_{μ} of 0.029 produces a slightly greater shock movement, but produces a ΔC_l of 0.32. Figure A-25 shows that the changes on the lower surface conditions make up the differences between these lift increments. The shock movement is also illustrated on Figure 13. These photos are excerpts from color movie films taken during the program of oil flowing over the wing surface. The rearward shift of separation with the addition of vortex generators is seen to be identical to that shown on the pressure distribution plot.

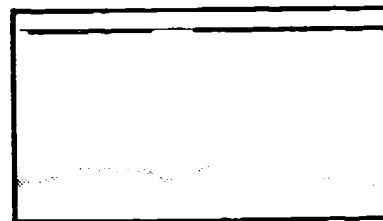
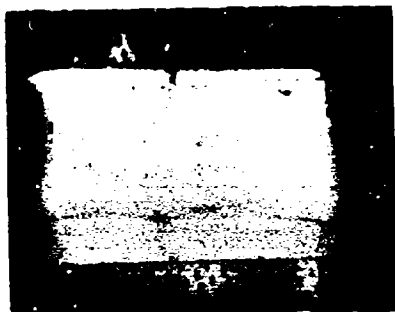
EFFECT OF REYNOLDS NUMBER

The effects of Reynolds number on longitudinal characteristics at Mach numbers from 0.7 to 0.95 are shown in Figures A-26 through A-30. The two Reynolds numbers compared are $2.5 \times 10^6/\text{ft}$ and $5.5 \times 10^6/\text{ft}$ in Figures A-26 and A-27. Data including a third Reynolds number of $6.5 \times 10^6/\text{ft}$ are shown in Figures A-28, A-29, and A-30.

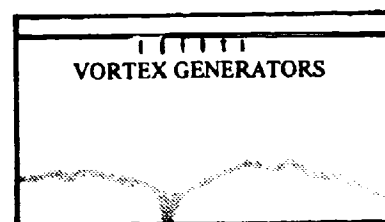
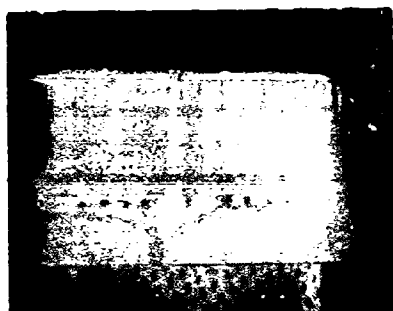
The comparison in Figure A-26 shows that at $R_N = 2.5 \times 10^6/\text{ft}$ there is a slight increase in lift at maximum angle of attack and a lower drag. These effects become more pronounced at $M = 0.80$ in Figure A-27 and at $M = 0.85$ in Figure A-28. Lift data at a Reynolds number of 6.5×10^6 in Figure A-28 fall between data for the other cases. Drag is highest for $R_N = 5.5 \times 10^6/\text{ft}$ while pitching moment changes are negligible at low lift and become slightly less negative at high lift at this Reynolds number. At $M = 0.90$ and $M = 0.95$, in Figures A-29 and A-30, Reynolds number effects exhibit similar trends as at the lower Mach numbers, but the increments are smaller particularly at the higher angles of attack.



(a) BASIC WING



(b) BLOWING, $C_{\mu} = .015$



(c) BLOWING, $C_{\mu} = .015$
PLUS VORTEX GENERATORS

Figure 13. Oil Flow Visualization, at $M = 0.85$, $\alpha = 8^\circ$, $\theta_f = 88^\circ$

In order to provide some insight into the behavior of the longitudinal characteristics with Reynolds number, pressure distribution plots have been prepared in Figures A-31 through A-34. In Figure A-31 for $M = 0.80$ and $R_N = 5.5 \times 10^6/\text{ft}$ it is seen that a shock occurs earlier on the airfoil at approximately $x/c = 0.45$ and this is accompanied by shock induced separation. At the lower Reynolds number a shock develops at about $x/c = 0.55$, but does not cause separation. In Figure A-32 at $M = 0.85$, flow separation occurs at all three Reynolds numbers with a shock forming earliest at $x/c = 0.50$ for $R_N = 5.5 \times 10^6/\text{ft}$. A similar situation is shown in Figure A-33 where the pressure distributions for $R_N = 2.5 \times 6.5 \times 10^6/\text{ft}$ are in close agreement. At $M = 0.95$ in Figure A-34, Reynolds number effects are negligible.

Since the tests were conducted under free transition conditions, the preceding variations with Reynolds number may be explained as follows. As Reynolds number increases, for example, from 2.5 to $5.5 \times 10^6/\text{ft}$, transition moves forward. Since the rate of boundary layer growth is greater for a turbulent boundary layer than a laminar one, the displacement thickness at a given point may be larger than for a lower Reynolds number as shown in Figure 14. As Reynolds number increases further, the transition point moves forward until its location remains fixed near the leading edge. The displacement thickness δ^* decreases with further increase in Reynolds number. As a consequence, it is seen in Figure 15 that for free transition the shock location x/c is aft at the low Reynolds number as at (A) and then proceeds forward as at (B). With increasing Reynolds number the shock moves aft as at (C).

EVALUATION OF THRUST RECOVERY AND RESIDUAL DRAG

Thrust Recovery

Reference 8 defines thrust recovery as the reduction by jet flap action, at a fixed lift, of the drag which the unblown wing would experience if it could attain that lift in the absence of flow separation. This definition was developed for low speed analysis, but it is applicable to the present analysis if "flow separation" is taken to mean "shock induced separation." To provide a physical meaning of thrust recovery, however, it is better expressed as the ratio between the drag reduction defined as above, and the blowing momentum coefficient, as shown in Figure 16.

$$\text{Thrust recovery } \eta_T = \frac{C_d' - C_d}{C_\mu} \quad (7)$$

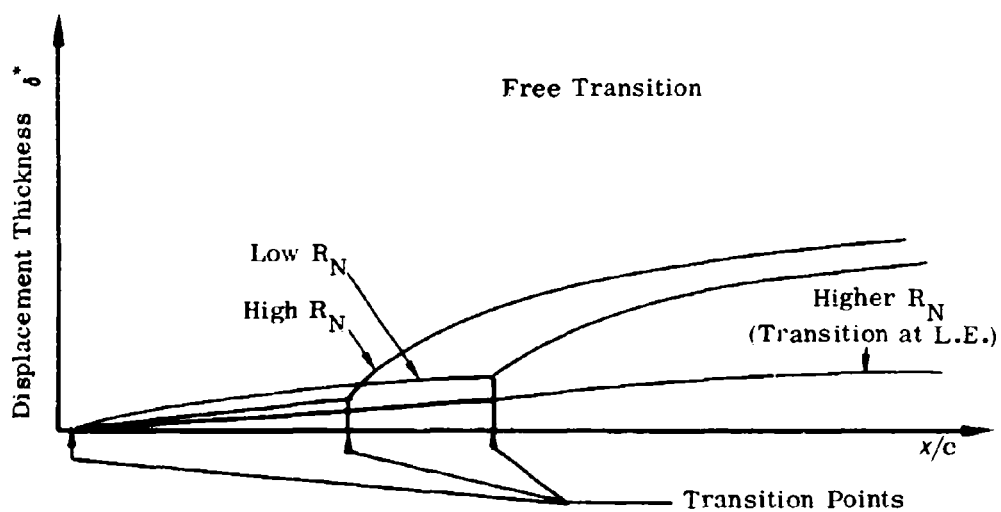


Figure 14. Effect of Reynolds Number on Displacement Thickness

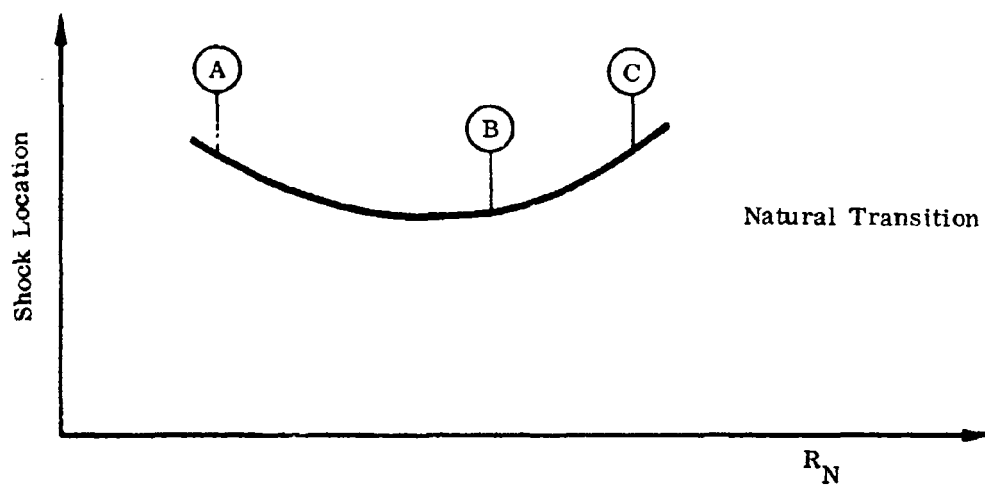


Figure 15. Variation of Shock Location with Reynolds Number

Note that the thrust is more realistically defined as C_μ rather than $C_\mu \cos(\theta_f + \alpha)$. The ideal is therefore $\eta_T = 100\%$ i. e., all the blowing momentum is recovered as thrust.

To obtain values of η_T we first have to define the unseparated drag polar for the unblown basic wing. This is done by assuming the drag can be represented by the equation

$$C'_d = C_{d_0} + KC_1^2 \quad (8)$$

One set of values for C_{d_0} and K were obtained by plotting all the unseparated data as C'_d versus C_1^2 and drawing a straight line through the points. The following equation best represented the data

$$C'_d = 0.026 + 0.058C_1^2 \quad (9)$$

Experimental values of thrust recovery were obtained using equation (7), where C_d was calculated for equation (9).

Figures A-35, A-36, and A-37 show the values of η_T obtained at $M = 0.85$ for values of $\theta_f = 0^\circ, 55^\circ$, and 88° . It might be expected that the thrust recovery would be proportional to the initial jet angle; however, the results show that $\eta_T = 100\%$ is obtained at all jet angles for some angle-of-attack values. Measuring techniques limit the accuracy of thrust recovery calculations at low angles of attack.

The $\theta_f = 88^\circ$ data show that 100% thrust recovery can be obtained with large jet angles, the jet apparently turning quickly after leaving the slot into the thrust direction with very little loss of momentum. Some values of η_T over 100% were obtained. They are thought to be associated again with (1) slight measuring inaccuracies and, (2) slight errors in using a common $C_d - C_1$ polar to describe the basic wing characteristics.

Residual Drag

Residual drag is defined as the difference in drag at fixed lift between the total drag with blowing and the drag due to lift of the unblown wing. Figure 16 illustrates this definition, and the data on Figures A-35, A-36, and A-37 show residual drag numbers for three jet angles $0^\circ, 55^\circ$, and 88° at a Mach number of 0.85.

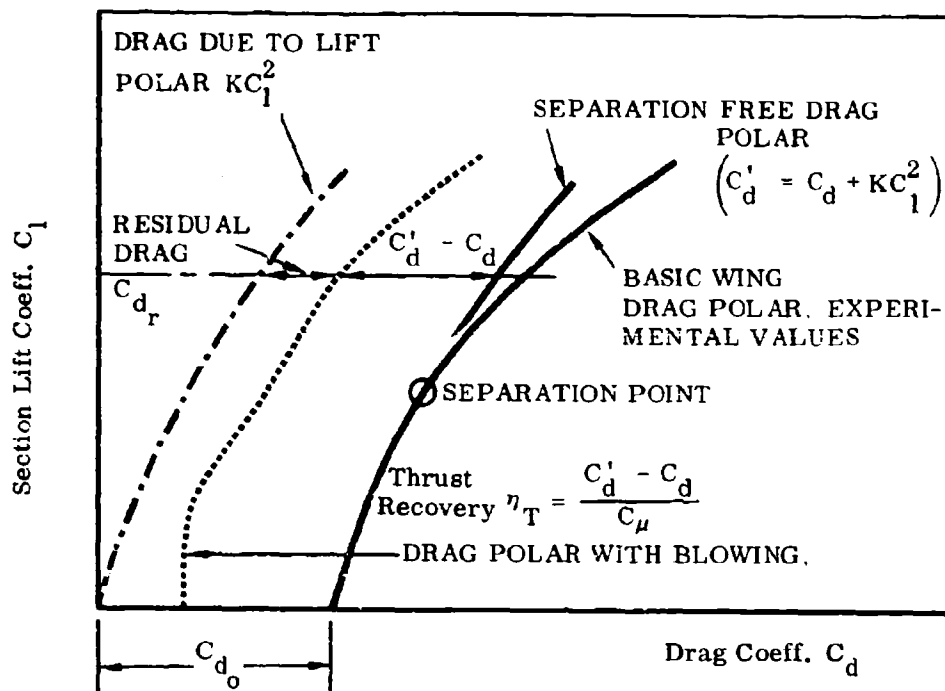


Figure 16. Definition of Thrust Recovery and Residual Drag

BUFFET ONSET ANALYSIS

There are several methods which can be used to determine buffet onset, and of these, six methods based on static force measurements have been applied. The methods include the following:

- | | |
|--------------------------------------|----------------------------|
| 1. Lift curve break | C_l vs α |
| 2. Trailing edge pressure divergence | $C_{p_{T.E.}}$ vs α |
| 3. Trailing edge pressure divergence | $C_{p_{T.E.}}$ vs Mach No. |
| 4. Lift peak Mach number | C_l vs Mach No. |
| 5. Axial force break | C_a vs α |
| 6. Drag due to lift break | C_l^2 vs C_d |

Buffet onset according to these methods is assumed to occur at particular points on curves of the above characteristics, as illustrated in Figure 17.

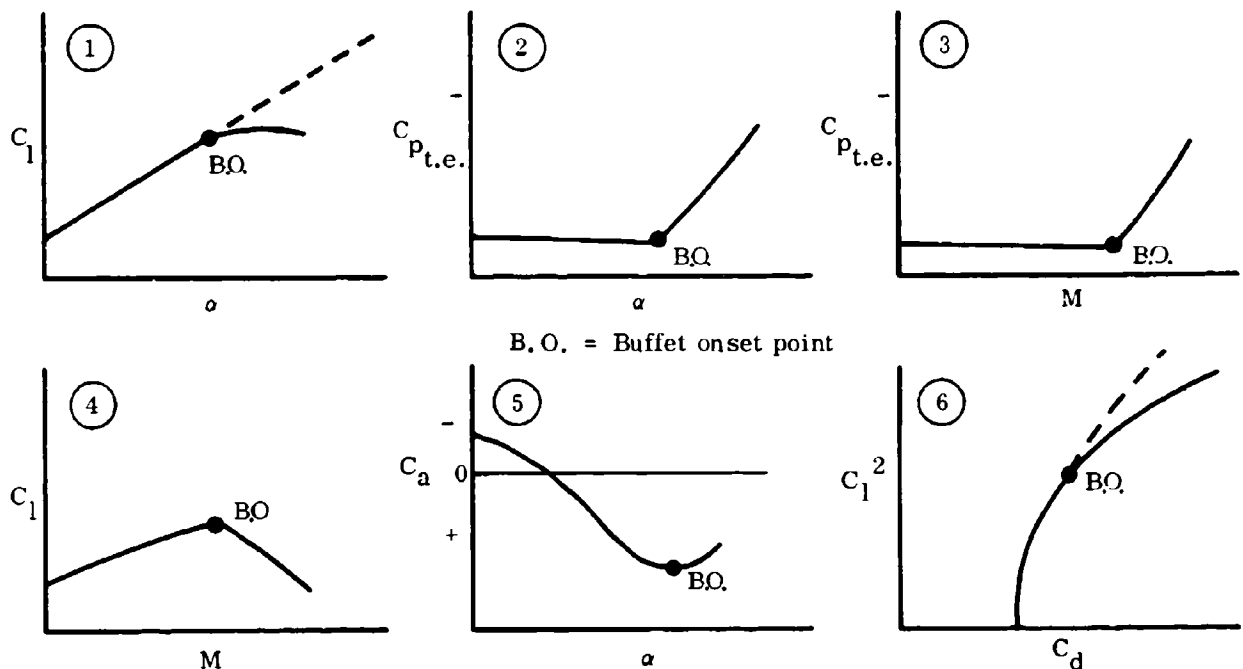


Figure 17. Buffet Onset Methods

From curves such as these, buffet onset data were derived; they are presented in Figure A-38. The data exhibit a fair amount of scatter, as is to be expected. In order to obtain a relative comparison between blowing and no blowing, an upperbound curve was fitted to the data. It is evident from this that blowing has a significant effect in raising the buffet boundary.

SHOCK LOCATIONS AND SEPARATION

Shock waves begin to appear on the upper surface of the wing at the low Mach numbers at high angles of attack. As the Mach number increases, these waves become a part of the upper surface flow field at all conditions. As the free stream Mach number continues to increase, the shock wave becomes stronger until the pressure rise through this shock becomes sufficient to cause the flow to separate locally from the surface. Further increases in Mach number increase the size of this separation bubble until it covers the complete region between the shock and the wing trailing edge, as shown in Figure 18.(a). The flow is then completely separated and buffeting begins.

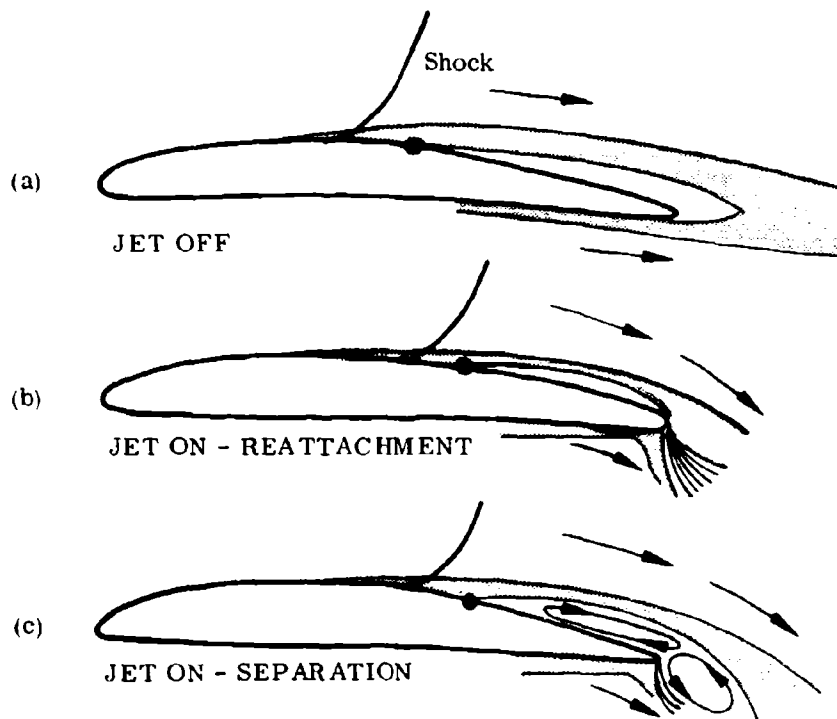


Figure 18. Flow Pattern Comparison

The location of the shock at any given time is such that its pressure rise and the other pressure changes occurring around the wing are in balance. Without the jet flap these pressure fields include the lower surface boundary layer, but with the jet flap a different balance can be reached as the jet flap effectively separates the upper and lower wing surfaces. Thus, we can expect a shift of the shock wave location when the jet flap is operating. As result of higher velocities over the upper surface of the wing with the jet on, it may be assumed that the boundary layer would be thinner and the shock would be shifted to a point downstream. As has been observed from oil flow visualization, even when there is a shift in shock, separation can still occur on the upper surface. Two possible flow patterns associated with flow separation may be assumed. One is the separation of the flow over the upper surface aft of the shock and then its reattachment at the trailing edge, as shown in Figure 18(b). The other is the separation of the flow over the entire wing aft of the shock, as illustrated in Figure 18(c). In this case, a certain degree of vorticity could exist in the separated flow region. The data shown previously in Figure A-12 indicate that the shock movement depends on the degree of flap deflection such that the $\theta_f = 0^\circ$ flap produces the smallest shock displacement and the maximum changes occur with the $\theta_f = 88^\circ$ flap. The effect is therefore proportional to the degree of super circulation effect of the jet flap.

Figure A-39 compares estimated shock locations for the basic 64A406 wing, and the modified wing with jet off and jet on. This figure shows the changes for a blowing rate of $C_{\mu} = 0.015$ at all test Mach numbers and a jet flap angle $\theta_f = 88^\circ$. It can be seen that there is a progressive rearward movement of the shock first with the modified airfoil jet off and then with jet on.

The effect of moving the shock rearwards is considered beneficial in reducing buffet intensity. Although no measurements were made during this test of buffet strength, the reduction of the separated area can be said qualitatively to be advantageous. The comparative plot in Figure A-40 shows the upper surface pressure variation for three conditions, namely, 1) jet off, 2) jet on $C_{\mu} = 0.015$, and 3) jet on $C_{\mu} = 0.015$ with vortex generators. The results clearly show the large shock movement with the application of successive boundary layer control. A maximum shift of $30\% x/c$ occurs at $M = 0.85$, $\alpha = 8^\circ$ for a jet angle of 88° . The approximate separation locations are also shown and are based on flow visualization photographs as presented in Figure 13. The shock locations from pressure measurements shown on Figure A-40 were defined according to Figure 19. The pressures were obtained at the 50% span station.

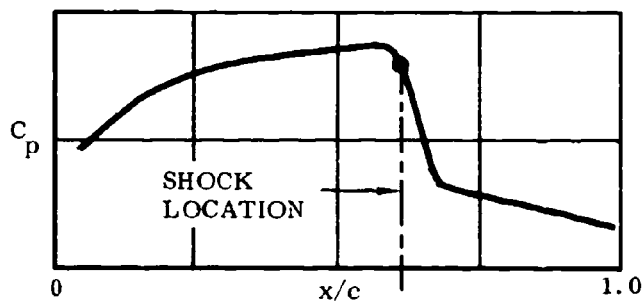


Figure 19. Definition of Shock Location

Other measuring stations occasionally indicated a slightly different shock location, but for consistency only the 50% span data were used. This variation in shock location is associated with local Mach number gradients over the airfoil. If the local Mach number variations are small, then large shock wave variations are to be expected for small changes in local conditions. The test airfoil has gentle pressure gradient, and therefore some variation in shock location is to be expected. Evidence of this variation is shown later in Figure A-43 where the midspan pressures were different from those obtained at other spanwise locations.

COMPARISON OF TEST AIRFOIL WITH NACA 64A406

Although the main purpose of this study was concerned with determining incremental effects (i. e., the effect of a jet flap of various strengths and directions on a given airfoil), it is of interest to compare the performance of the test airfoil with the basic NACA 64A406 airfoil (Reference 10). The test airfoil was thicker aft of the 65% chord and had a blunt trailing edge. Both of these modifications had a noticeable effect on drag rise and separation effects. Blunting can, without too much of a drag penalty, be very helpful in increasing the transonic drag rise Mach Number M_{DD} , as shown in Reference 11.

Additionally, blunting the trailing edge reduced the camber on the test airfoil, compared to the original, and therefore, an effective "nose down" attitude resulted. This effect may be noted, for example, in considering the shift in the angle of zero lift on Figure A-41. This figure shows the lift and drag coefficients for both airfoils at $M = 0.8$ and 0.85 . There is also a basic difference in Reynolds number between the two sets of data which would contribute to the difference between the curves.

A further comparison is made on Figure A-42, which shows the section C_p distribution for three different angles of attack for the upper surface of the wing for $Mach = 0.80$. The C_p distributions have been compared at approximately equal C_l values of 0.2 , 0.8 , and 0.95 , resulting in angle-of-attack differences varying between 2° to 4° . The C_p distributions are shown to be in good agreement.

SPANWISE PRESSURE DISTRIBUTION

A correlation of pressures at the midchord point for a spanwise variation of y/s between 0.15 and 0.50 is presented in Figure A-43. These data were prepared to illustrate the two dimensionality of the flow over the wing. Several conditions are shown on these figures in order to provide an overall picture of how well two-dimensional flow was achieved. These include the effects of Mach number from 0.7 to 0.95 , angle of attack of 0° , 4° , and 8° and the effect of blowing at $C_\mu = 0.022$. As may be observed, pressure levels across the span are relatively constant at $\alpha = 0^\circ$ and 4° for all Mach numbers. At $\alpha = 8^\circ$, for Mach numbers of 0.80 and 0.85 , there is a local shock effect at midspan at the 50% chord location which causes the increase in pressures. Blowing tends to restore the pressures at midspan to the levels established at the other spanwise locations. The increase in pressure may be attributed to earlier transition resulting possibly from a local surface disturbance. The curves demonstrate clearly that two-dimensional flow was indeed achieved.

SECTION IV

CONCLUSIONS

The data presented and analyzed in the report have provided information to determine the feasibility of using a jet flap for transonic maneuvering. Accordingly the following conclusions are stated:

1. The lift boundary for buffet onset was improved with the jet flap.
2. Shock induced separation was reduced as shocks were shifted rearward with jet flap blowing. Maximum reduction occurred when vortex generators were combined with jet flap blowing.
3. High levels of thrust recovery and lifting efficiency were obtained which were consistent with results of previous studies.
4. A Reynolds number comparison indicated a loss in lift and increase in drag at a Reynolds number of $5.5 \times 10^6/\text{ft}$ compared to $2.5 \times 10^6/\text{ft}$.
5. Comparisons of the effects of jet flap angle showed that maximum lift improvement and rearward shift of shocks occurred at $\theta_f = 88^\circ$. Drag was lowest at $\theta_f = 35^\circ$. Pitching moment increased negatively with jet angle and was highest at $\theta_f = 88^\circ$.

SECTION V

REFERENCES

1. Cahill, J. F., and Cooper, B. L. "Flight Test Investigation of Transonic Shock-Boundary Layer Phenomena, " AFFDL-TR-68-84.
2. Peitzman, F. W., "Data Report of a Transonic Wind Tunnel Test of Three Two-Dimensional Wings, " NOR-67-46, June 1967.
3. Butler, R., "Two-Dimensional Jet Flap Test, " PC0969, A.R.O., Inc. Arnold Air Force Station, Tenn.
4. Hoekman, R. J., "Calibration of Five Jet Flaps, " NOR-69-128, September 1969.
5. Spence, D. A., "The Lift Coefficient of a Thin, Jet Flapped Wing, " Proc. of The Royal Soc., Series A, Mathematical and Physical Sciences, Vol 238, No. 1212, December 1956.
6. Jacobs, W. F., and Paterson, J. H., "The Jet Flapped Wing in Two- and Three-Dimensional Flow, " I.A.S. Meeting Preprint No. 791, January 1958.
7. Poisson-Quinton, Ph, and Jousserandot, P., "Influence of Air-Blowing Near the Trailing Edge of a Wing on its High Speed Aerodynamic Characteristics, " O.N.E.R.A. Report No. 56, February 1957.
8. Hynes, C. S., "The Lift, Stalling and Wake Characteristics of a Jet-Flapped Airfoil in a Two-Dimensional Channel, " SUDAAR No. 363, Stanford University.
9. Foley, W. M., and Reid, E. G., "Jet Flap Thrust Recovery, " Journal of The Aero/Space Sciences, June 1959.
10. Stivers, L. D., Jr., "Effects of Subsonic Mach Number on the Forces and Pressure Distributions on Four NACA 64A-Series Airfoil Sections at Angles of Attack as High as 28°, " NACA Technical Note 3162.
11. Cleary, J. W. and Stevens, G. L., "The Effects at Transonic Speeds of Thickening the Trailing Edge of a Wing with a 4% Thick Circular Arc Airfoil, " NACA RM A51 J11.

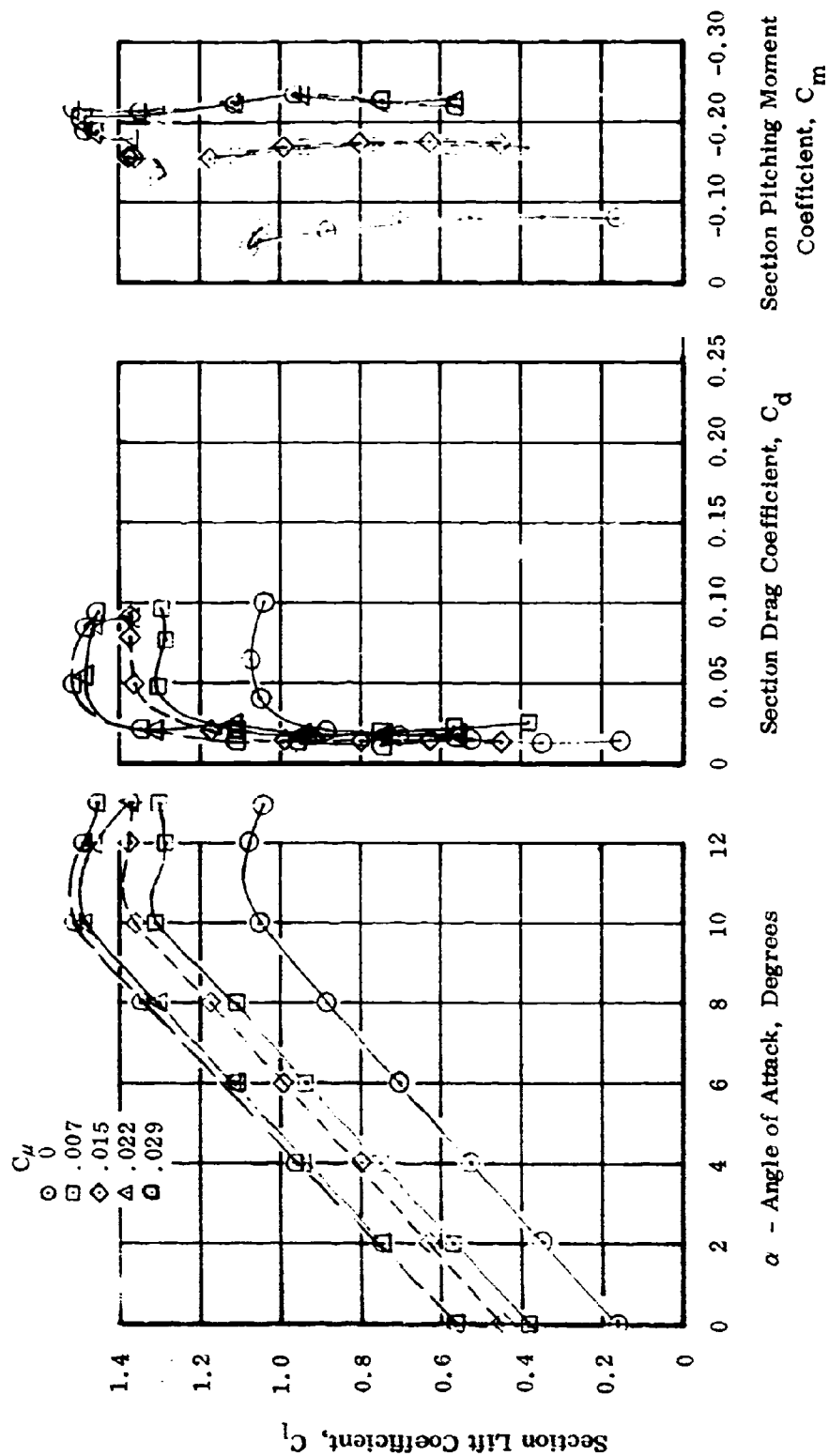
APPENDIX - LIST OF RELATED FIGURES

| <u>Figure</u> | <u>Title</u> | <u>Page</u> |
|---------------|--|-------------|
| A-1 | Effect of Blowing Momentum, $M = 0.70$ | 35 |
| A-2 | Effect of Blowing Momentum, $M = 0.80$ | 36 |
| A-3 | Effect of Blowing Momentum, $M = 0.85$ | 37 |
| A-4 | Effect of Blowing Momentum, $M = 0.90$ | 38 |
| A-5 | Effect of Blowing Momentum, $M = 0.95$ | 39 |
| A-6 | Effect of Blowing Momentum on Pressure Distribution, $M = 0.70$ | 40 |
| A-7 | Effect of Blowing Momentum on Pressure Distribution, $M = 0.80$ | 41 |
| A-8 | Effect of Blowing Momentum on Pressure Distribution, $M = 0.85$ | 42 |
| A-9 | Effect of Blowing Momentum on Pressure Distribution, $M = 0.90$ | 43 |
| A-10 | Effect of Blowing Momentum on Pressure Distribution, $M = 0.95$ | 44 |
| A-11 | Variation of Longitudinal Characteristics with Jet Angle | 45 |
| A-12 | Variation of Pressure Distribution with Jet Angle. | 46 |
| A-13 | Jet Induced Circulation Lift, $\alpha = 0^\circ$ | 47 |
| A-14 | Section Drag Coefficient Versus C_μ , $M = 0.70$ | 48 |
| A-15 | Section Drag Coefficient Versus C_μ , $M = 0.85$ | 49 |
| A-16 | Section Drag Coefficient Versus C_μ , $M = 0.95$ | 50 |
| A-17 | Section Lift Coefficient Versus Mach No., $C_\mu = 0$ | 51 |
| A-18 | Section Lift Coefficient Versus Mach No., $C_\mu = 0.022$ | 51 |
| A-19 | Section Drag Coefficient Versus Mach No. | 52 |
| A-20 | Section Pitching Moment Versus Mach No. | 53 |
| A-21 | Lift Efficiency Versus Mach No. at $\alpha = 0^\circ$ | 54 |
| A-22 | Effect of Vortex Generators, $M = 0.70$ | 55 |
| A-23 | Effect of Vortex Generators, $M = 0.80$ | 56 |
| A-24 | Effect of Vortex Generators, $M = 0.85$ | 57 |
| A-25 | Effect of Vortex Generators on Pressure Distribution, $M = 0.85$ | 58 |
| A-26 | Effect of Reynolds Number, $M = 0.70$ | 59 |
| A-27 | Effect of Reynolds Number, $M = 0.80$ | 60 |
| A-28 | Effect of Reynolds Number, $M = 0.85$ | 61 |
| A-29 | Effect of Reynolds Number, $M = 0.90$ | 62 |
| A-30 | Effect of Reynolds Number, $M = 0.95$ | 63 |

APPENDIX - LIST OF RELATED FIGURES (Continued)

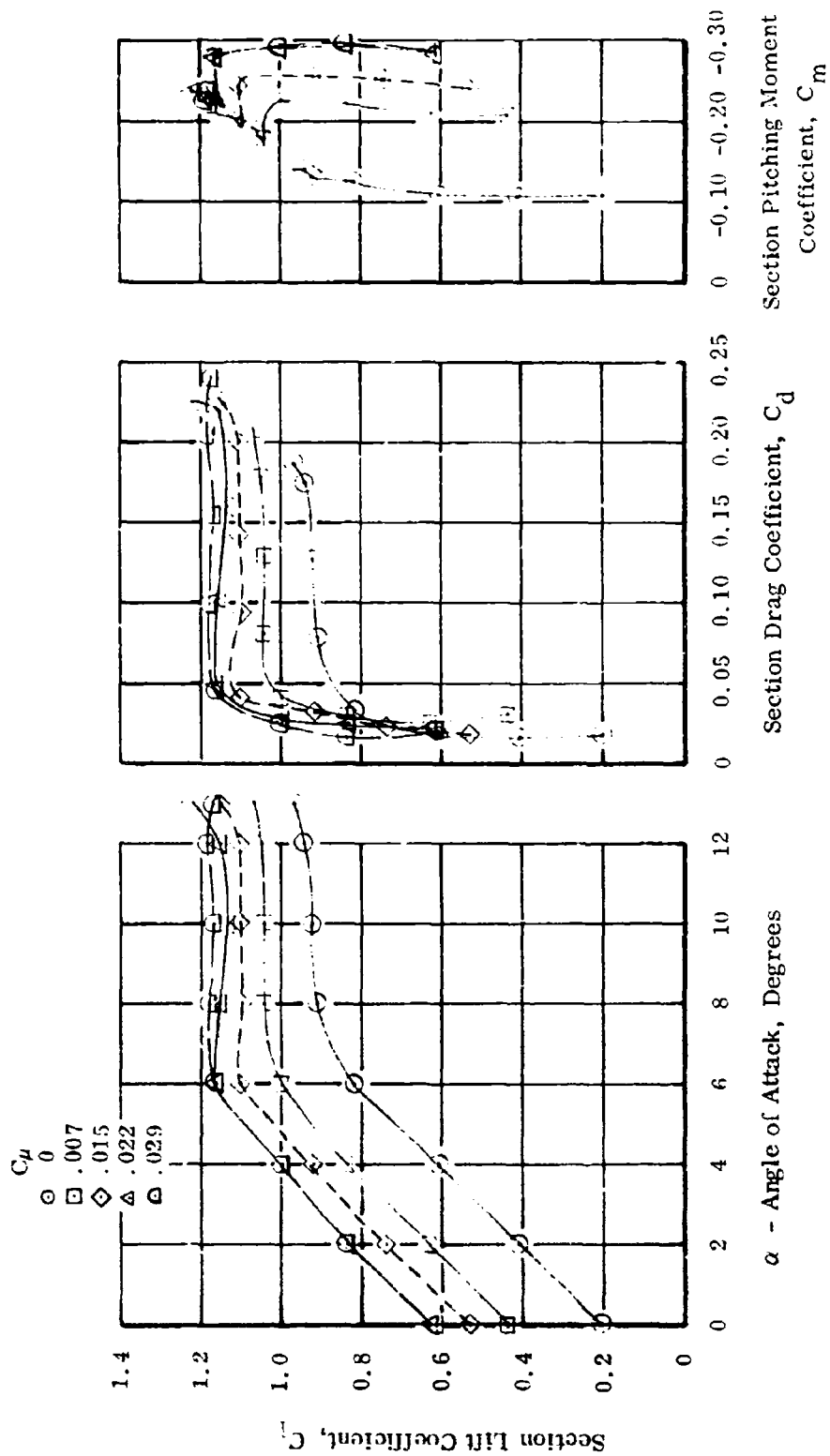
| <u>Figure</u> | <u>Title</u> | <u>Page</u> |
|---------------|---|-------------|
| A-31 | Effect of Reynolds Number on Pressure Distribution, $M = 0.80$. . . | 64 |
| A-32 | Effect of Reynolds Number on Pressure Distribution, $M = 0.85$. . . | 65 |
| A-33 | Effect of Reynolds Number on Pressure Distribution, $M = 0.90$. . . | 66 |
| A-34 | Effect of Reynolds Number on Pressure Distribution, $M = 0.95$. . . | 67 |
| A-35 | Thrust Recovery at $\theta_f = 0^\circ$ | 68 |
| A-36 | Thrust Recovery at $\theta_f = 55^\circ$ | 69 |
| A-37 | Thrust Recovery at $\theta_f = 88^\circ$ | 70 |
| A-38 | Buffet Onset Method Comparison | 71 |
| A-39 | Comparisons of Estimated Shock Locations | 72 |
| A-40 | Upper Surface Pressure Comparison | 73 |
| A-41 | Comparison of Test Airfoil and NACA 64A406 | 74 |
| A-42 | Comparison of Test Airfoil and NACA 64A406 Upper Surface Pressures at $M = 0.80$ | 75 |
| A-43 | Spanwise Pressure Distributions | 76 |

$$R_N = 5.5 \times 10^6 / \text{FT} \quad , \quad \theta_f = 88^\circ$$



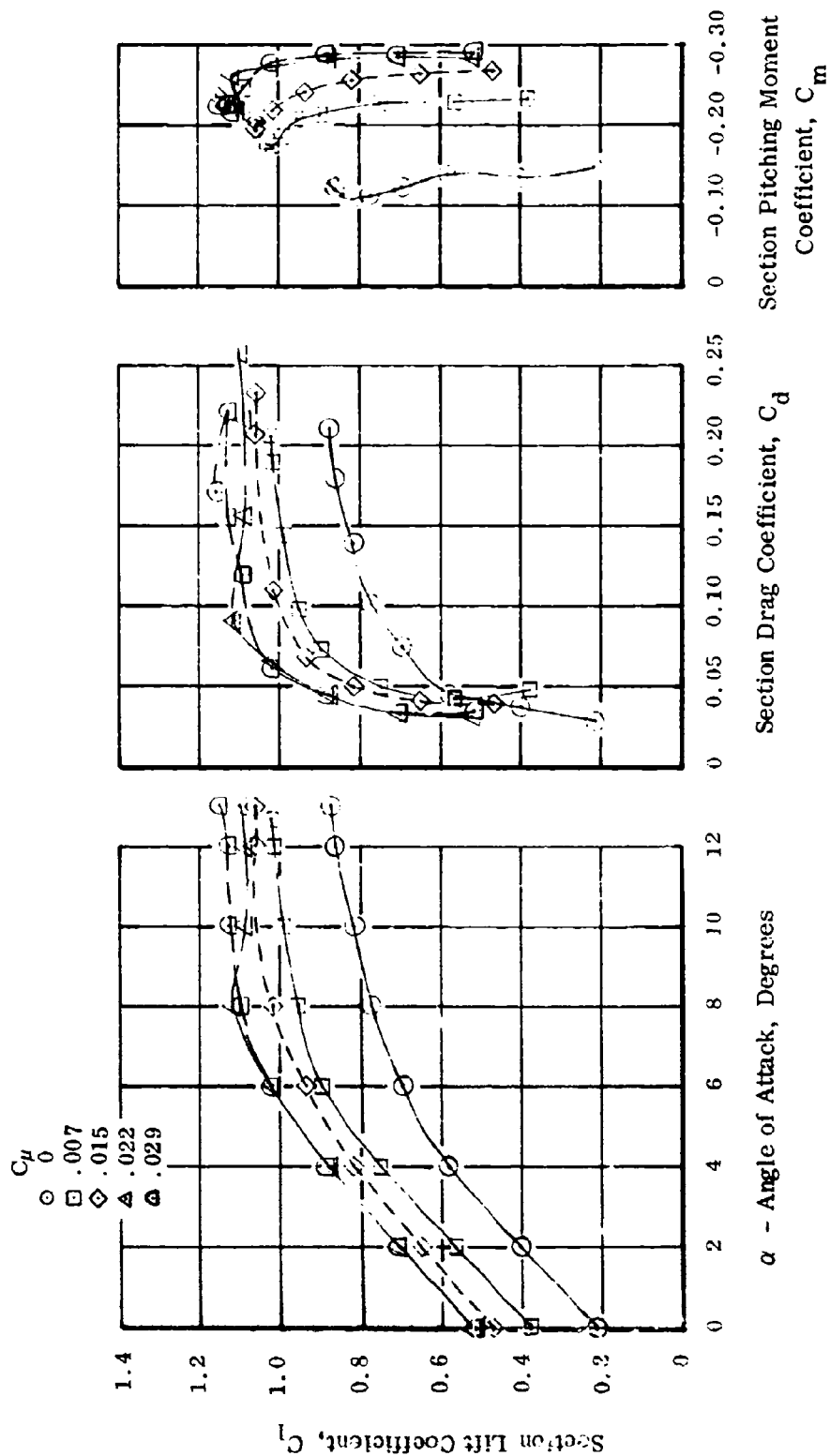
A-1. Effect of Blowing Momentum, $M = 0.70$

$$R_N = 5.5 \times 10^6 / \text{FT}^2, \theta_f = 88^\circ$$



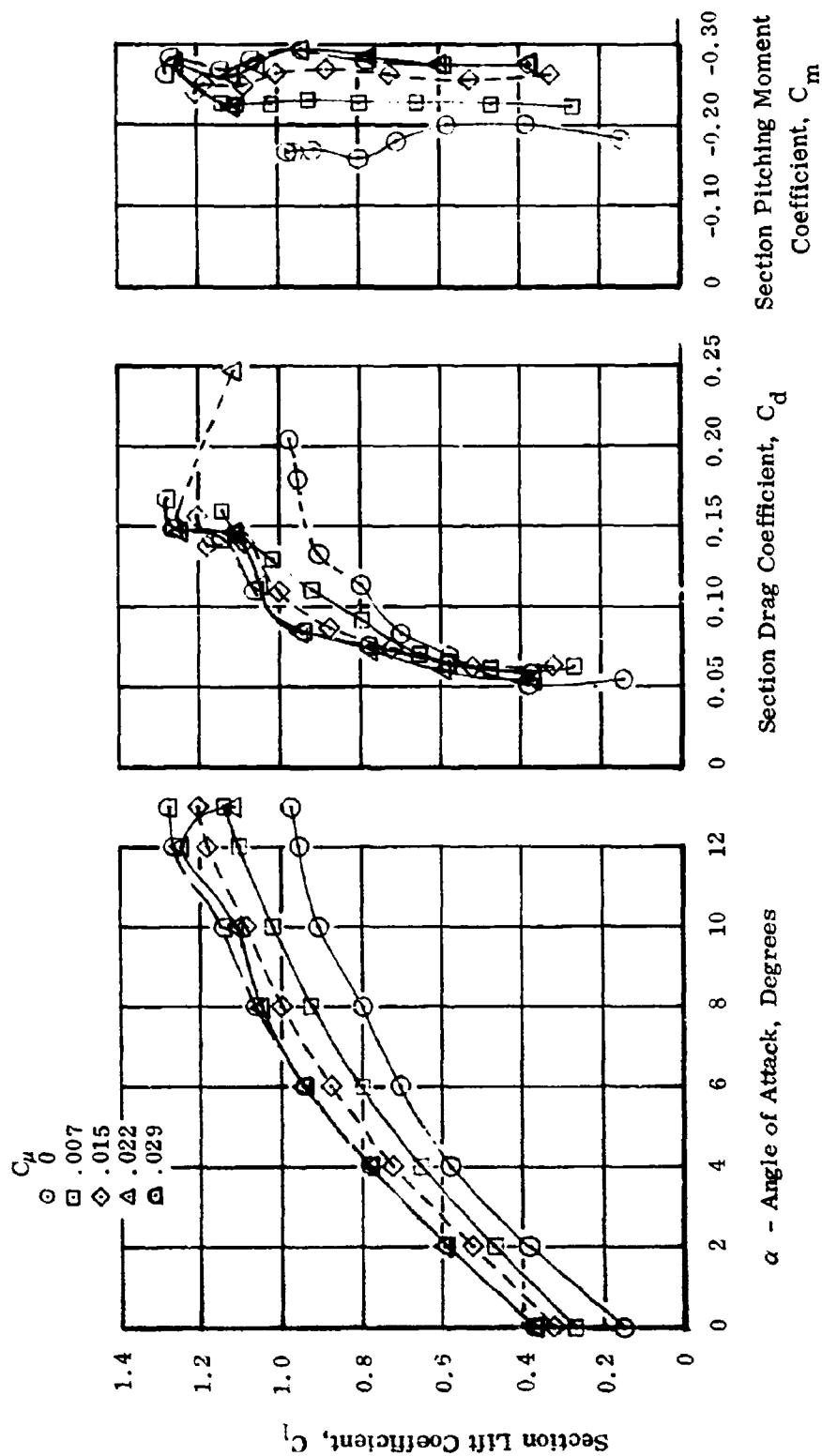
A-2. Effect of Blowing Momentum, $M = 0.80$

$$R_N = 5.5 \times 10^6 / \text{FT} \quad , \quad \theta_i = 88^\circ$$



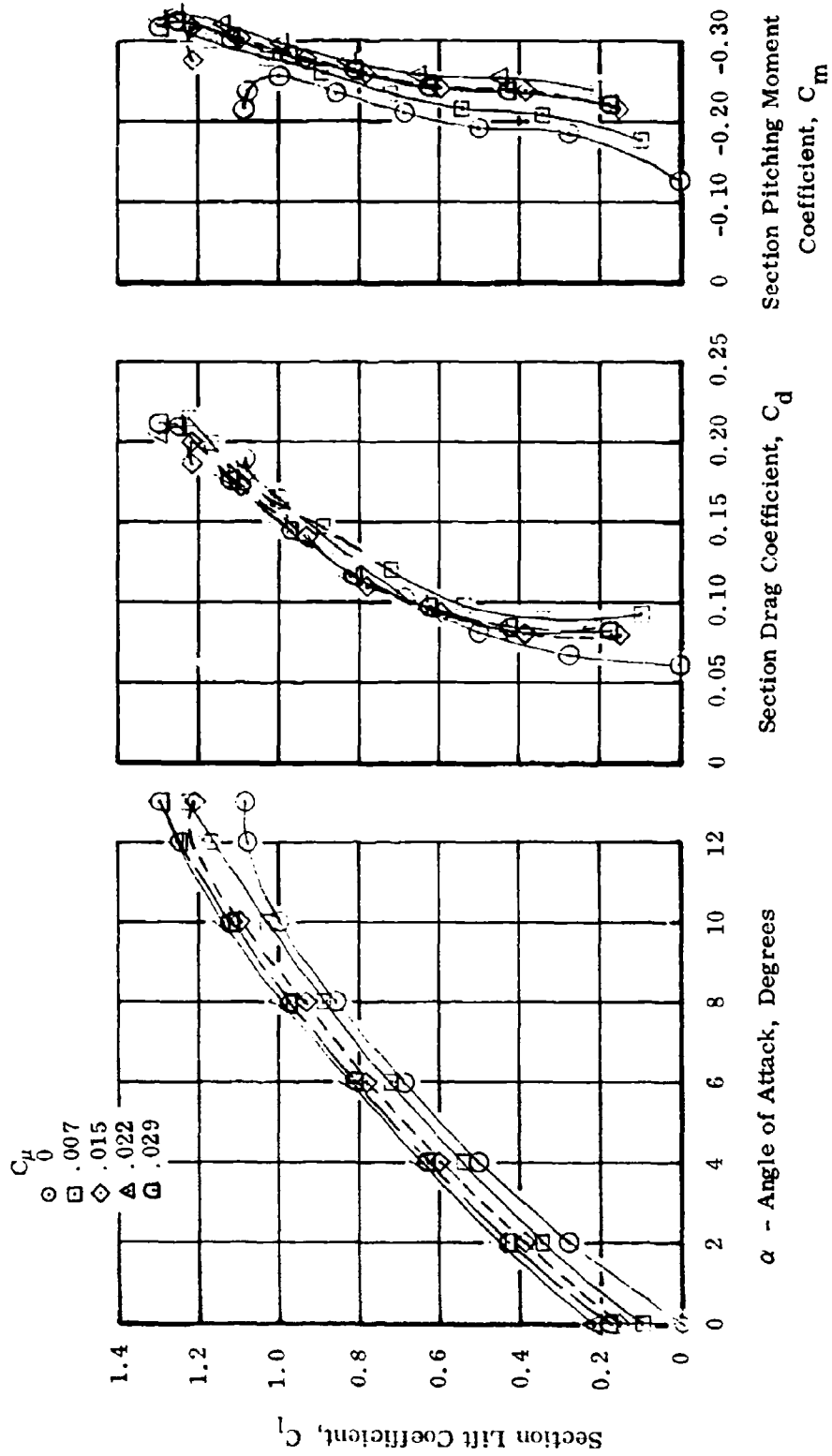
A-3. Effect of Blowing Momentum, $M = 0.85$

$$R_N = 5.5 \times 10^6 / \text{FT} \quad , \quad \theta_f = 88^\circ$$



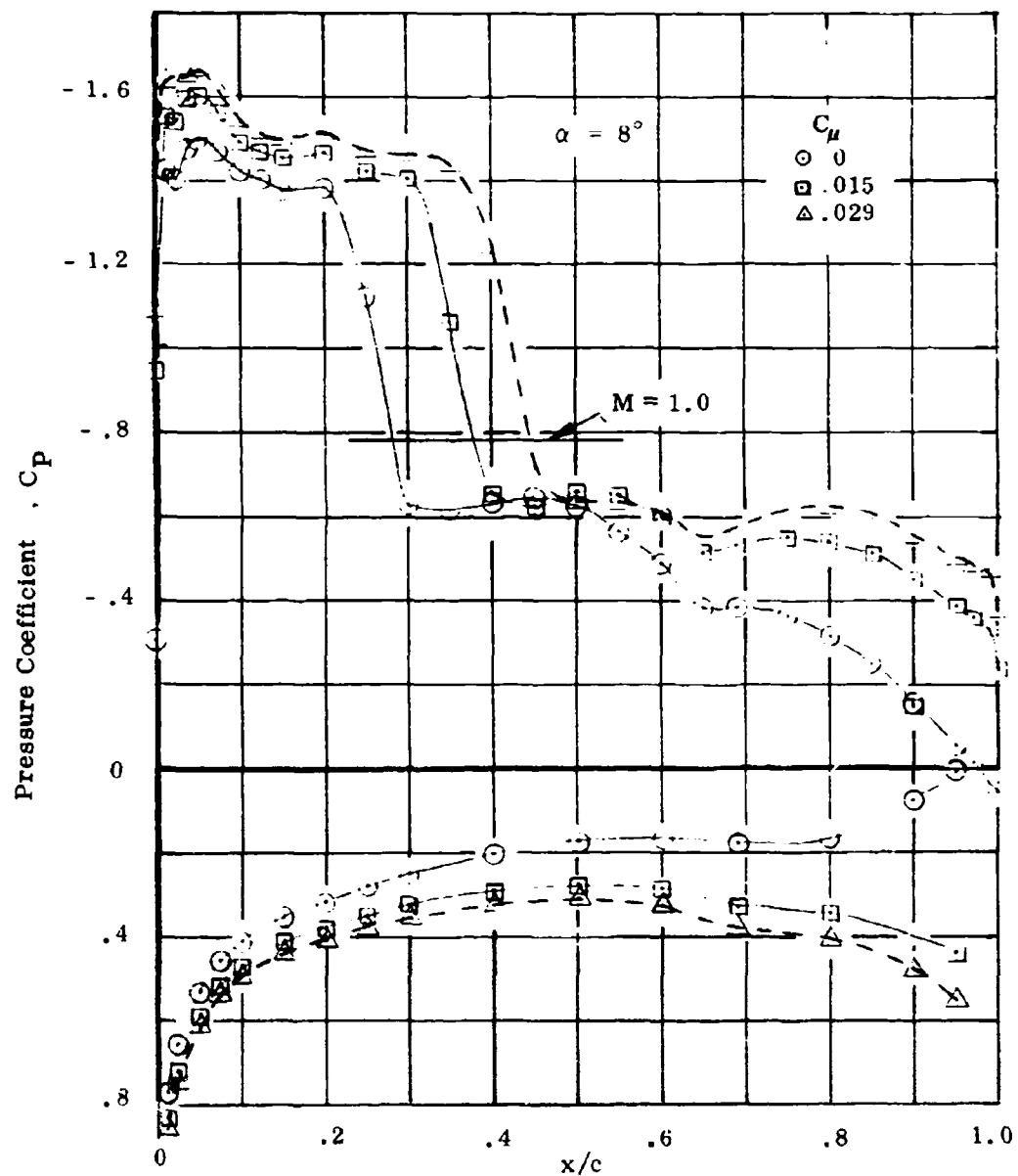
A-4. Effect of Blowing Momentum, $M = 0.90$

$$R_N = 5.5 \times 10^6 / \text{FT} \quad , \quad \theta_f = 88^\circ$$



A-5. Effect of Blowing Momentum, $M = 0.95$

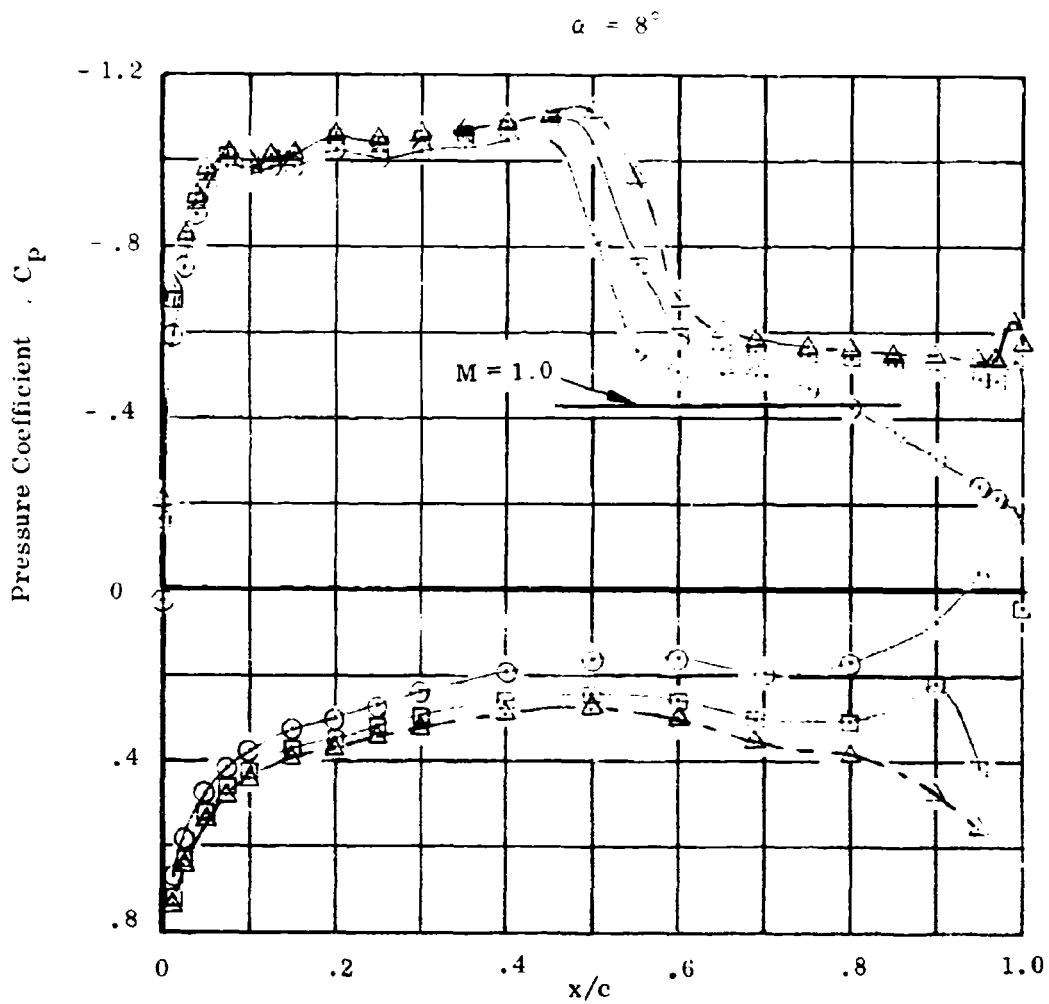
$$R_N = 5.5 \times 10^6 / \text{FT} \quad , \quad \theta_f = 88^\circ$$



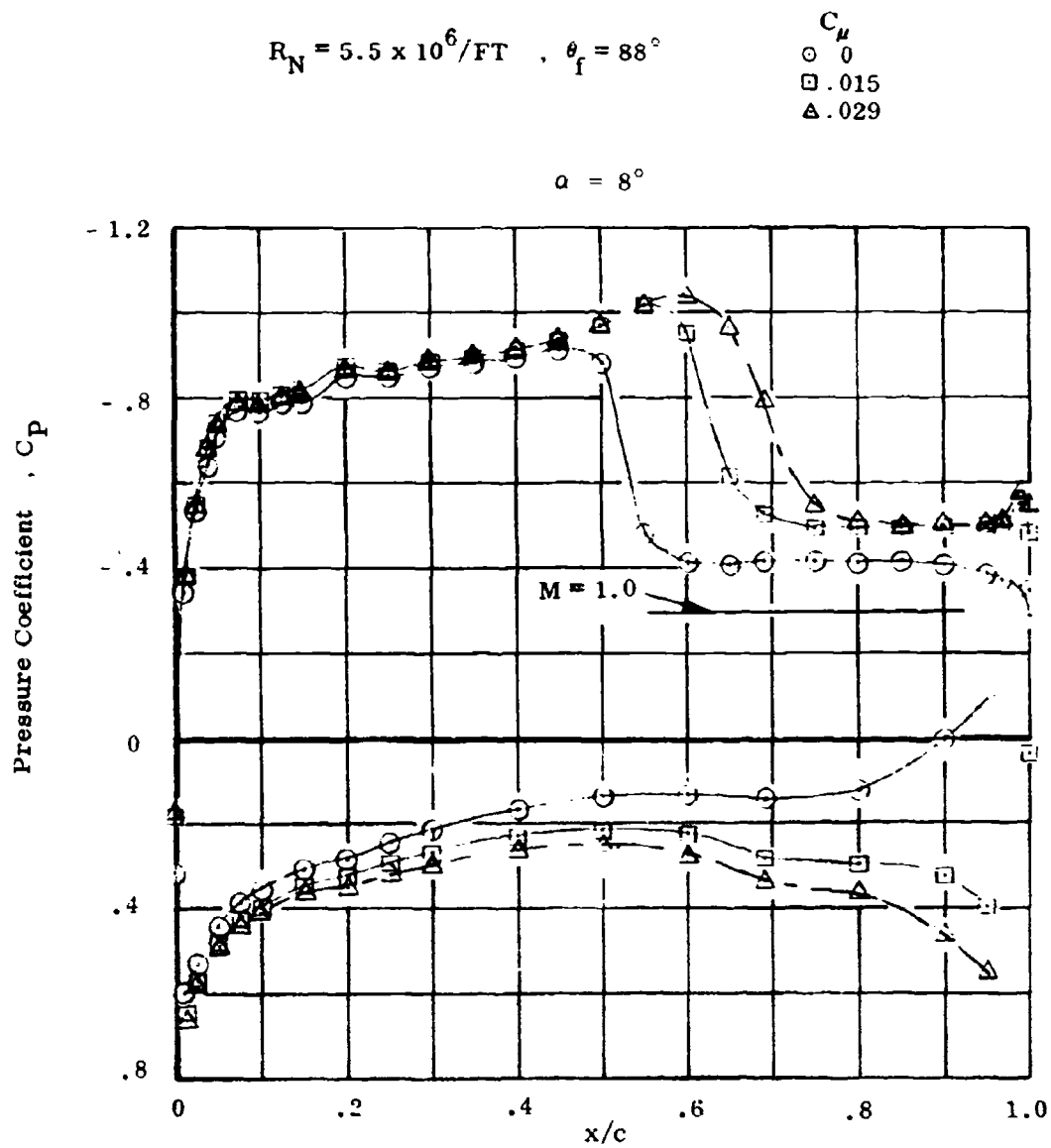
A-6. Effect of Blowing Momentum on Pressure Distribution, $M = 0.70$

$$R_N = 5.5 \times 10^6 / \text{FT} \quad , \quad \theta_f = 88^\circ$$

C_μ
 \circ 0
 \square .015
 \triangle .029



A-7. Effect of Blowing Momentum on Pressure Distribution, $M = 0.80$

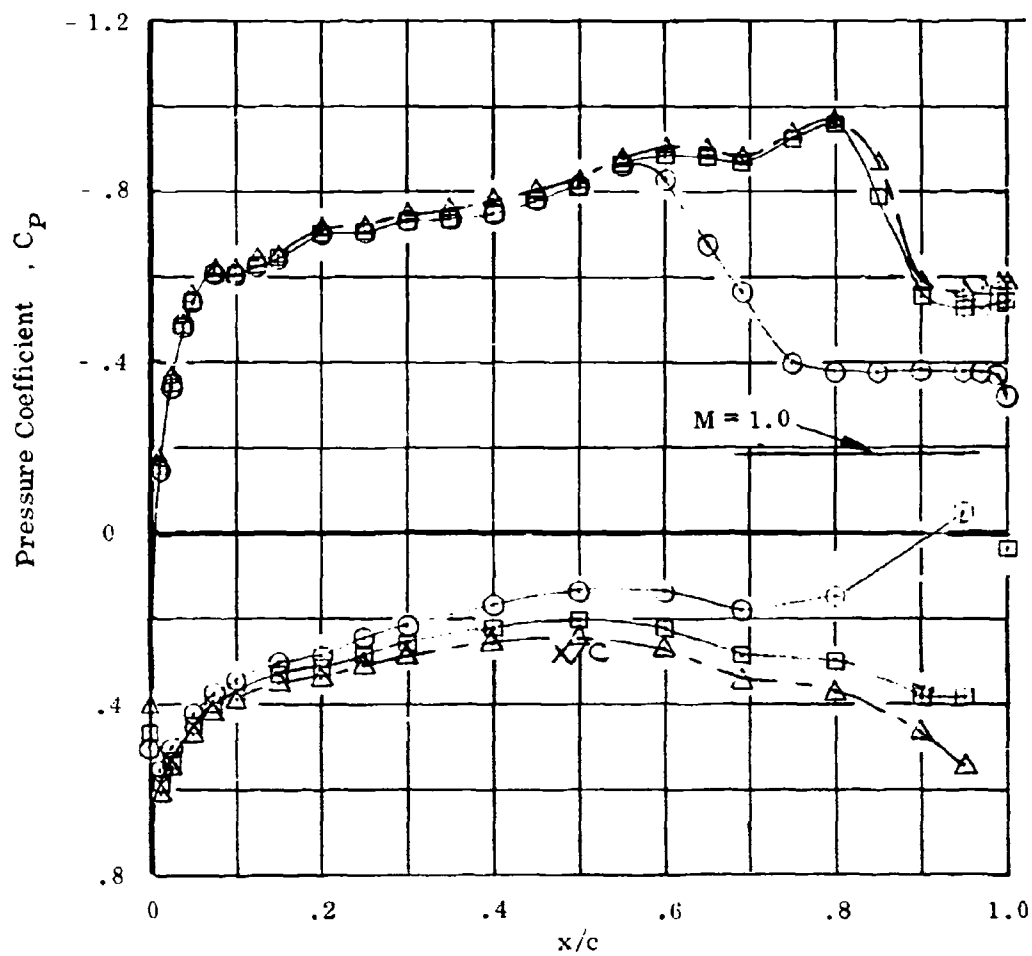


A-8. Effect of Blowing Momentum on Pressure Distribution, $M = 0.85$

$$R_N = 5.5 \times 10^6 / FT \quad , \quad \theta_f = 88^\circ$$

C_μ
 \circ 0
 \square .015
 \triangle .029

$$\alpha = 8^\circ$$

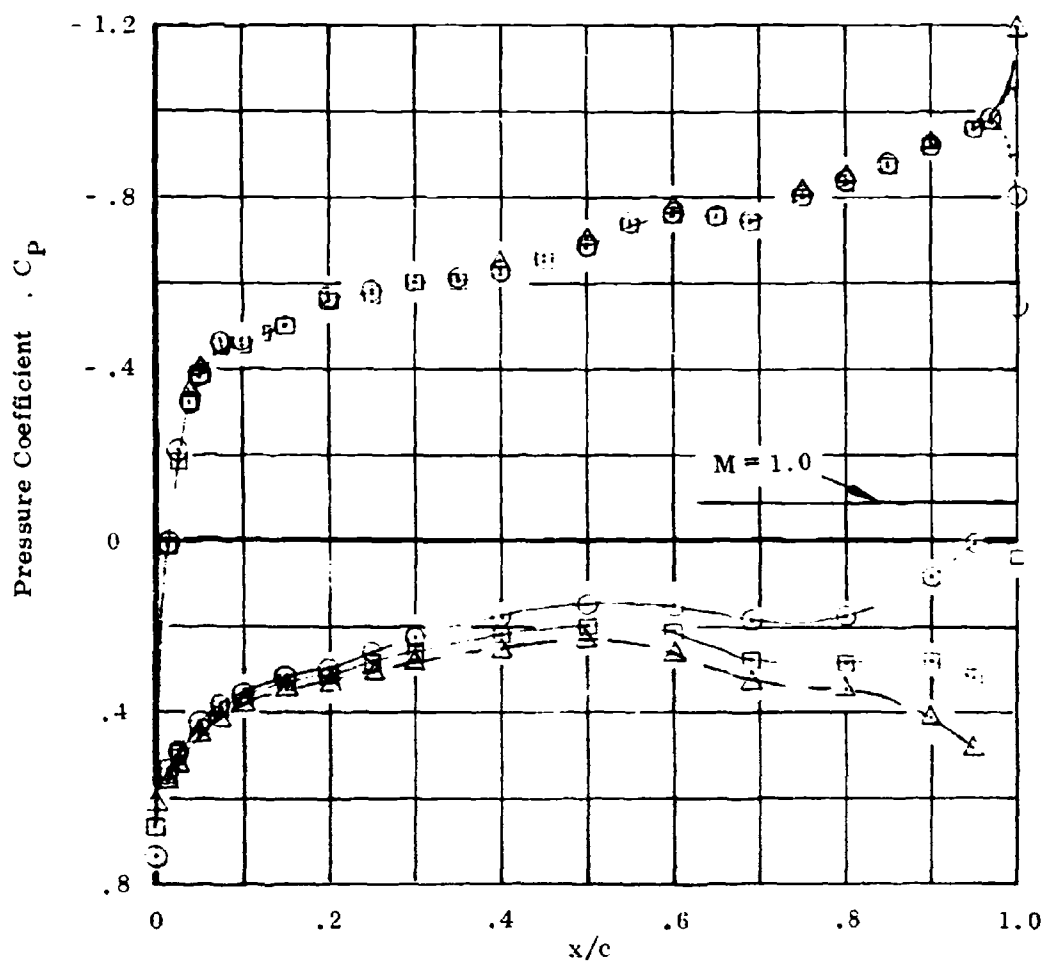


A-9. Effect of Blowing Momentum on Pressure Distribution, $M = 0.90$

$$R_N = 5.5 \times 10^6 / \text{FT} \quad , \quad \theta_f = 88^\circ$$

C_μ
 \circ 0
 \square .015
 \triangle .029

$$\alpha = 8^\circ$$

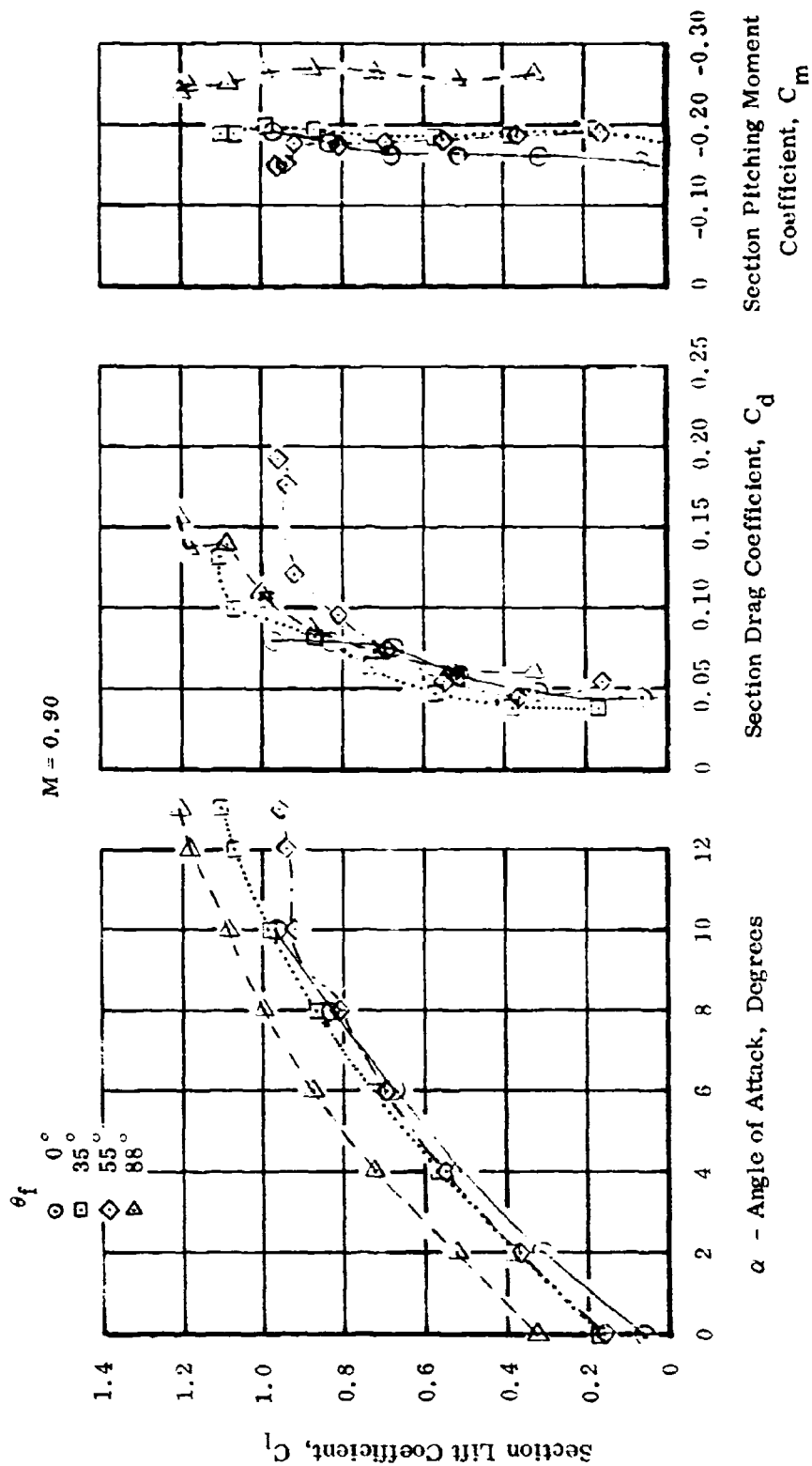


A-10. Effect of Blowing Momentum on Pressure Distribution, $M = 0.95$

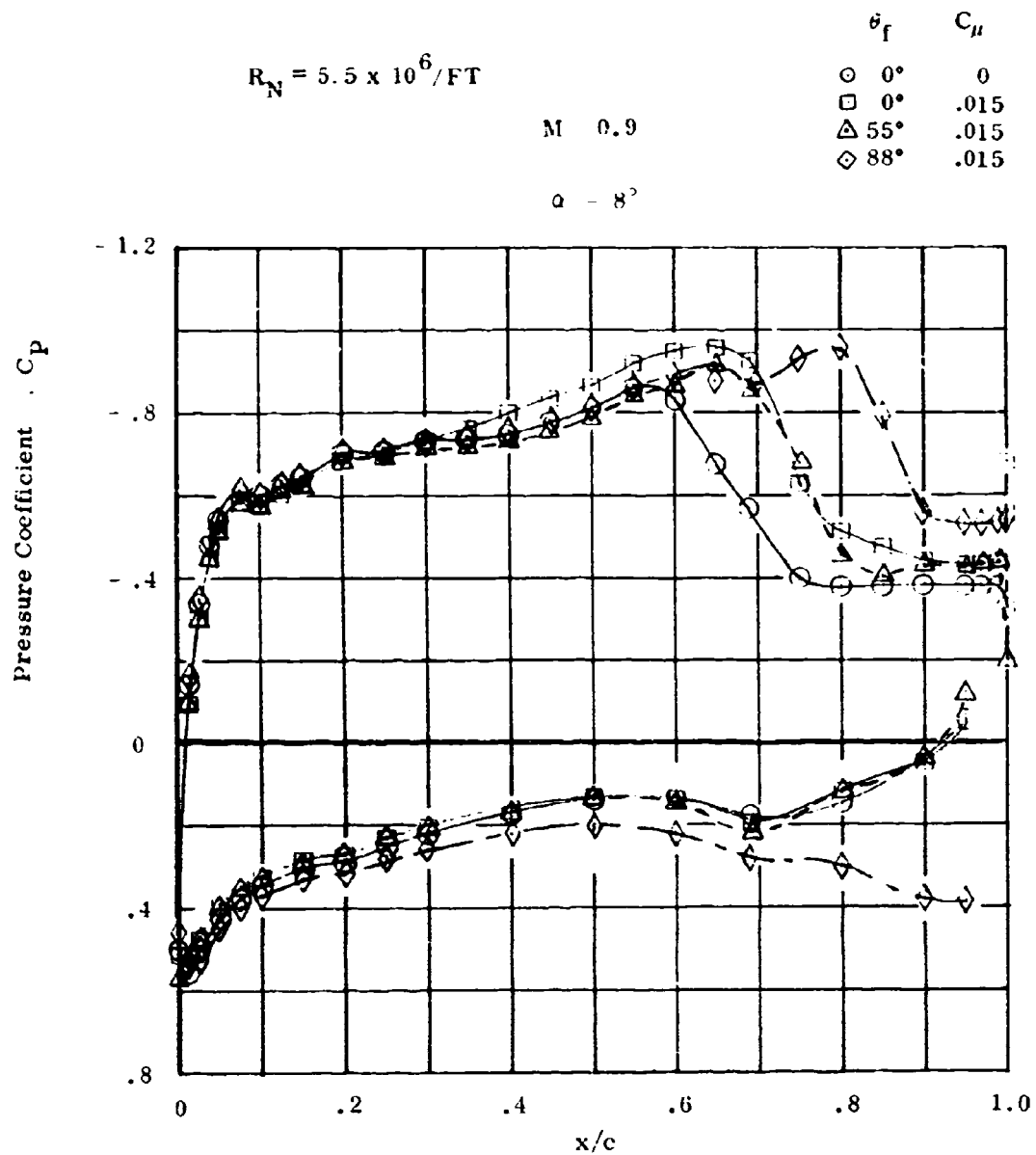
$$R_N = 5.5 \times 10^6 / \text{FT}$$

$$C_{\mu} = .015$$

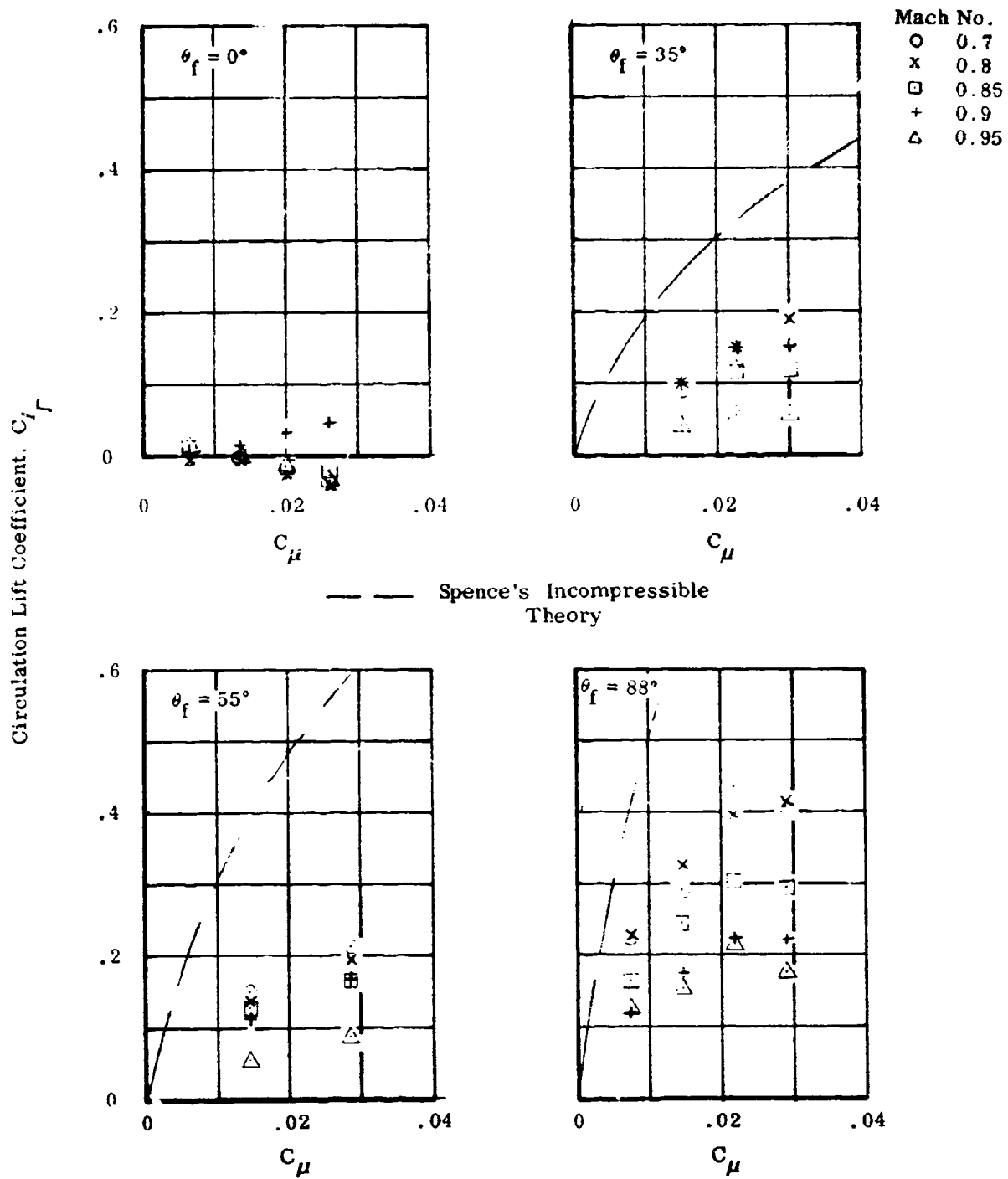
$$M = 0.90$$



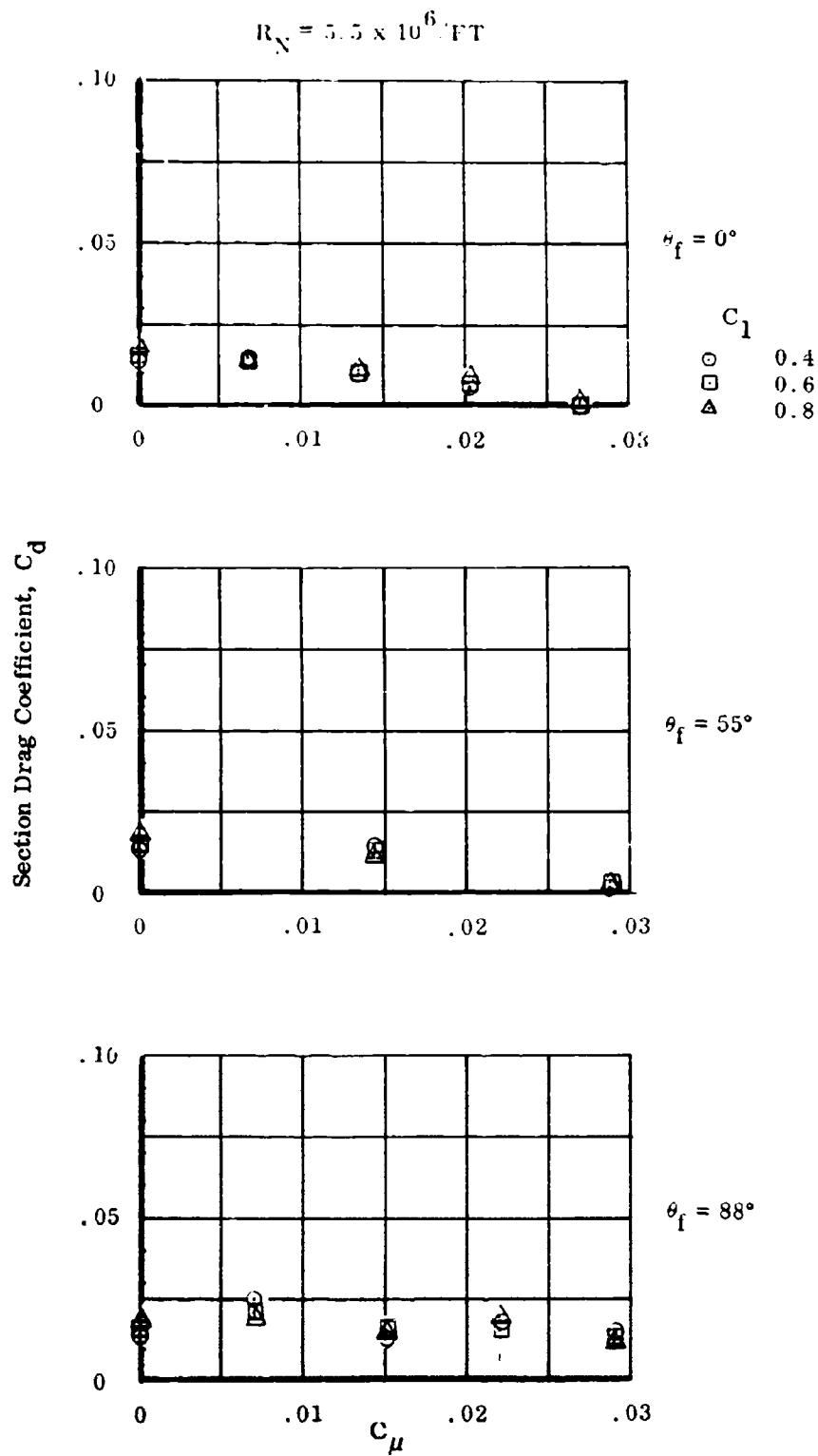
A-11. Variation of Longitudinal Characteristics with Jet Angle



A-12. Variation of Pressure Distribution with Jet Angle

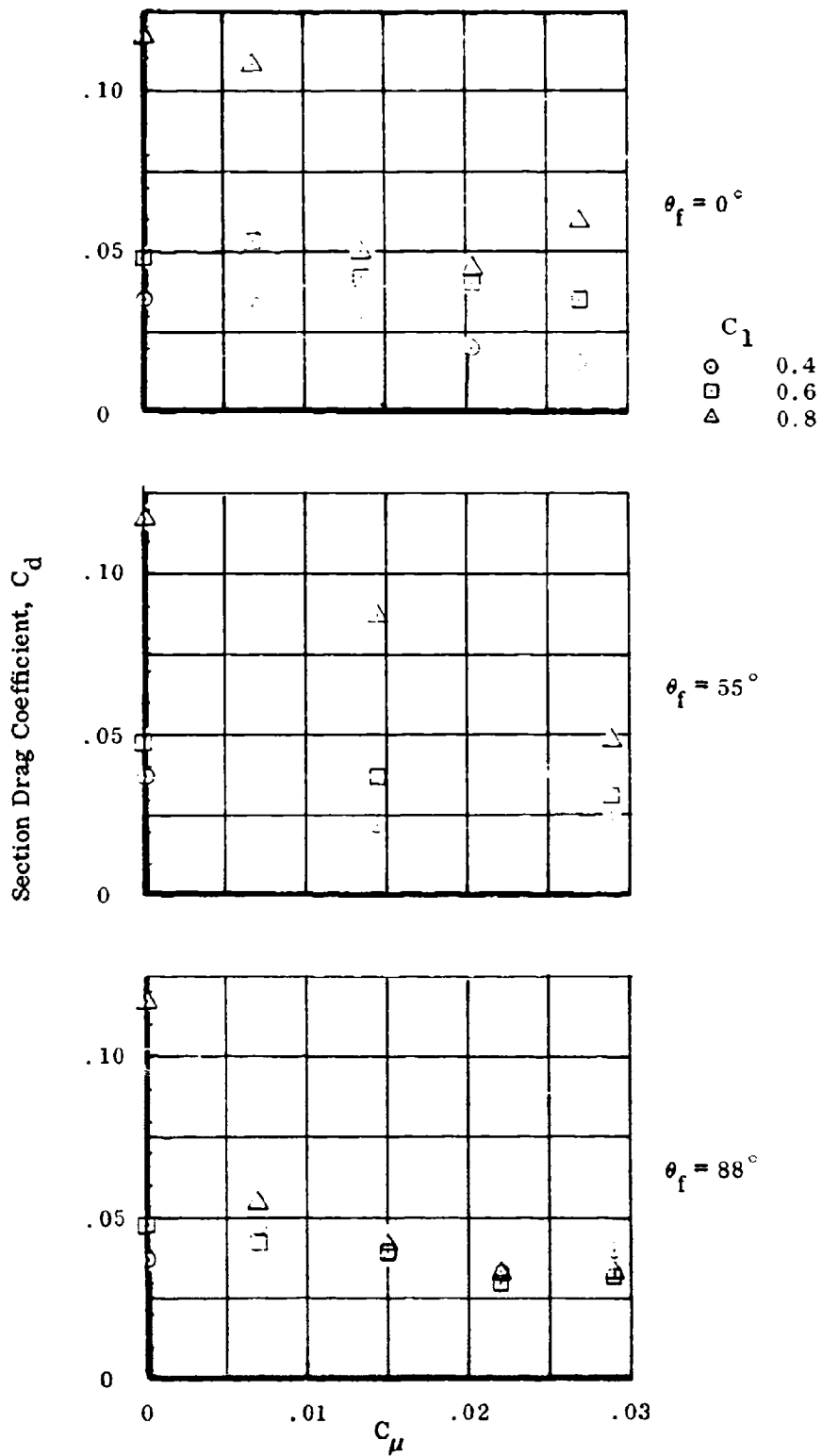


A-13. Jet Induced Circulation Lift, $\alpha = 0^\circ$



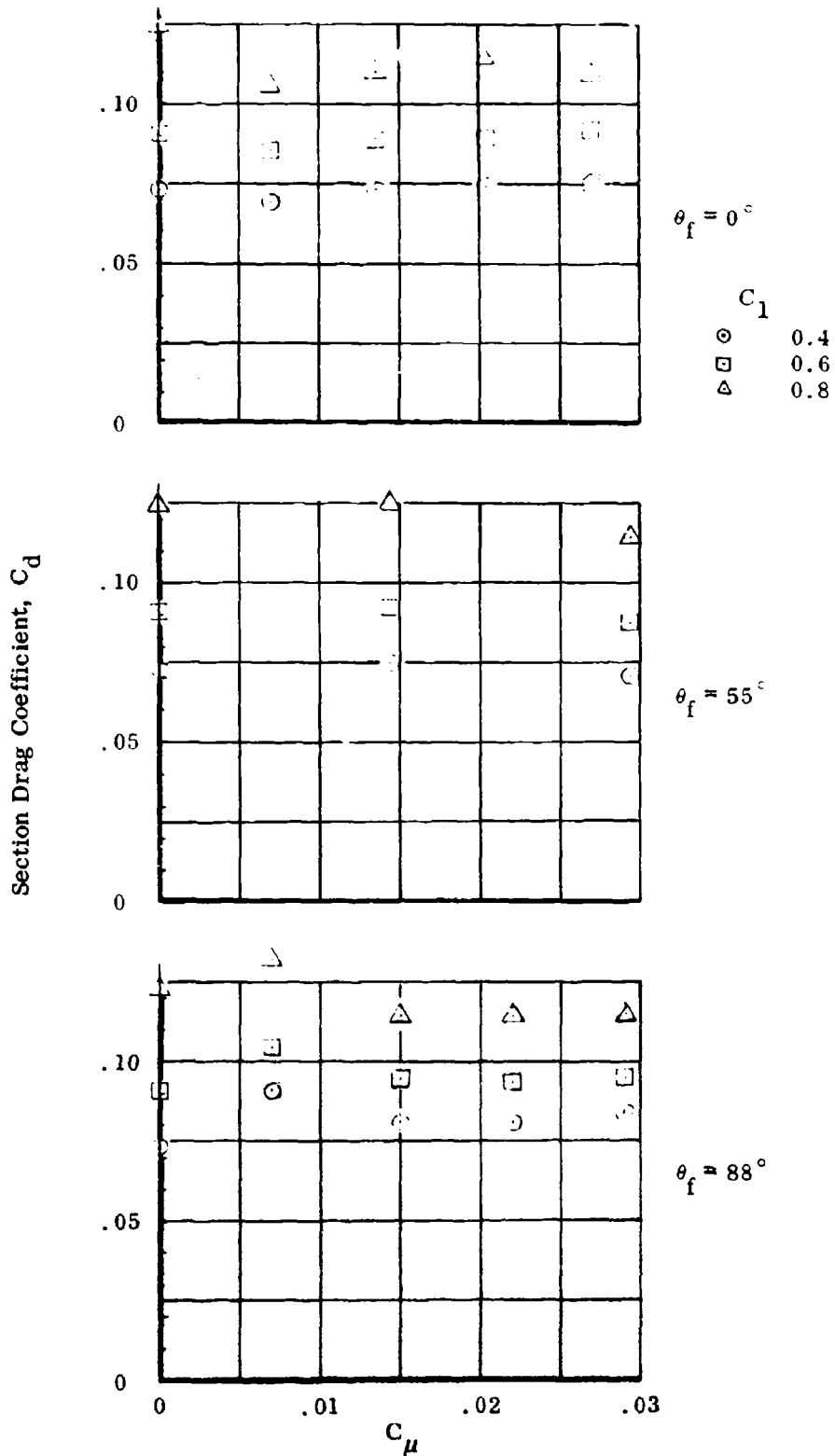
A-14. Section Drag Coefficient Versus C_μ , $M = 0.70$

$$R_N = 5.5 \times 10^6 / \text{FT}$$



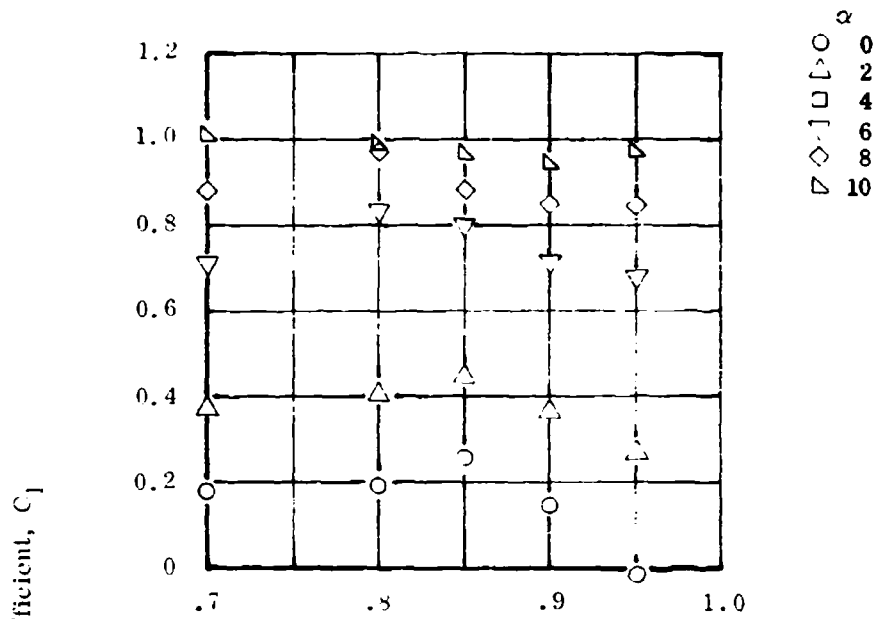
A-15. Section Drag Coefficient Versus C_μ , $M = 0.85$

$$R_N = 5.5 \times 10^6 / \text{FT}$$

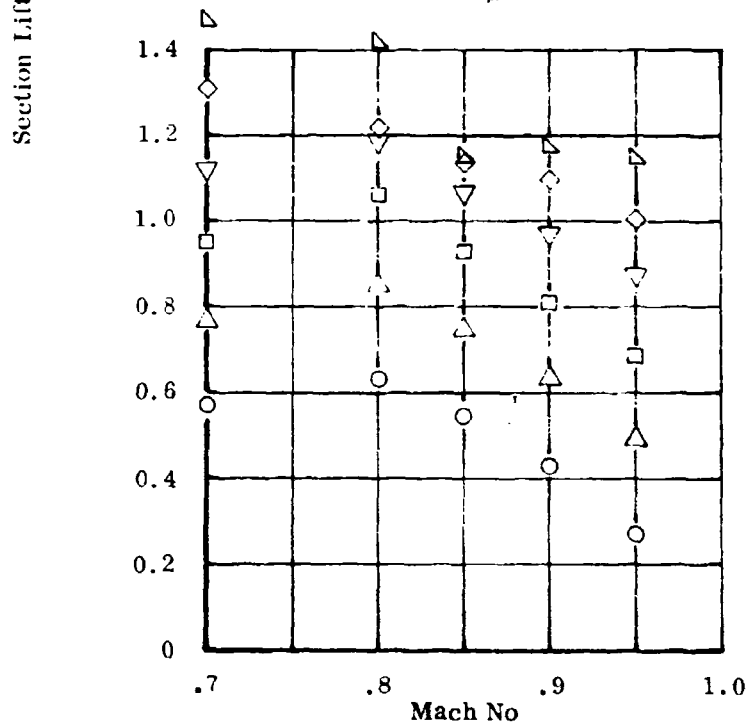


A-16. Section Drag Coefficient Versus C_μ , $M = 0.95$

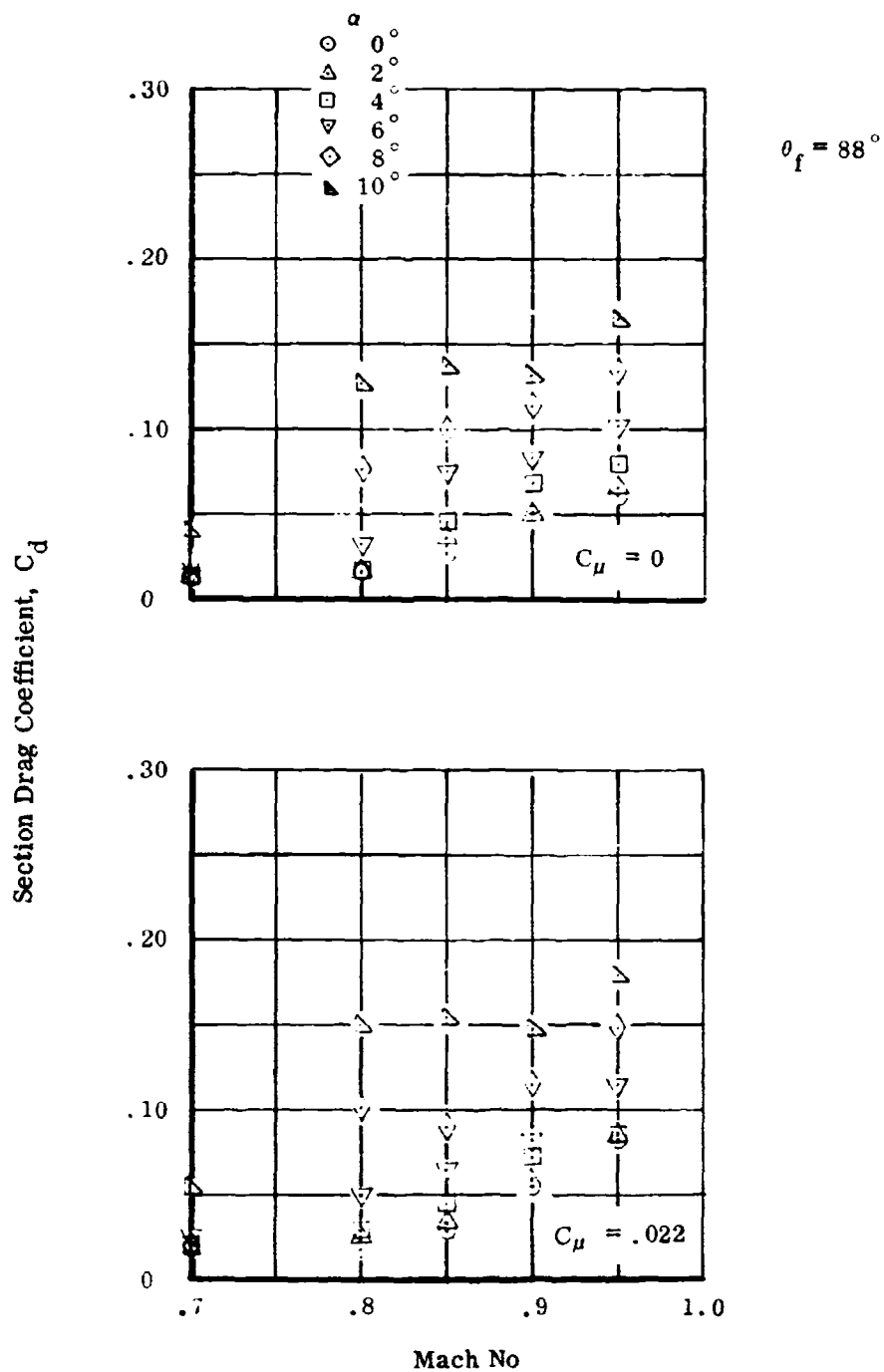
$$R_N = 5.5 \times 10^6 / \text{FT} \quad \theta_f = 8^\circ$$



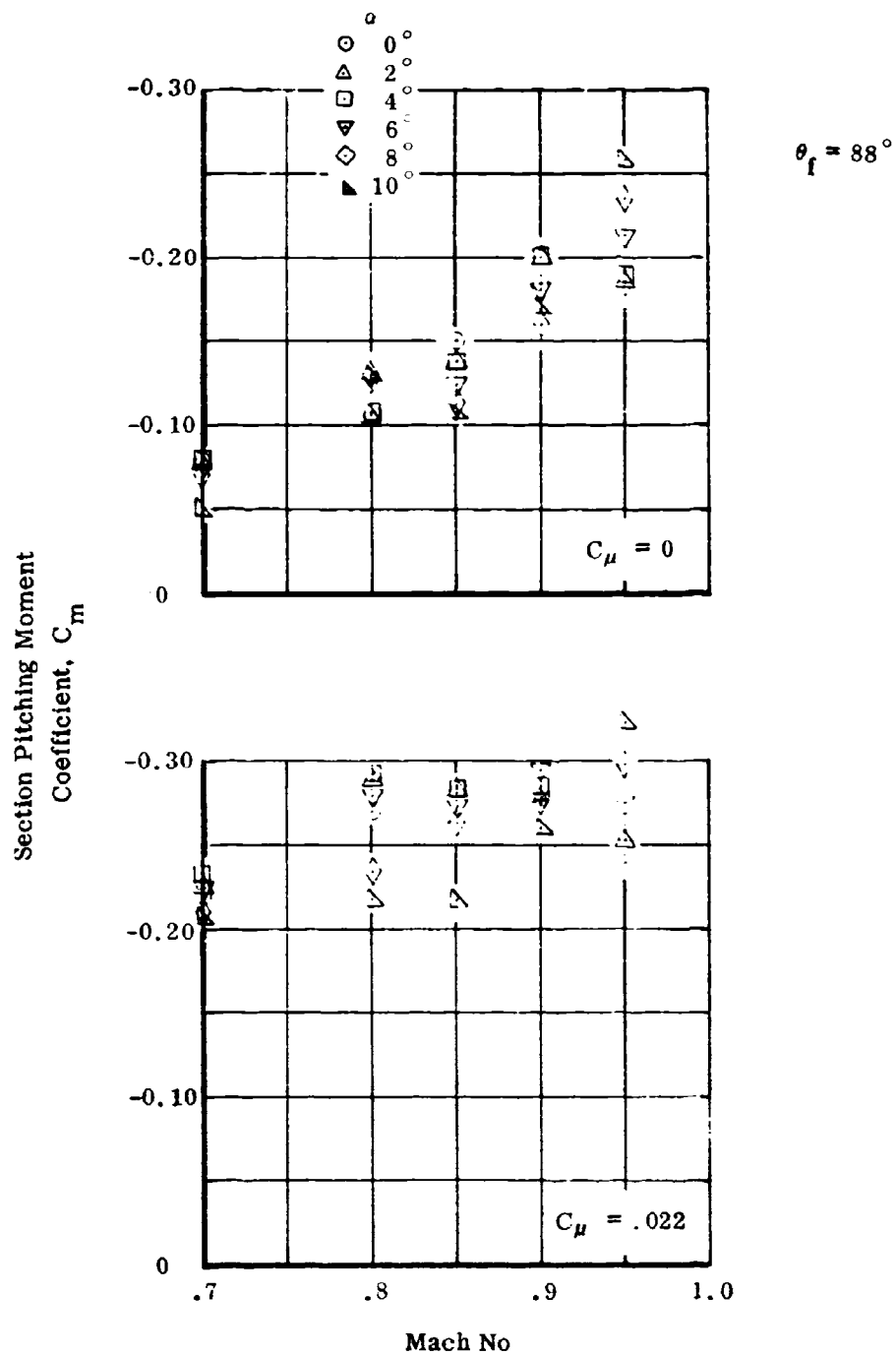
A-17. Section Lift Coefficient Versus Mach No., $C_\mu = 0$



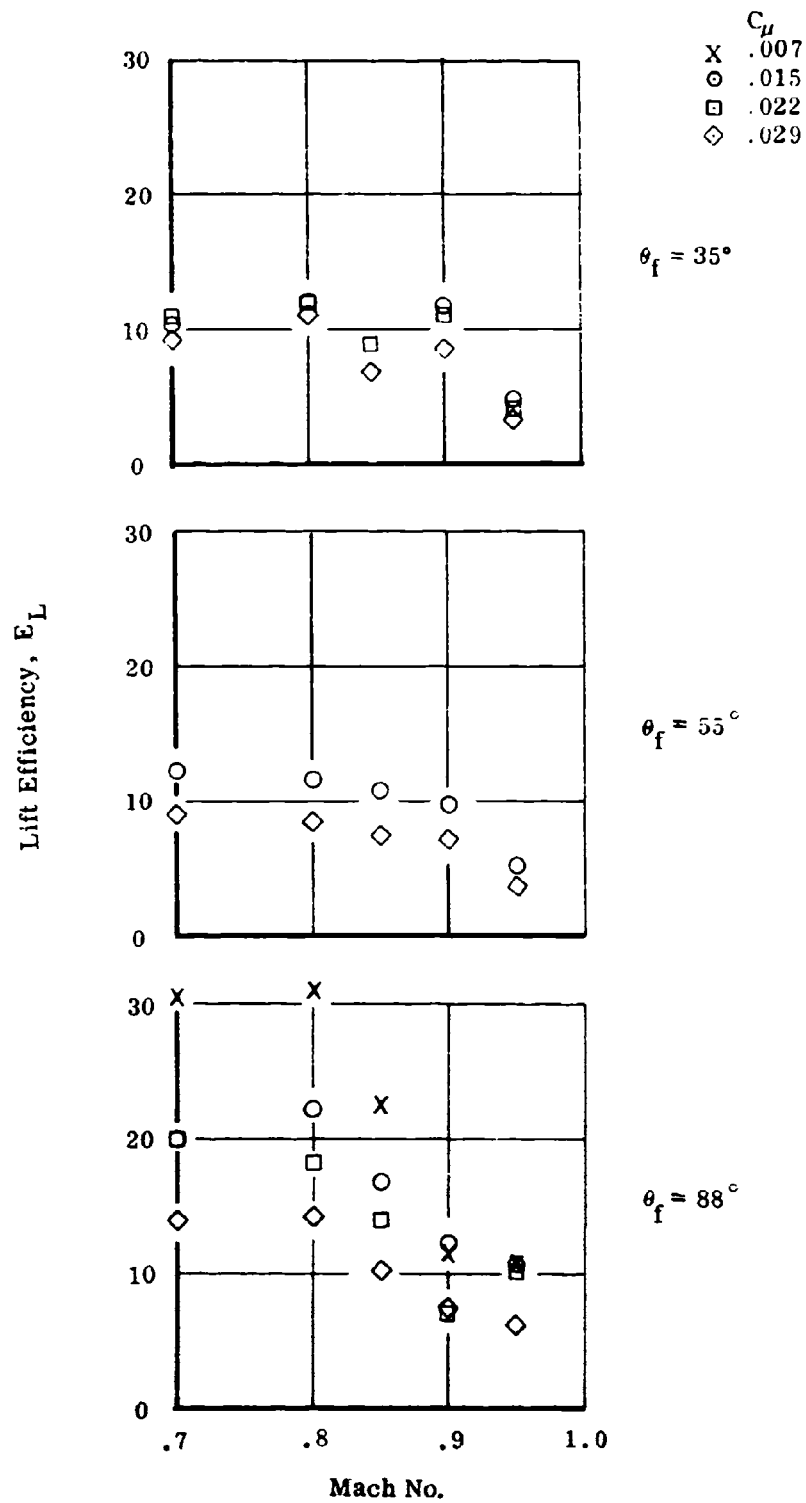
A-18. Section Lift Coefficient Versus Mach No., $C_\mu = 0.022$



A-19. Section Drag Coefficient Versus Mach No.

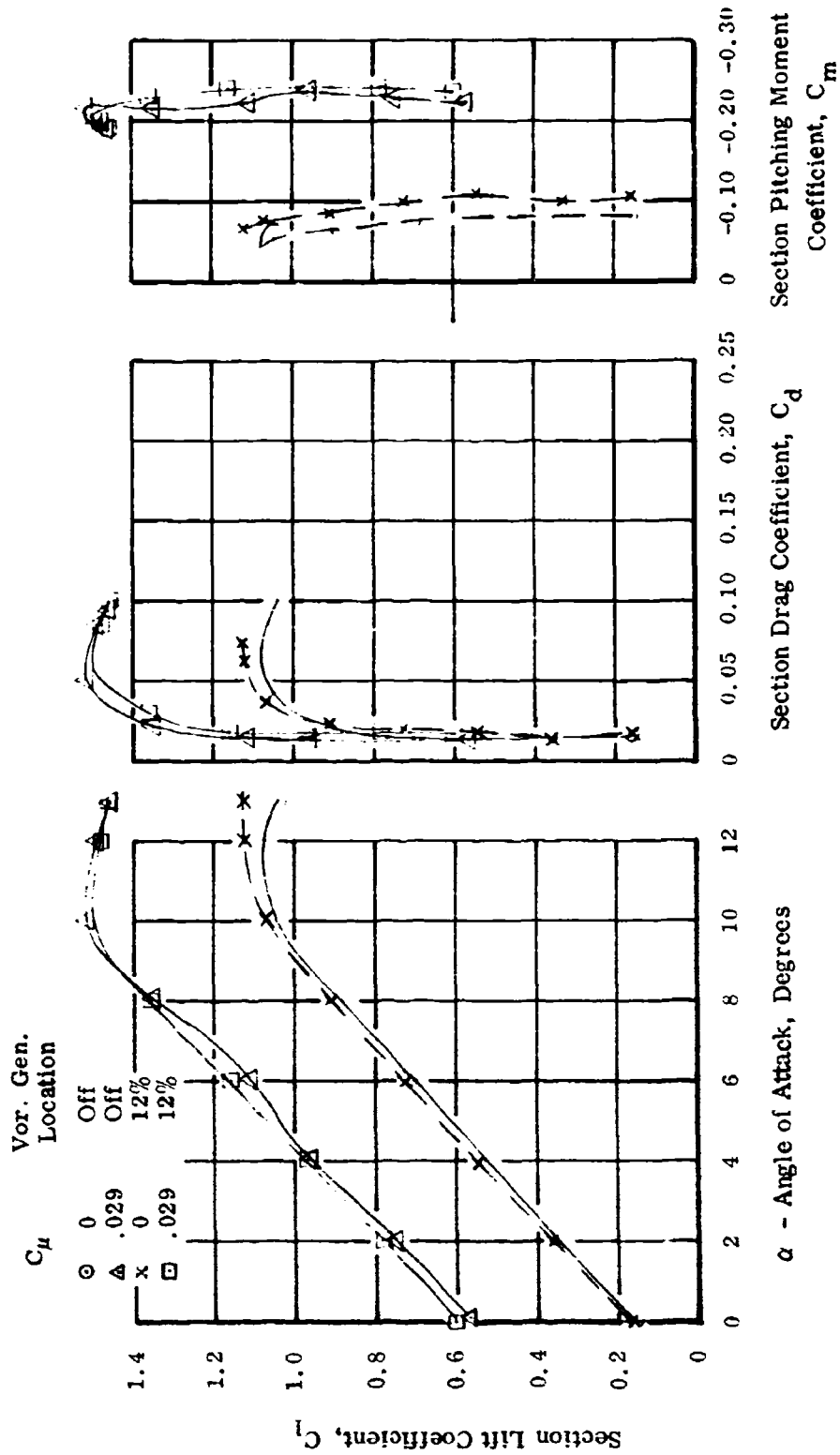


A-20. Section Pitching Moment Versus Mach No.



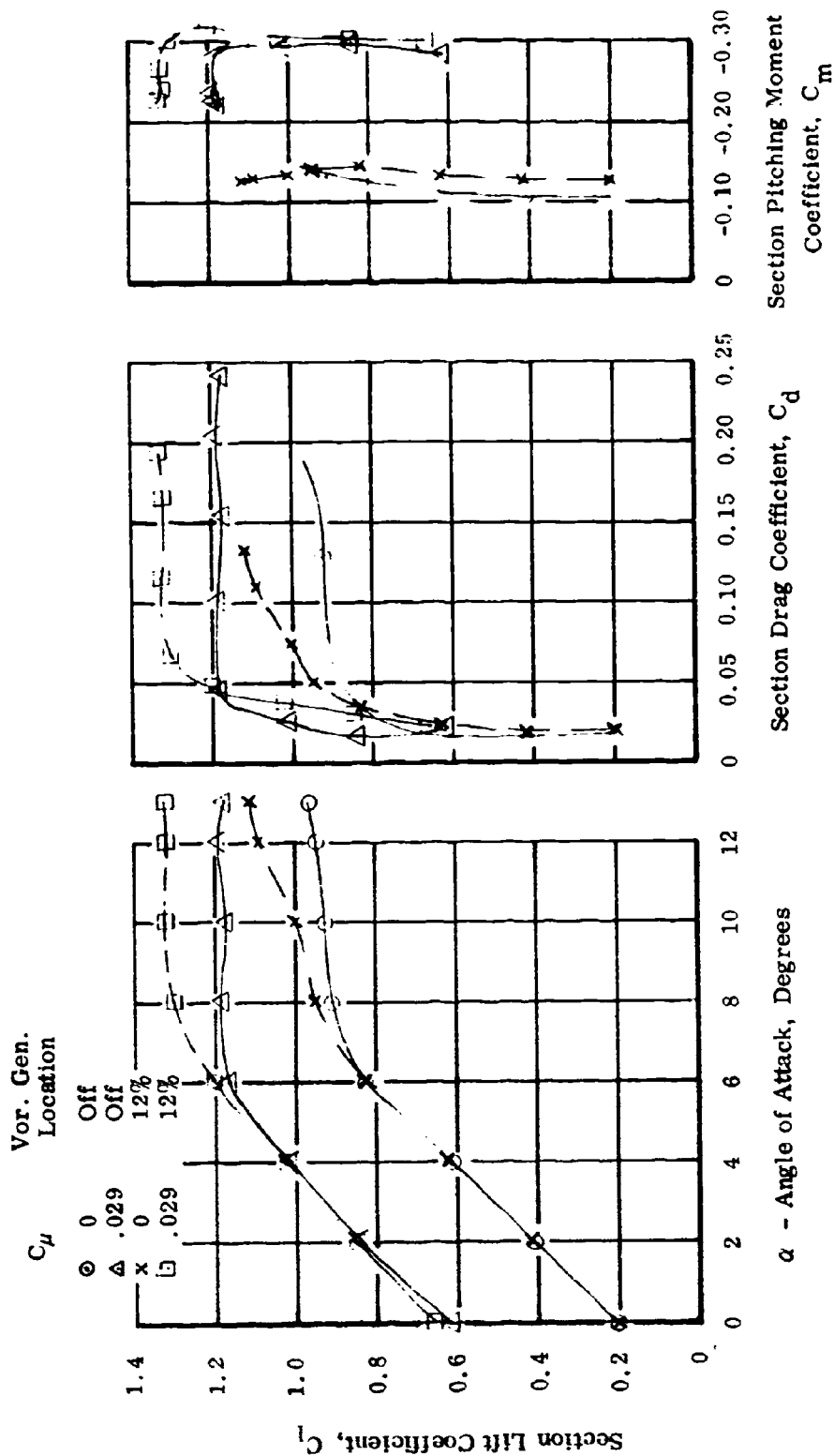
A-21. Lift Efficiency Versus Mach No. at $\sigma = 0^\circ$

$$R_N = 5.5 \times 10^6 / \text{FT} \quad \theta_f = 88^\circ$$



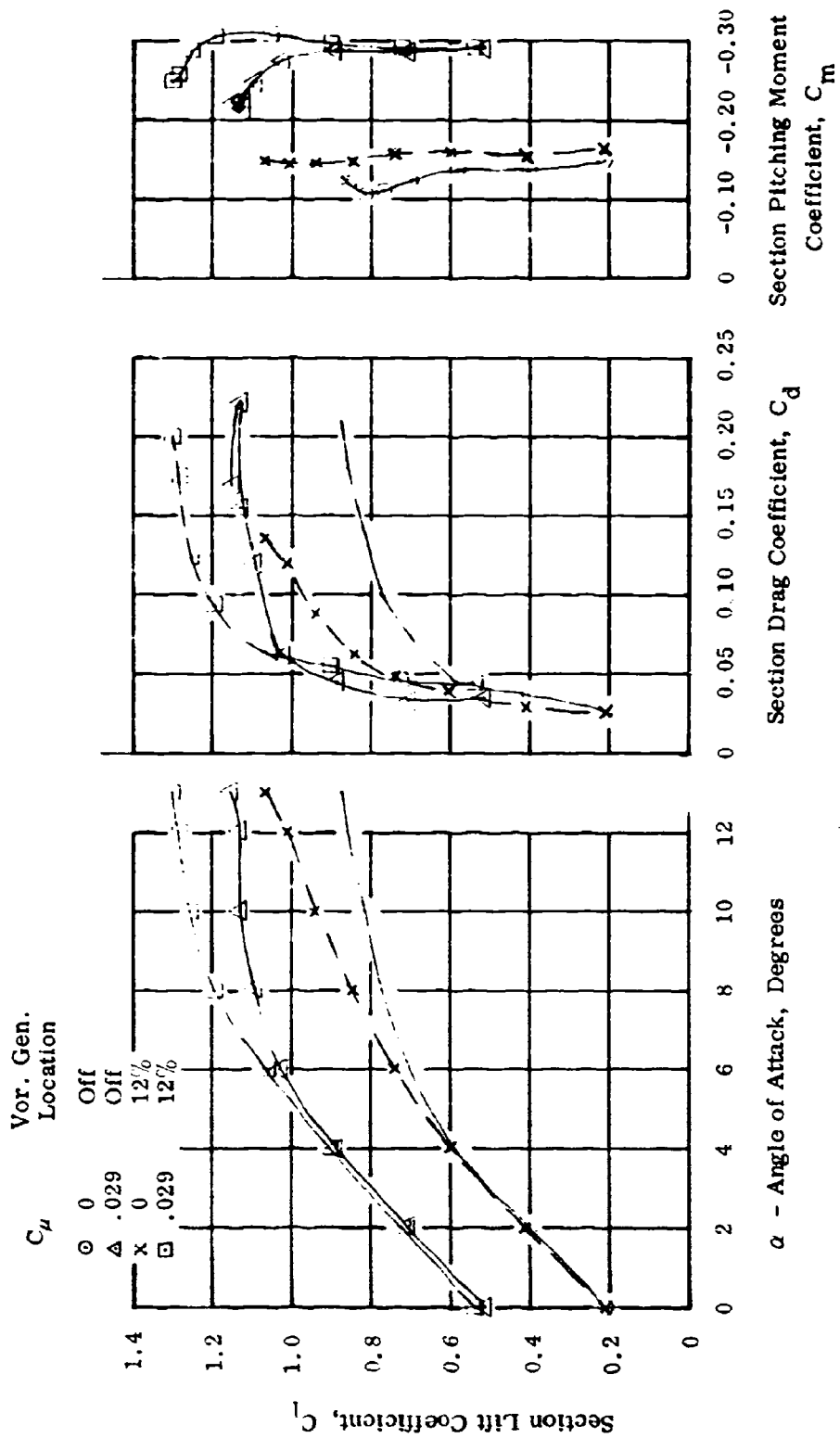
A-22. Effect of Vortex Generators, $M = 0.70$

$$R_N = 5.5 \times 10^6 / \text{FT} \quad , \quad \theta_f = 88^\circ$$

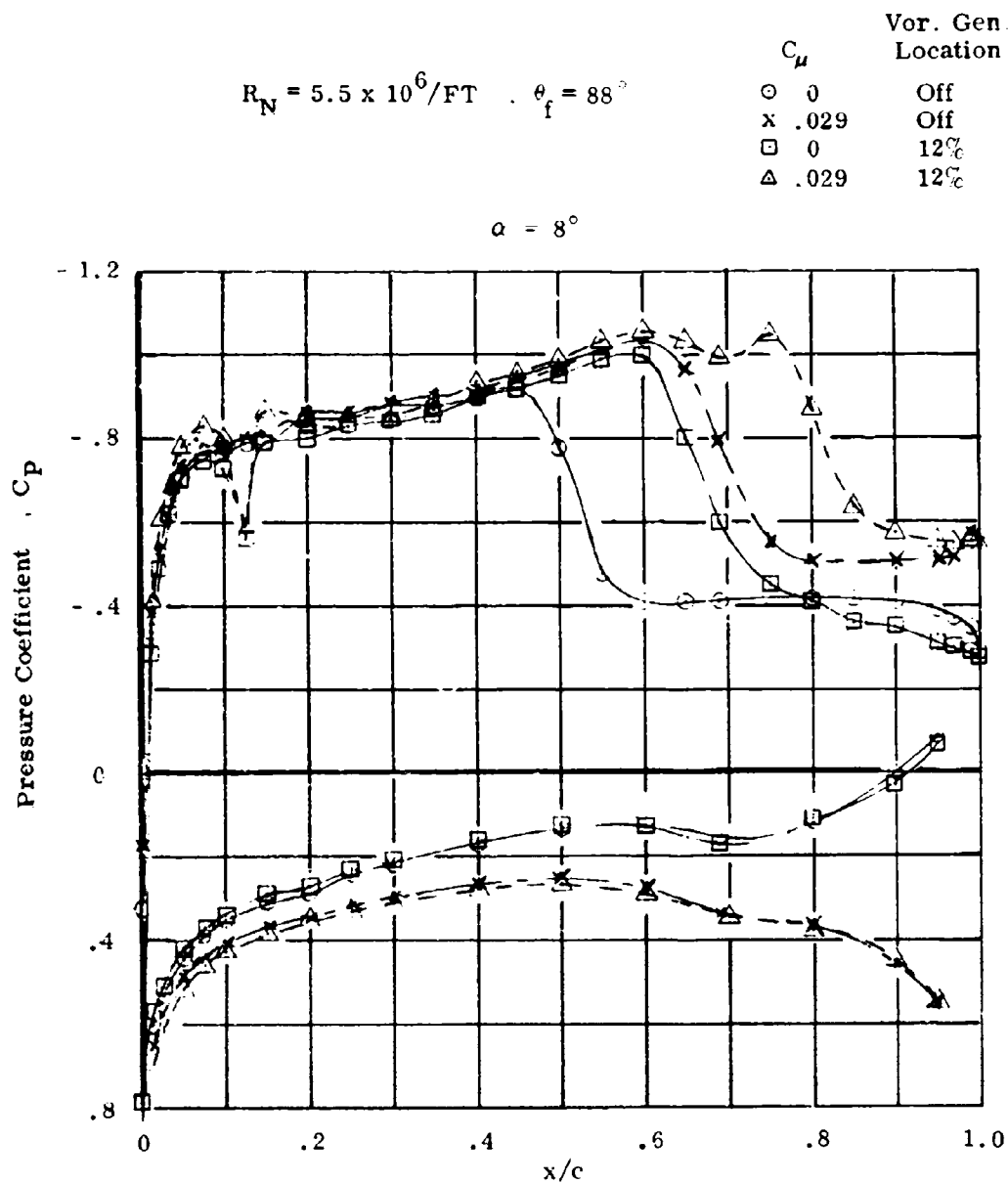


A-23. Effect of Vortex Generators, $M = 0.80$

$$R_N = 5.5 \times 10^6 / \text{FT} \quad , \quad \theta_f = 88^\circ$$

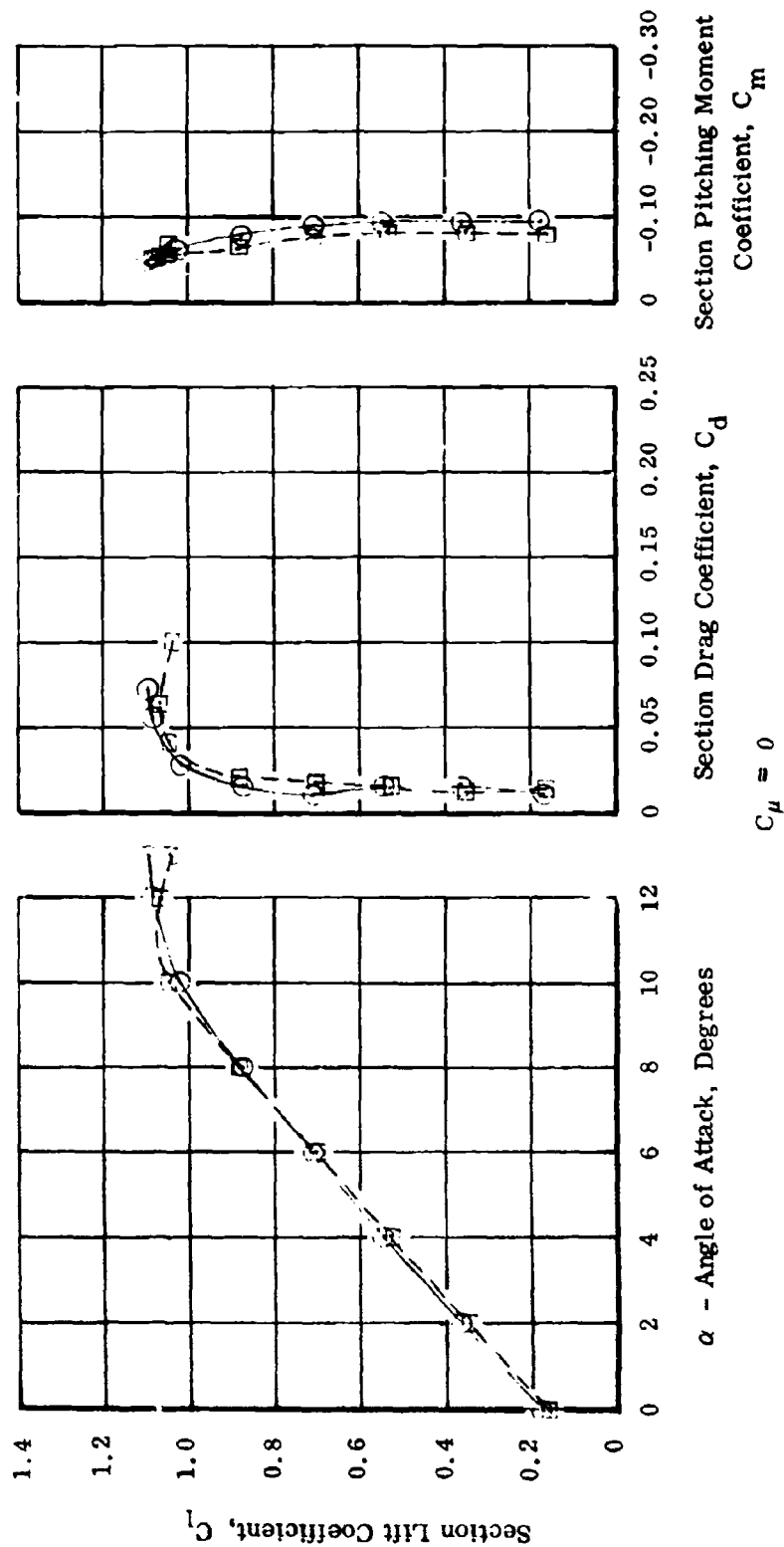


A-24. Effect of Vortex Generators, $M = 0.85$



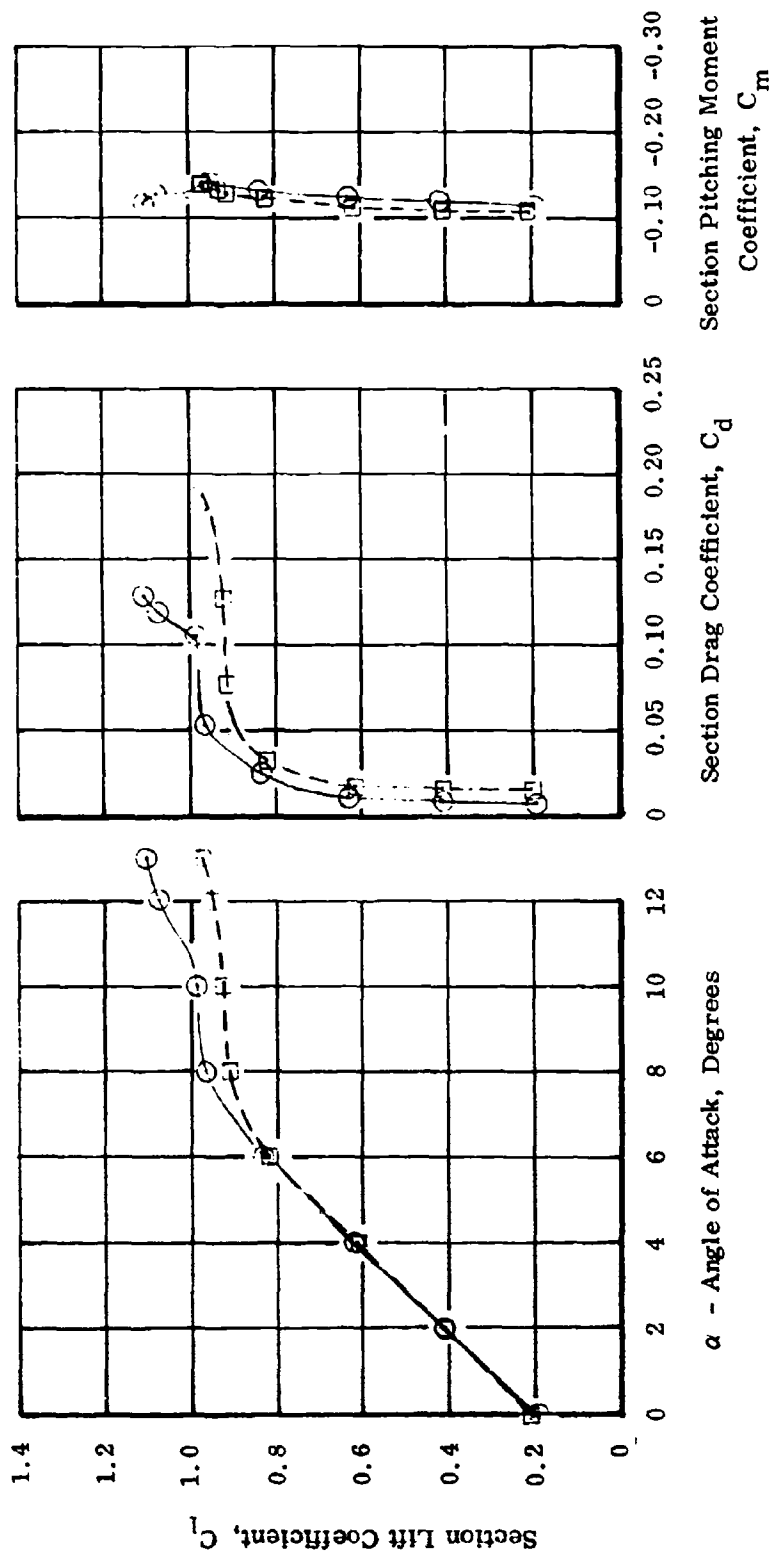
A-25. Effect of Vortex Generators on Pressure Distribution, $M = 0.85$

R_N
 $\circ 2.5 \times 10^6/\text{FT}$
 $\square 5.5 \times 10^6/\text{FT}$



A-26. Effect of Reynolds Number, $M = 0.70$

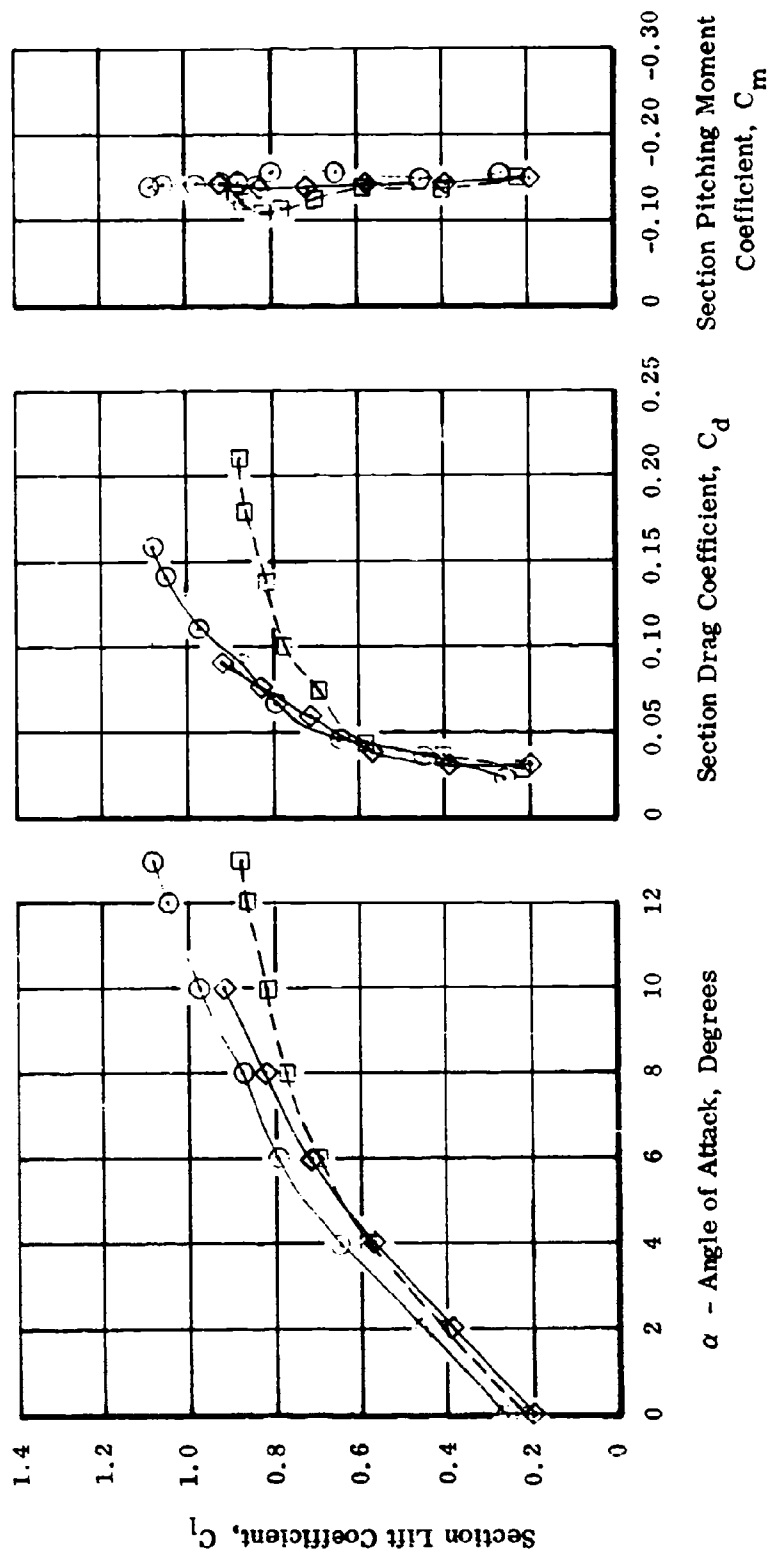
R_N
 $\bigcirc 2.5 \times 10^6/\text{FT}$
 $\square 5.5 \times 10^6/\text{FT}$



$C_{\mu} = 0$

A-27. Effect of Reynolds Number, $M = 0.80$

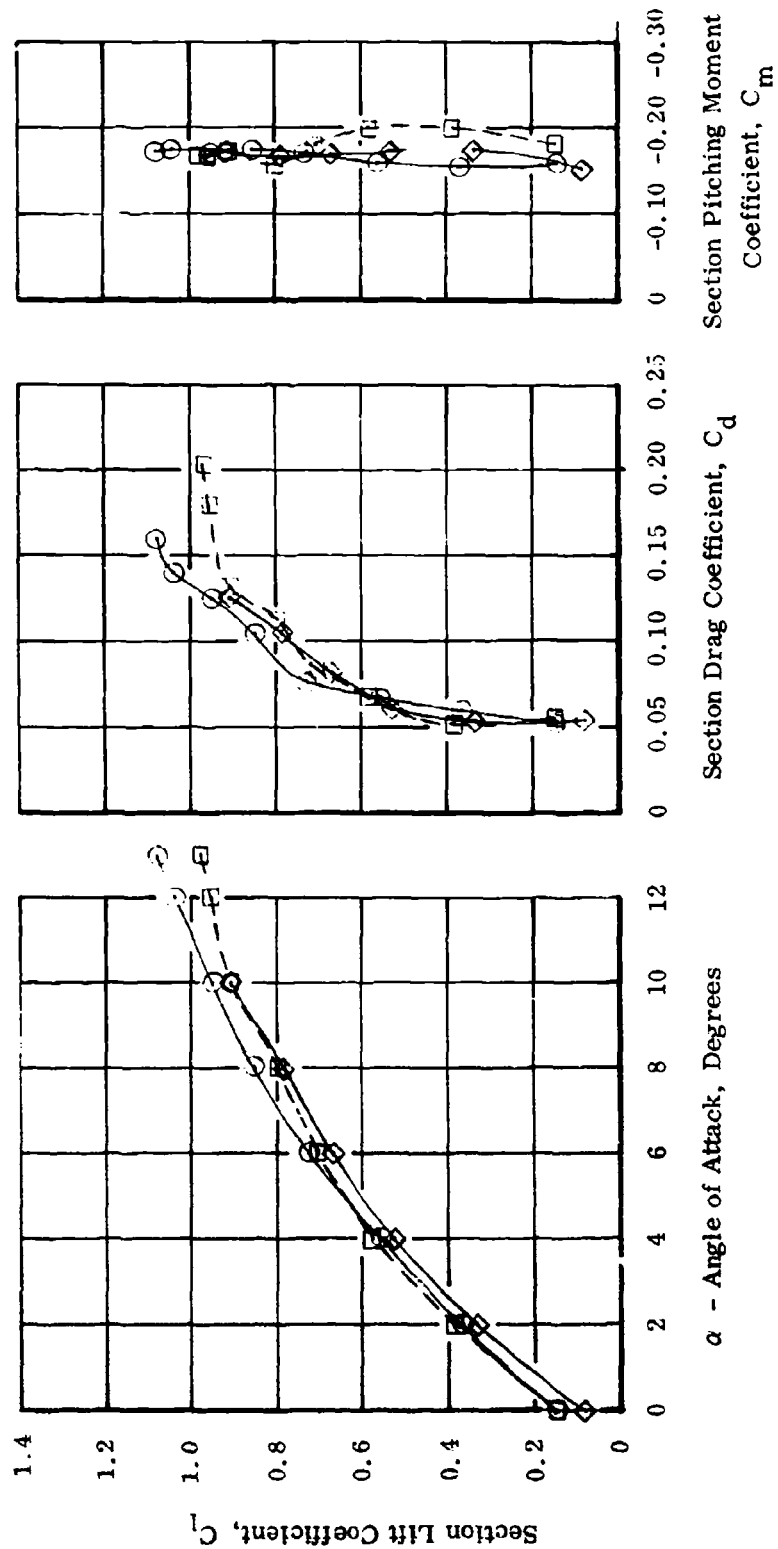
R_N
 $\circ 2.5 \times 10^6/\text{FT}$
 $\square 5.5 \times 10^6/\text{FT}$
 $\diamond 6.5 \times 10^6/\text{FT}$



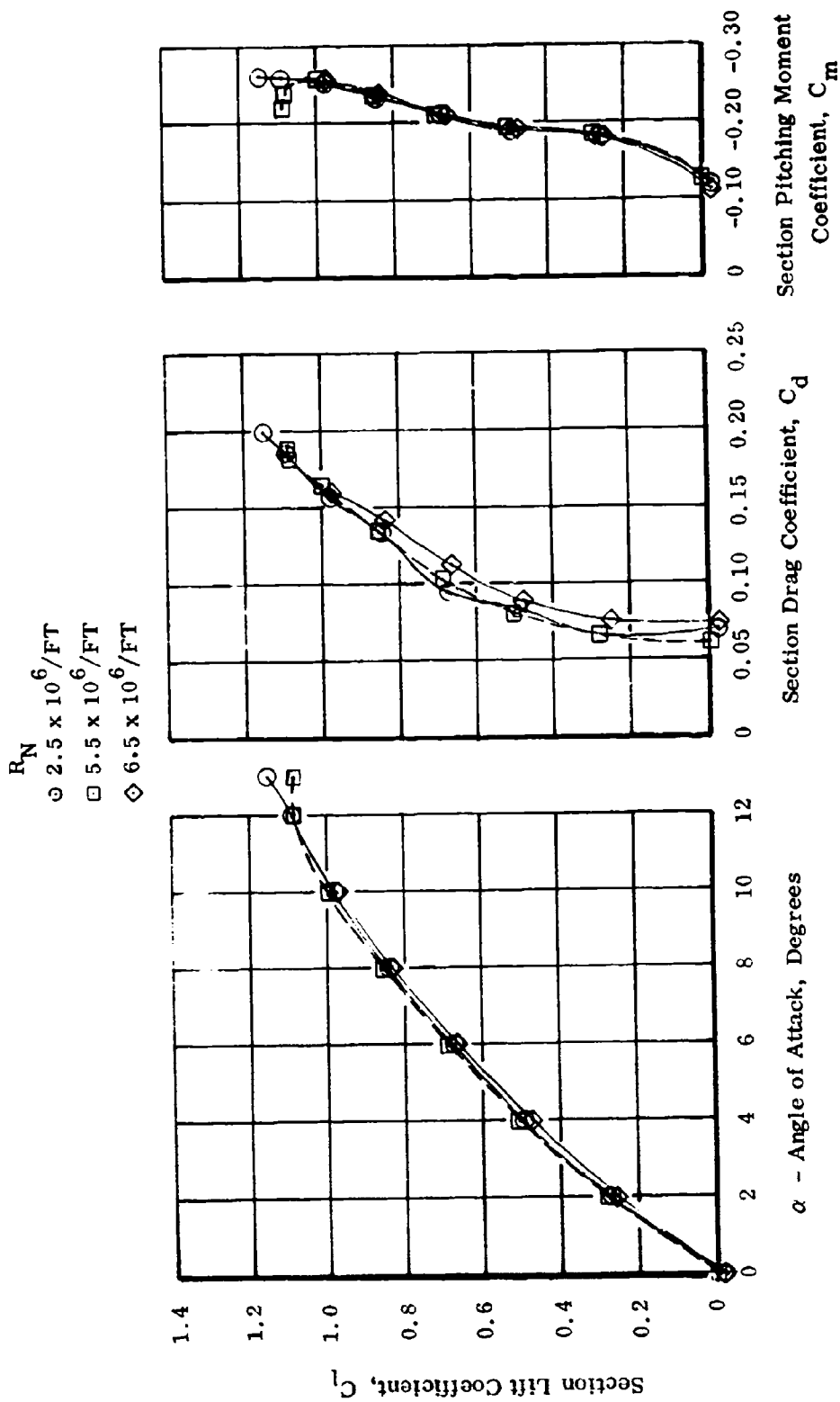
$C_{\mu} = 0$

A-28. Effect of Reynolds Number, $M = 0.85$

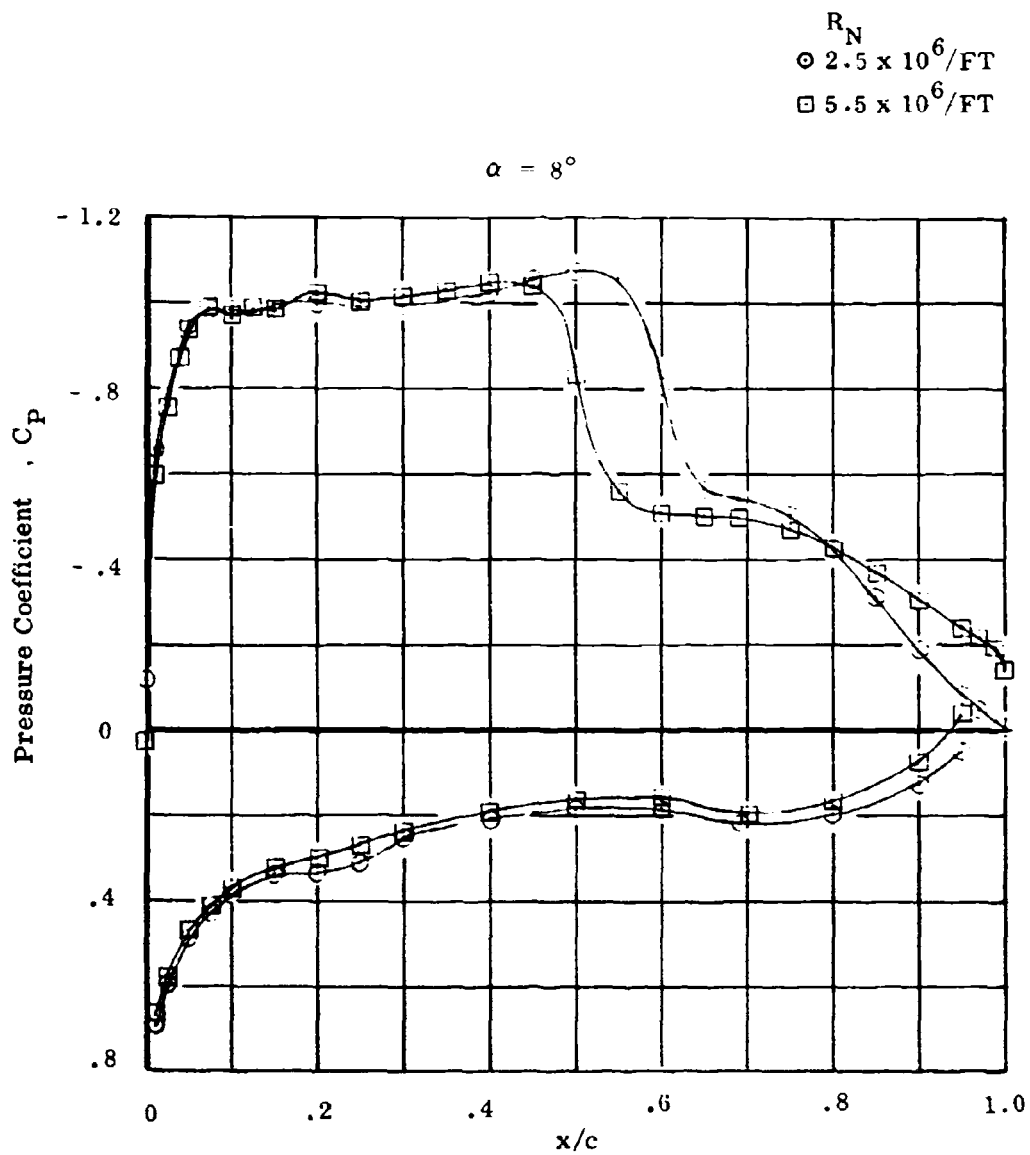
R_N
 $\circ 2.5 \times 10^6/\text{FT}$
 $\square 5.5 \times 10^6/\text{FT}$
 $\diamond 6.5 \times 10^6/\text{FT}$



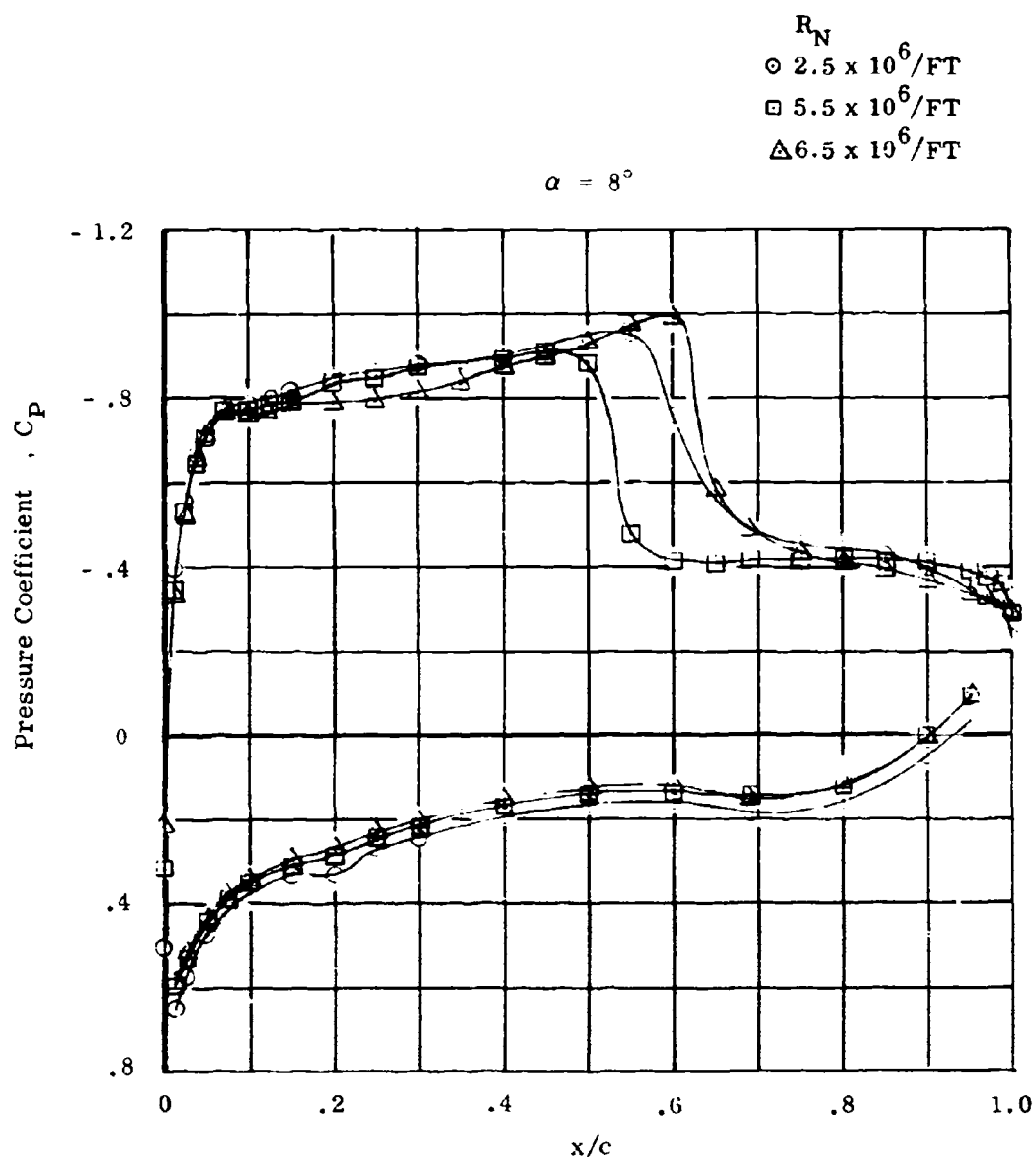
A-29. Effect of Reynolds Number, $M = 0.90$



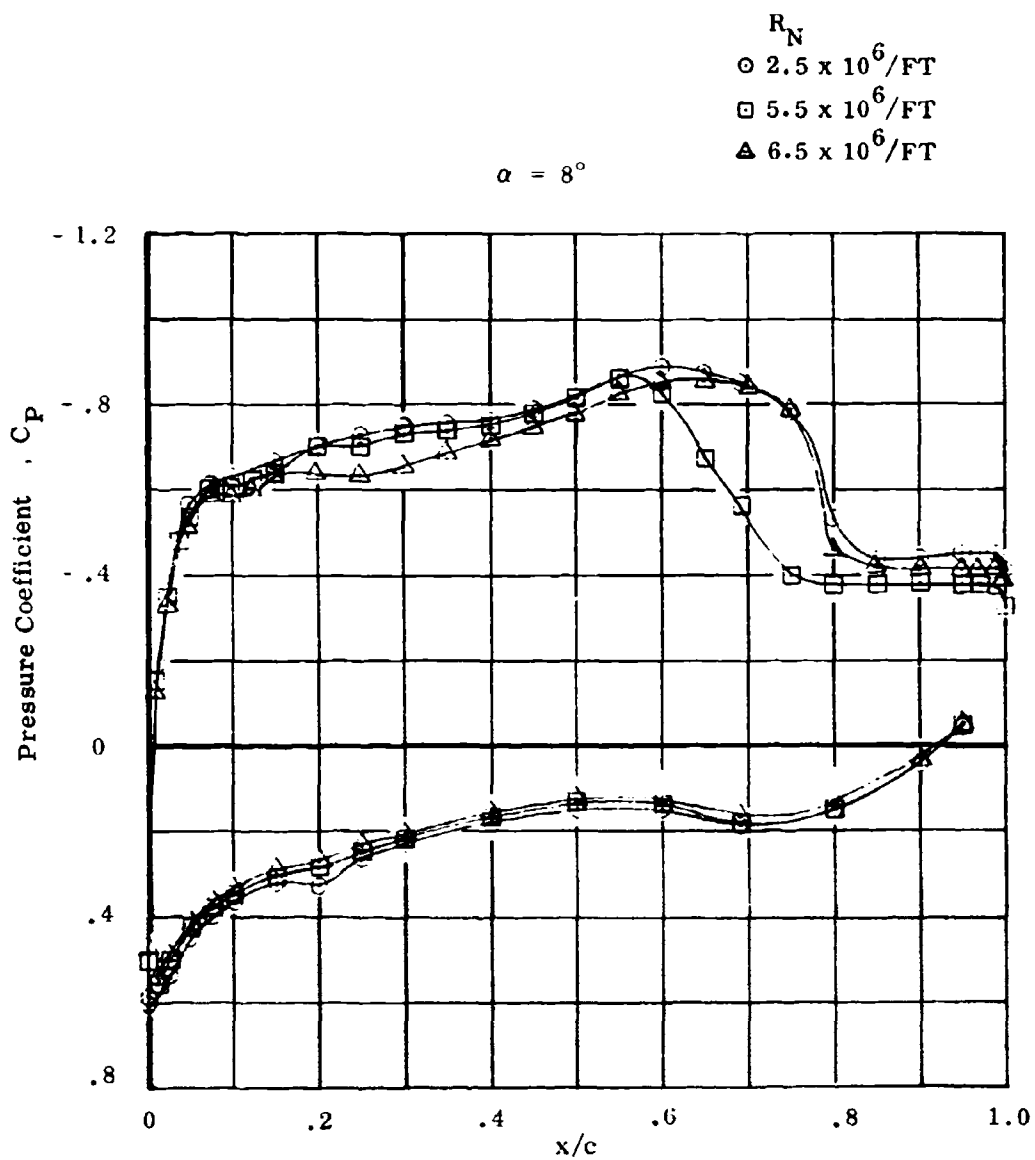
A-30. Effect of Reynolds Number, $M = 0.95$



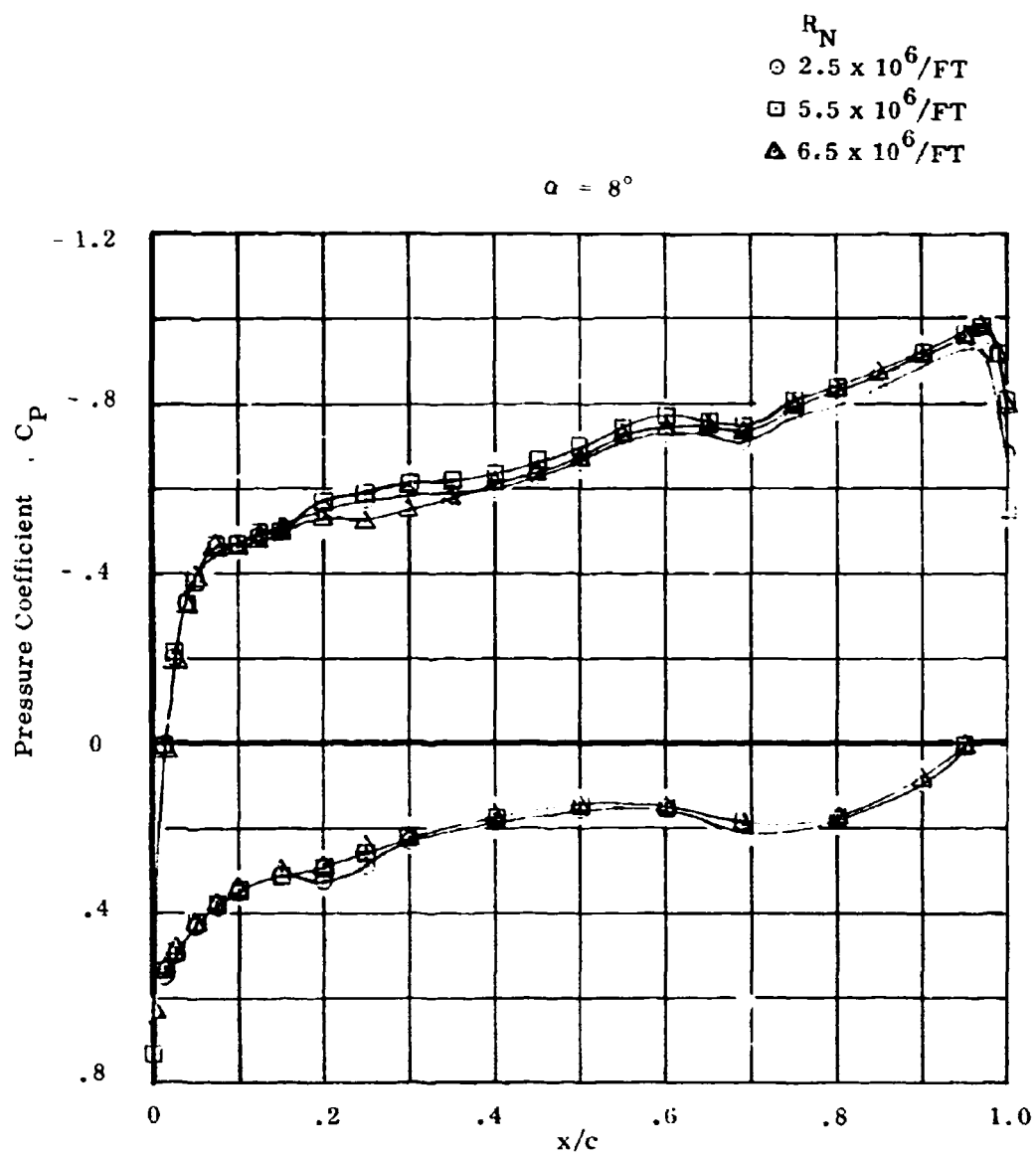
A-31. Effect of Reynolds Number on Pressure Distribution, $M = 0.80$



A-32. Effect of Reynolds Number on Pressure Distribution, $M = 0.85$



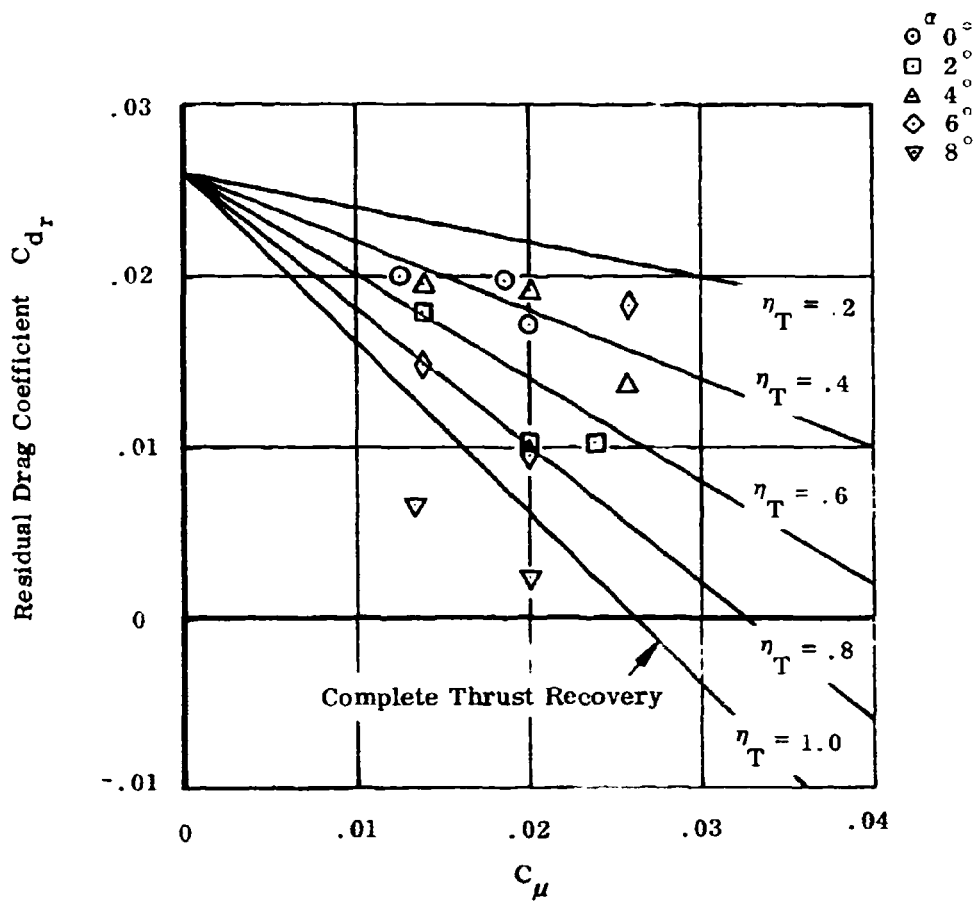
A-33. Effect of Reynolds Number on Pressure Distribution, $M = 0.90$



A-34. Effect of Reynolds Number on Pressure Distribution, $M = 0.95$

Mach No. = 0.85

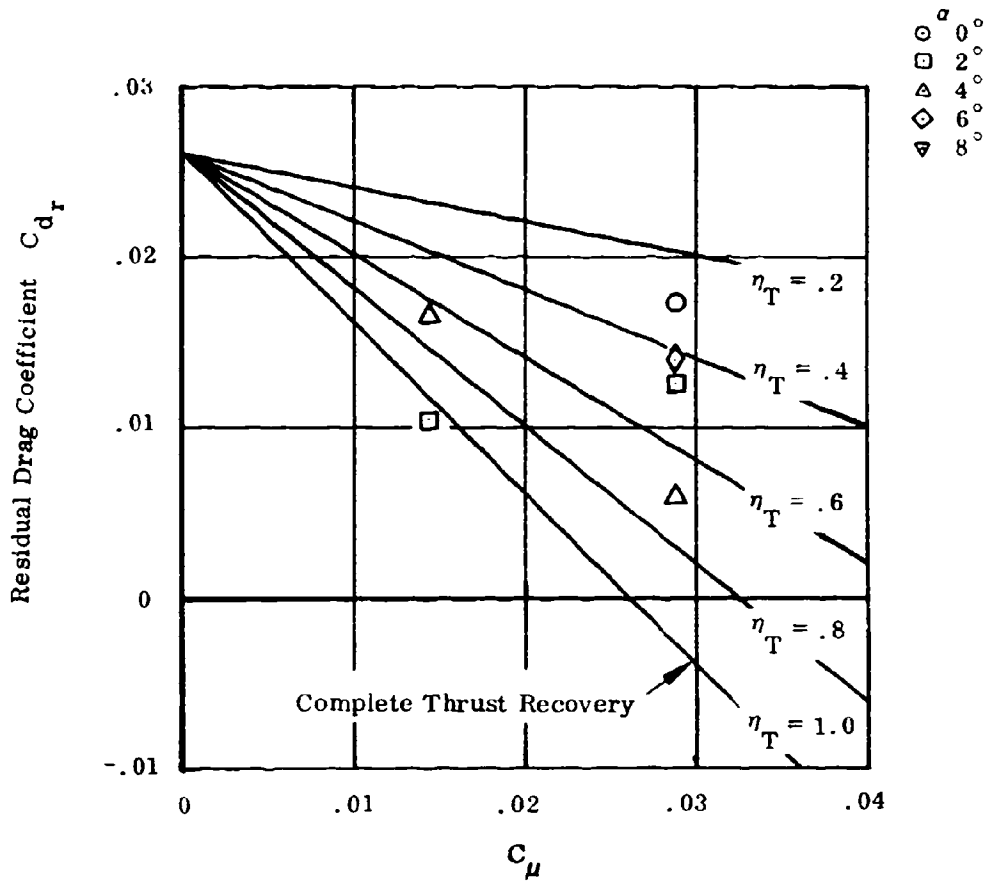
$R_N = 5.5 \times 10^6 / FT$



A-35. Thrust Recovery at $\theta_f = 0^\circ$

Mach No. = 0.85

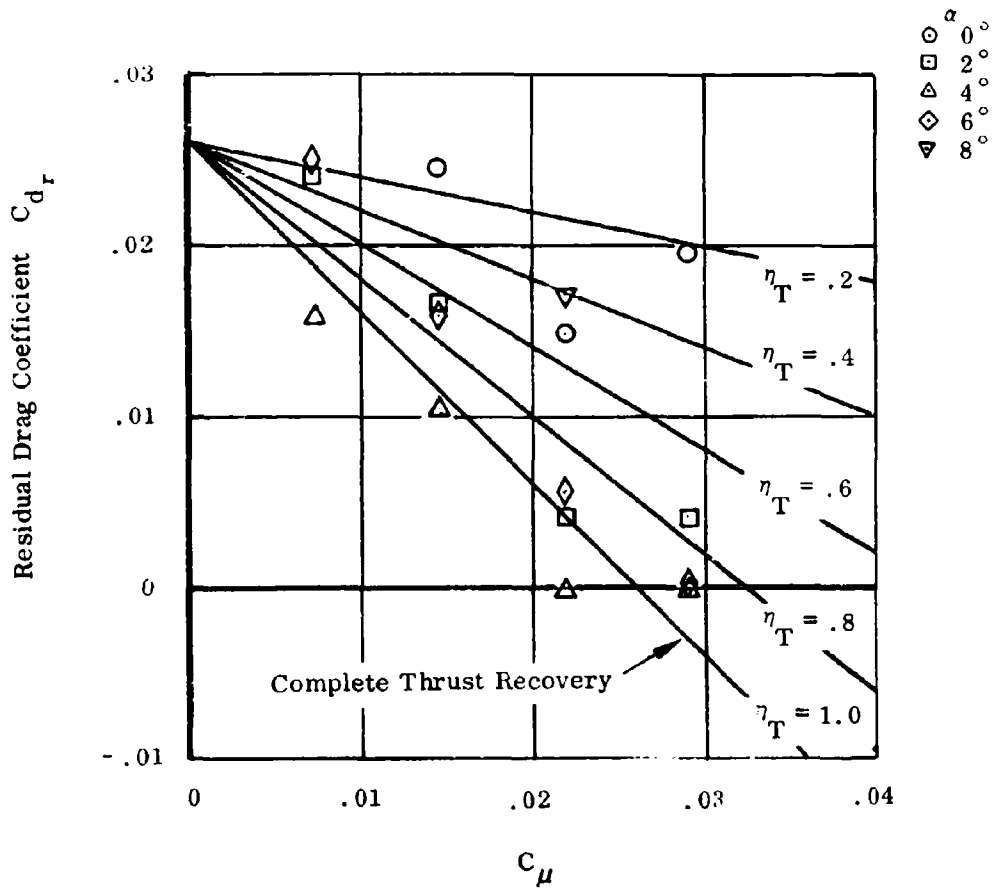
$R_N = 5.5 \times 10^6 / \text{FT}$



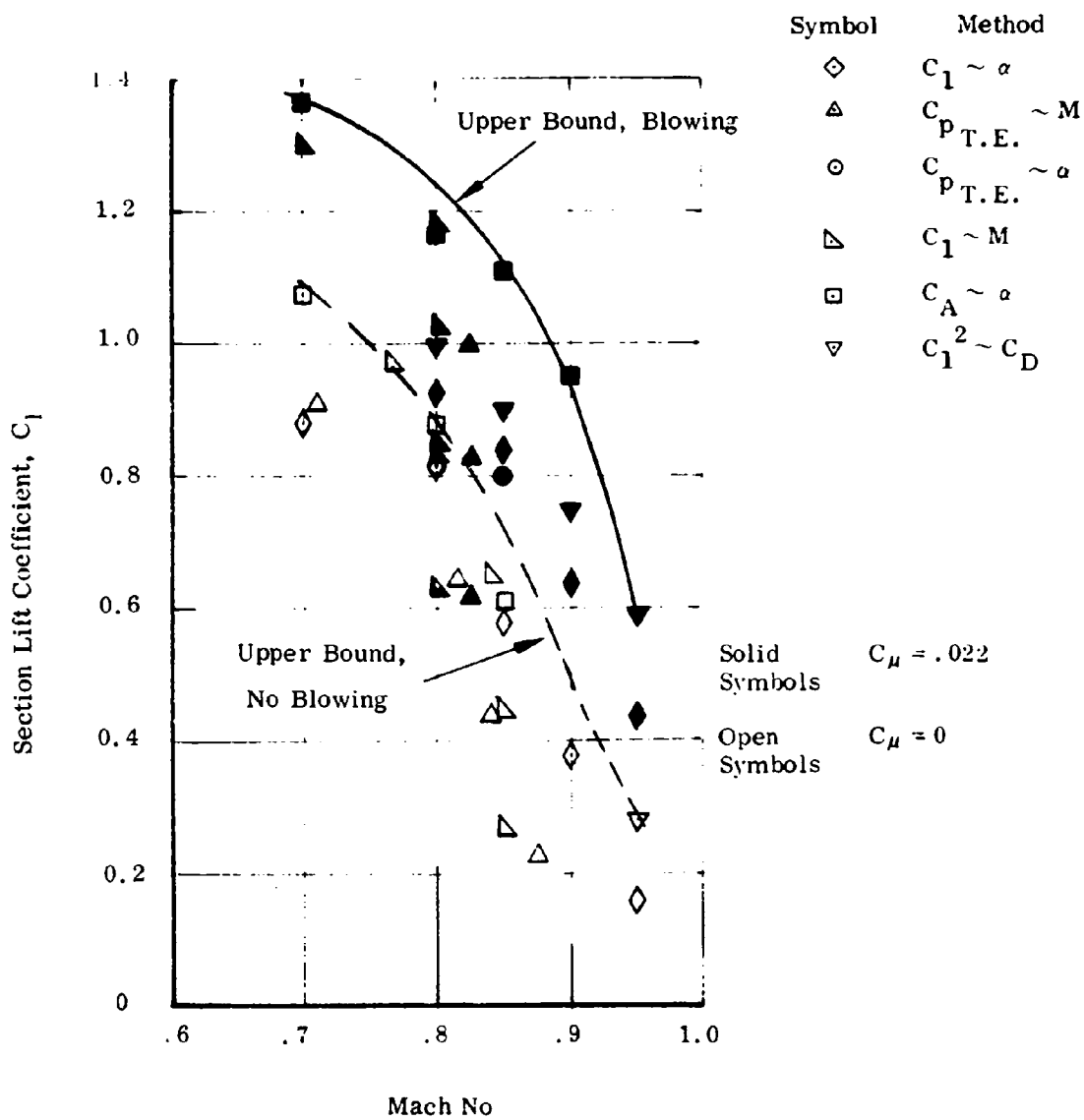
A-36. Thrust Recovery at $\theta_f = 55^\circ$

Mach No. = 0.85

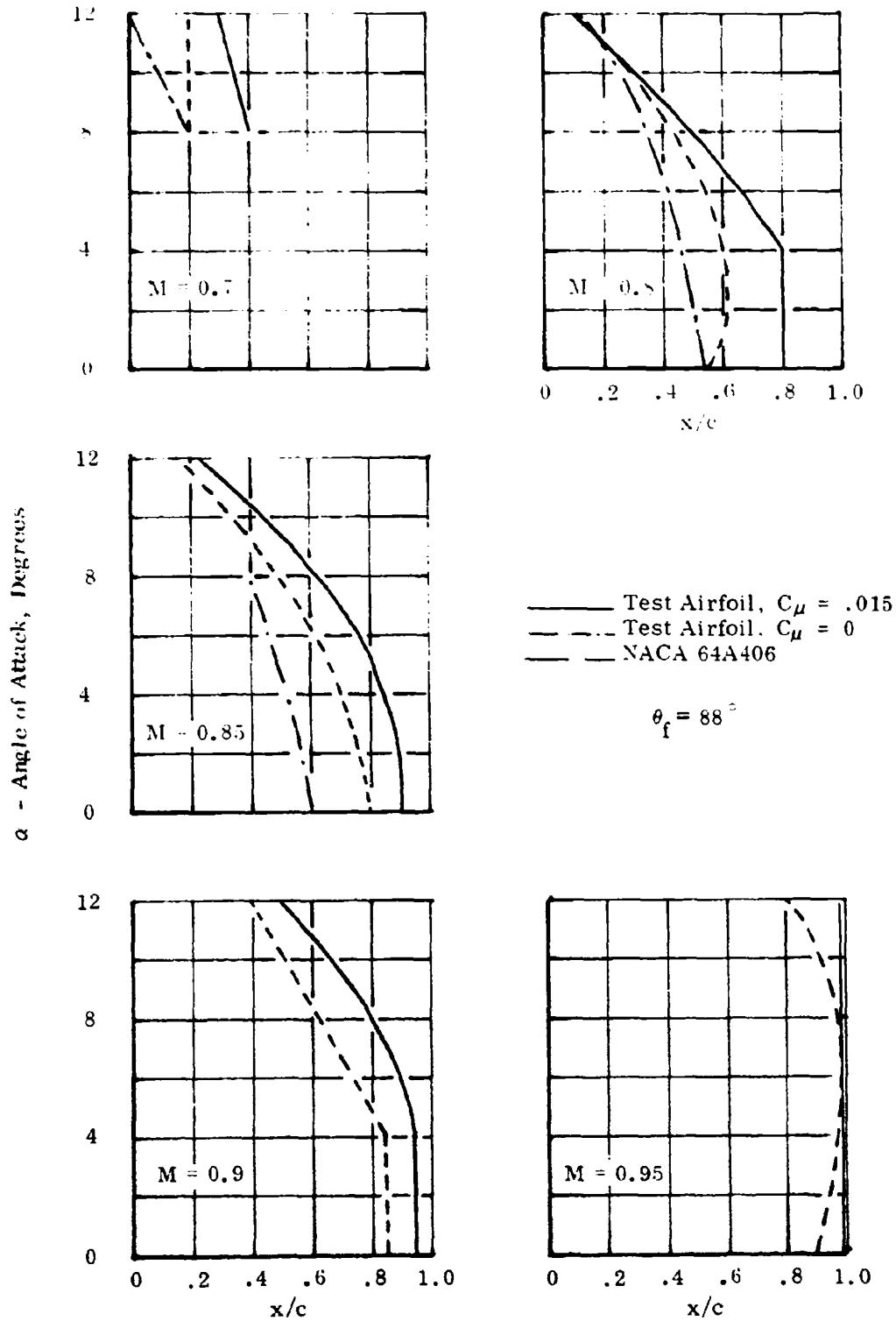
$R_N = 5.5 \times 10^6 / FT$



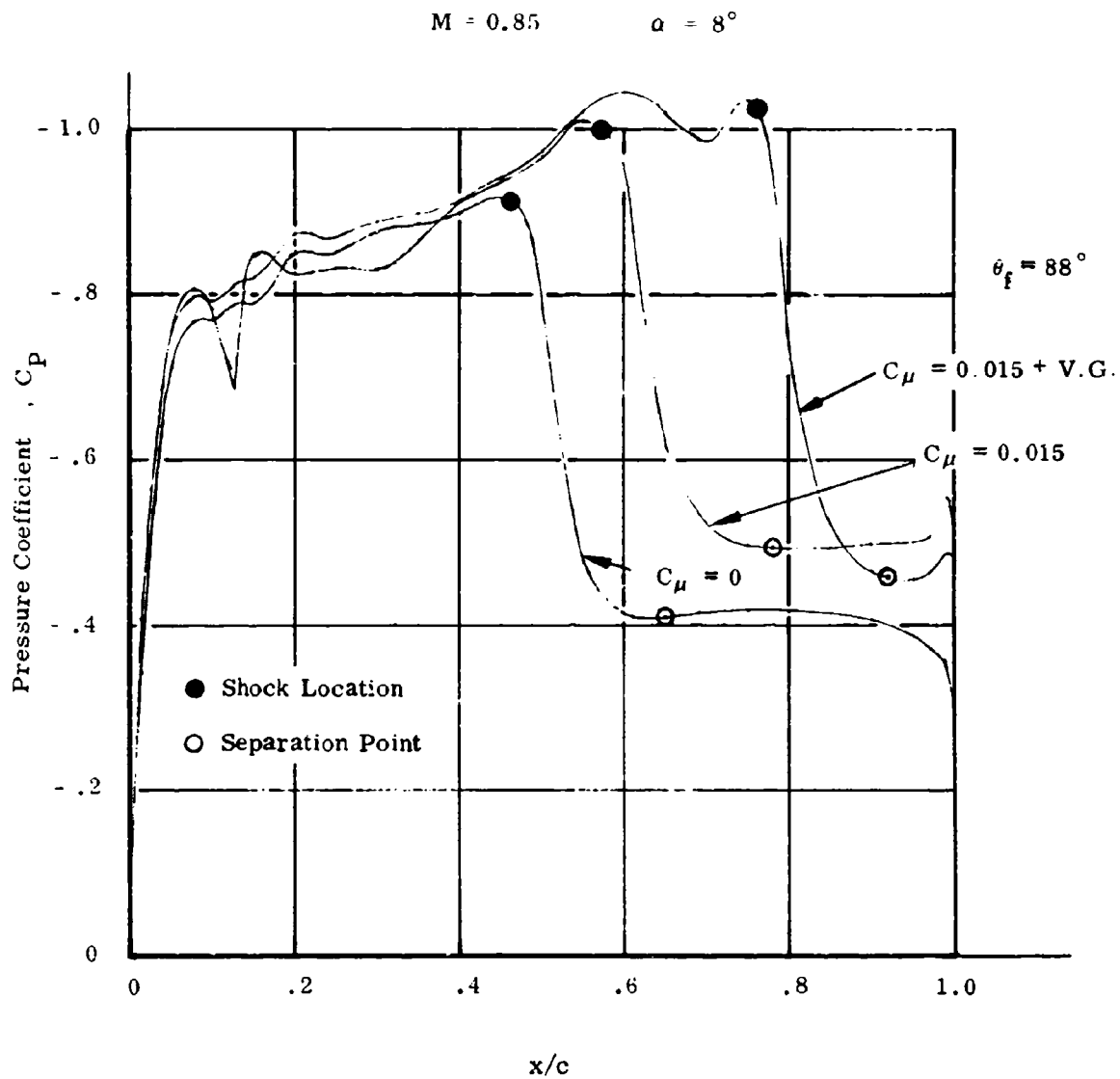
A-37. Thrust Recovery at $\theta_f = 88^\circ$



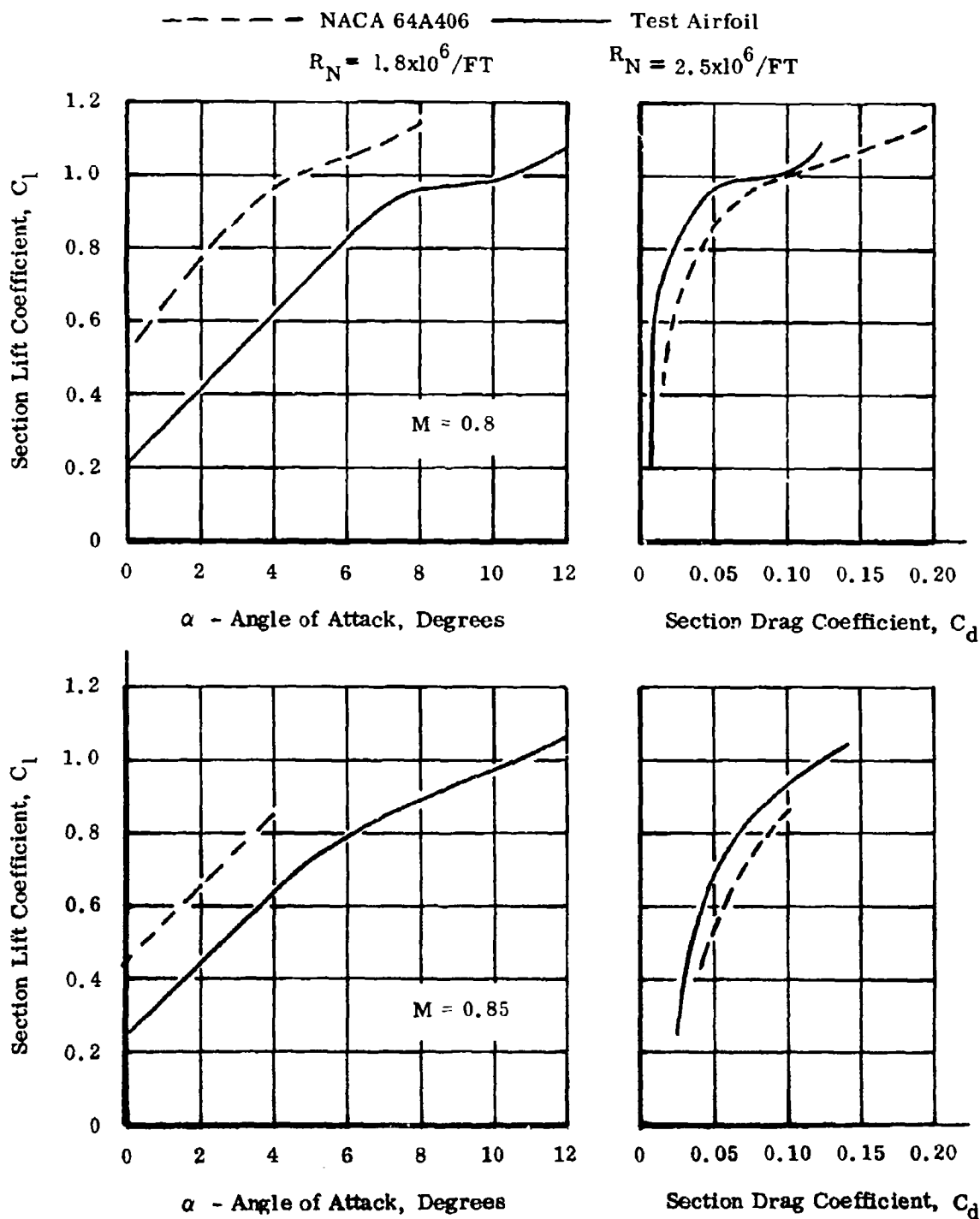
A-38. Buffet Onset Method Comparison



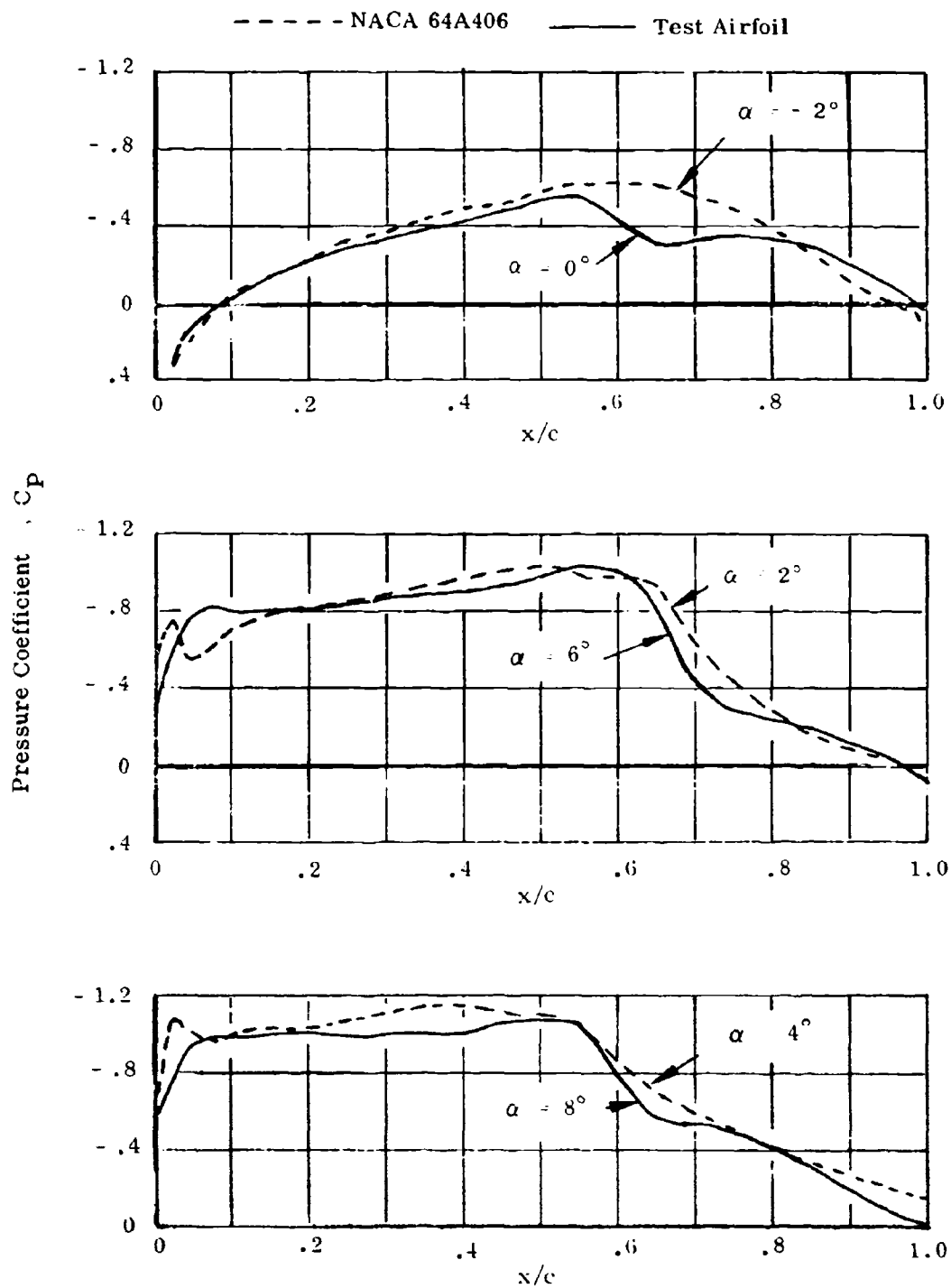
A-39. Comparisons of Estimated Shock Locations



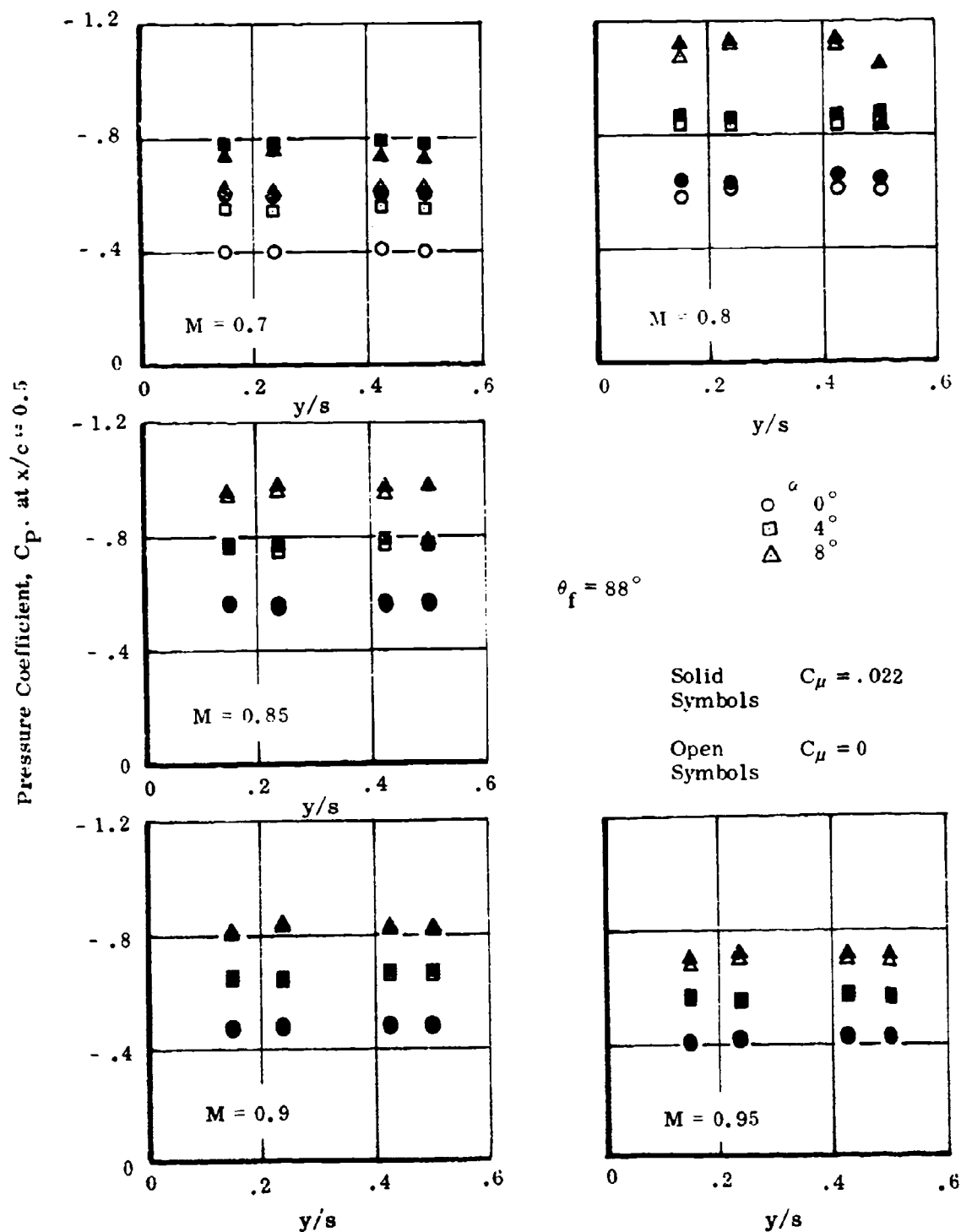
A-40. Upper Surface Pressure Comparison



A-41. Comparison of Test Airfoil and NACA 64A406



A-42. Comparison of Test Airfoil and NACA 64A406 Upper Surface Pressures at $M = 0.80$



A-43. Spanwise Pressure Distributions

Unclassified

Security Classification

| DOCUMENT CONTROL DATA - R & D | | |
|---|---|--|
| (Security classification of title, body of abstract and indexing annotation must be entered when the overall report is classified) | | |
| 1. ORIGINATING ACTIVITY (Corporate author) Northrop Corporation Aircraft Division 3901 W. Broadway, Hawthorne, California 90250 | | 2a. REPORT SECURITY CLASSIFICATION Unclassified |
| | | 2b. GROUP |
| 3. REPORT TITLE JET FLAP INVESTIGATION AT TRANSONIC SPEEDS | | |
| 4. DESCRIPTIVE NOTES (Type of report and inclusive dates) Final Technical Report - 10 February 1969 through 10 November 1969 | | |
| 5. AUTHOR(S) (First name, middle initial, last name) William E. Grahame Jack W. Headley | | |
| 6. REPORT DATE February 1970 | 7a. TOTAL NO. OF PAGES 84 | 7b. NO. OF REFS 11 |
| 8a. CONTRACT OR GRANT NO. F33615-69-C-1429 | 9a. ORIGINATOR'S REPORT NUMBER(S) AFFDL-TR-69-117 | |
| b. PROJECT NO. 1366 | | |
| c. Task No. 136619 | 9b. OTHER REPORT NO(S) (Any other numbers that may be assigned this report) | |
| d. Work Unit No. 136619006 | NOR 69-143 | |
| 10. DISTRIBUTION STATEMENT This document is subject to special export controls and each transmittal to foreign governments or foreign nationals may be made only with prior approval of the Flight Dynamics Laboratory (FDMM) Wright-Patterson Air Force Base, Ohio, 45433 | | |
| 11. SUPPLEMENTARY NOTES | 12. SPONSORING MILITARY ACTIVITY Air Force Flight Dynamics Laboratory Air Force Systems Command Wright-Patterson AFB, Ohio 45433 | |
| 13. ABSTRACT A transonic wind tunnel test of a two-dimensional airfoil with a jet flap was conducted to obtain data relative to determining the feasibility of using a jet flap for transonic maneuvering. Tests were performed at Mach numbers of 0.70, 0.80, 0.85, and 0.95 for an angle of attack range from zero up to the angle of attack corresponding to maximum lift coefficient at nominal jet flap angles of 0°, 30°, 45°, 60°, and 90°. Lift and drag characteristics were obtained by integrating pressures measured over the wing and by a wake rake. The results show significant lift improvement at low Mach number which diminished as Mach number increased. Test results were compared on the basis of lifting efficiency E_L and thrust recovery η_T at various jet angles and jet momentum values. The results indicated that the values of E_L and η_T obtained generally agreed with those which have been presented from other tests. The jet flap at the largest angle (θ_f nominally 90°) with a row of vane vortex generators positioned at 12% chord produced the greatest rearward movement of shock induced separation. Effects of Reynolds number showed that lift characteristics were lower at $R_N = 5.5 \times 10^6/\text{ft}$ than at $R_N = 2.5 \times 10^6/\text{ft}$ while drag was higher throughout the Mach number range. A correlation of six methods, which predict the onset of buffet, illustrated the ability of the jet flap to improve the buffet boundary. This abstract is subject to special export controls and each transmittal to foreign governments or foreign nationals may be made only with prior approval of the Flight Dynamics Laboratory (FDMM), Wright-Patterson AFB, Ohio 45433. | | |

DD FORM 1473
1 NOV 66

Unclassified

Security Classification

Unclassified
Security Classification

| 14 KEY WORDS | LINK A | | LINK B | | LINK C | |
|-------------------------------|--------|----|--------|----|--------|----|
| | ROLE | WT | ROLE | WT | ROLE | WT |
| Transonic Flow | | | | | | |
| Jet Flap | | | | | | |
| Shock Waves | | | | | | |
| Shock Induced Separation | | | | | | |
| Buffet Analysis | | | | | | |
| Wind Tunnel Test | | | | | | |
| Static Pressure Distributions | | | | | | |
| Two-Dimensional Flow | | | | | | |
| Vortex Generators | | | | | | |

Unclassified
Security Classification